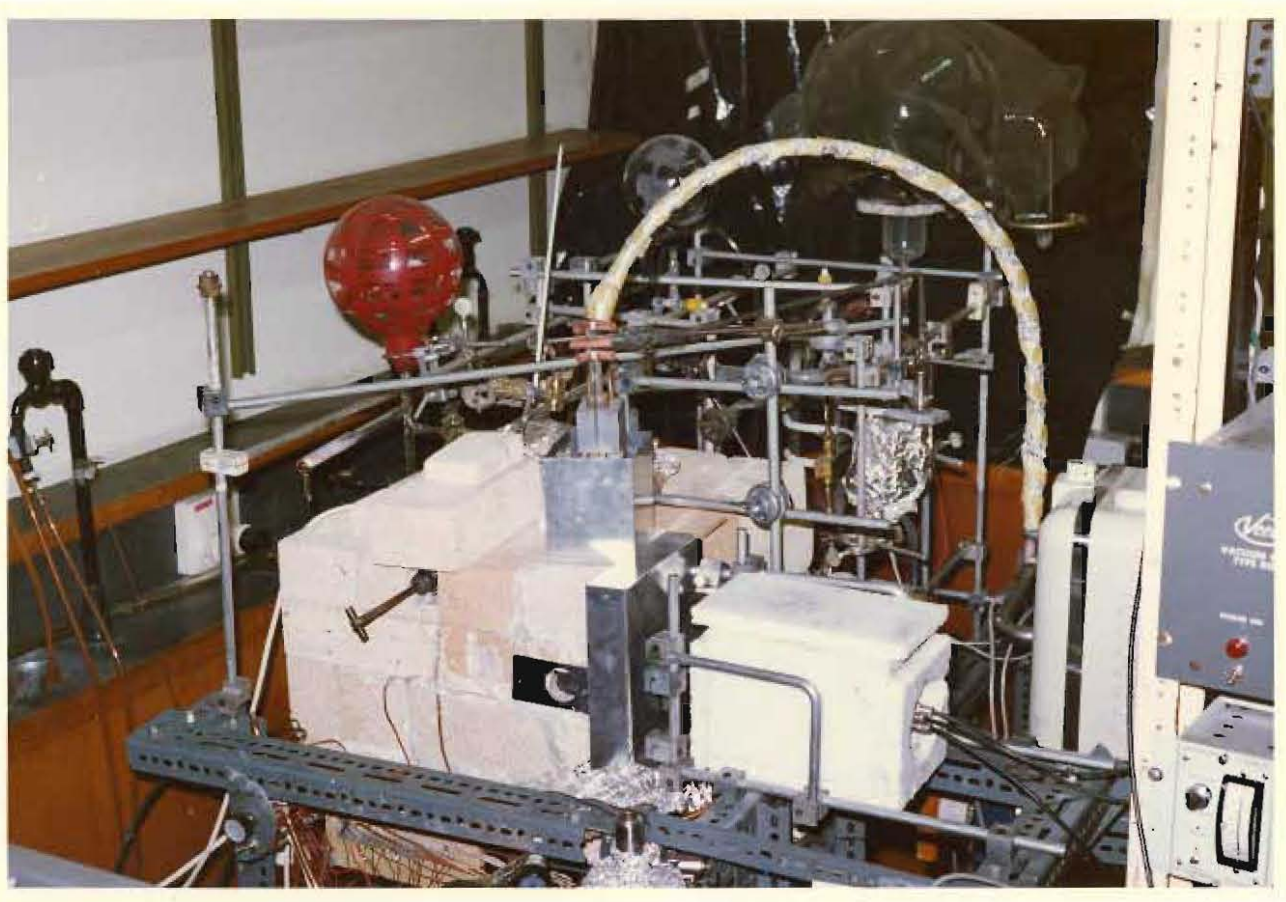

EXPERIMENTAL APPARATUS

OPTICAL STUDIES OF METAL VAPOURS

A thesis
submitted in partial fulfilment
of the requirements for the Degree
of
Doctor of Philosophy in Chemistry
in the
University of Canterbury
by

Christopher John Nokes

University of Canterbury
1982

ACKNOWLEDGEMENT

During the course of this work there have been numerous people whose assistance has been greatly appreciated and to whom I owe my thanks. Foremost amongst these is Professor L.F. Phillips who has always been ready to give of his time and to offer advice when it was sought. For his patient help and his enthusiasm over these years I am sincerely grateful. Also, I wish to thank Dr A. Metcalfe for the sharing of his chemical knowledge (and for his many "true" stories that provided light relief in moments of frustration) which has often been a help during this work.

I am grateful to the Chemistry Department for the award of a Teaching Fellowship over three years.

For the tolerance and assistance of the department's technical staff, I am indebted; in particular, I wish to thank Messrs. A.M. Ferguson, R.W. Gillard, R. Dalley and R.A. Loeffen.

I am grateful to Mrs J. Warburton for her rapid and efficient typing of the text and her concern over its appearance.

For her tolerance, also, and her encouragement and help with proof-reading, I am indebted to Sheila.

Finally, it is an appropriate place to express, in addition to my gratitude for their help in their own fields of expertise, my sincere thanks to my parents for providing for an education that has enabled me to undertake this study.

C.J. Nokes

1982

C.J. Nokes.

ABSTRACT

The kinetics of the $CdNH_3^*$ 430 nm emission band at 550 K have been studied using steady-illumination and conventional phase-shift techniques in addition to a laser fluorescence technique that has enabled the phase shift of the metastable $Cd(^3P_0)$ species to be measured. The data from these measurements require the system kinetics to be modelled on a mechanism in which an unstabilized complex $CdNH_3^\dagger$, having a lifetime in the range 10^{-9} - 10^{-13}s with respect to dissociation to NH_3 plus either $Cd(^3P_1)$ or $Cd(^3P_0)$, is present. The phase-shift measurements give values of 2×10^{-5} s for the radiative lifetime of $CdNH_3^*$ and 9.1×10^{-13} cm^3 $molecule^{-1}$ s^{-1} for the rate constant of the process

$$CdNH_3^* + NH_3 \rightarrow CdNH_3^\dagger + NH_3 \quad .$$

The laser fluorescence measurements yield values of 2.1×10^{-11} and 8.7×10^{-11} cm^3 $molecule^{-1}$ s^{-1} for the rate constants of the processes

$$Cd(^3P_0) + NH_3 \rightarrow CdNH_3^\dagger$$

and

$$Cd(^3P_1) + NH_3 \rightarrow CdNH_3^\dagger \ ,$$

respectively. The steady-illumination measurements show that at low ammonia pressures production of an unstabilized cadmium excimer $Cd_2^\dagger$ competes with production of $CdNH_3^\dagger$, providing an additional energy reservoir in this system. The lifetime of $Cd_2^\dagger$ is two or three orders of magnitude greater than that of $CdNH_3^\dagger$.

CONTENTS

LIST OF TABLES

LIST OF FIGURES

CHAPTER I

INTRODUCTION AND REVIEW

Reports of qualitative studies of the photophysical and photochemical properties of metal vapours were appearing frequently in the literature by the 1920s. Mercury vapour in particular received much attention because its relatively high vapour pressure facilitated the design and construction of experimental apparatus. This preferential interest in mercury has persisted to the present, with the result that a large body of information concerning the quenching and photosensitised reactions of this metal has accumulated. Many papers have appeared describing work on cadmium systems, and although in some cases the knowledge gained from the mercury studies has provided the basis for the understanding of the behaviour of the chemically similar metal, there are numerous instances where processes occurring in cadmium vapour systems do not parallel their mercury counterparts.

Four consequences of the collision of a ground state molecule or atom with a cadmium atom in the lowest lying excited singlet state, $Cd(5^1P_1)$,‡ or the first excited triplet manifold, $Cd(5^3P_{2,1,0})$, can be distinguished. Collision can result in:

---

‡ For brevity $Cd(5^1P_1)$ will be denoted by $Cd(^1P_1)$ or $^1P_1$, $Cd(5^3P_2)$ by $Cd(^3P_2)$ or $^3P_2$ and so on. $Cd(^3P_J)$ will denote any, or more than one, of the triplet manifold levels.

(i) An elastic collision, giving no change in the internal energy of either of the collision partners.

(ii) An inelastic collision, through which energy is lost or gained by the excited atom, leaving the quencher chemically unchanged.

(iii) A loss of energy from the excited atom causing chemical change in the quencher. These *photosensitised reactions* (i.e., those occurring in a species other than that absorbing the radiation, by the collisional transfer of energy from the sensitiser to the acceptor molecule) are of interest to those studying collision dynamics and also to synthetic chemists. Sensitisation makes possible the energization of molecules that are transparent in spectral regions convenient for excitation. It may also happen that quantum yields are greater for sensitised systems than for direct photolysis, or indeed the products may be entirely different.

(iv) A new, excited molecule being formed which subsequently decays radiatively to an unbound ground state and dissociates. Two types of excited molecule can be identified. Those made up of chemically identical partners - *excimers* (excited-dimers), and those composed of chemically different species - *exciplexes* (excited-complexes). It is the study of the formation of excimers and exciplexes in irradiated mixtures of cadmium vapour and ammonia with which this thesis is concerned.

In the review that follows, a brief summary of the present knowledge of cadmium vapour systems exhibiting cases (i) - (iii) is given, followed by a more detailed discussion of cadmium systems in which excimer and exciplex formation has been observed.

I ENERGY TRANSFER PROCESSES AND PHOTOSENSITISED REACTIONS IN CADMIUM SYSTEMS

(1) The Equilibrium between the $^3P_1$ and $^3P_0$ Levels.

Although electronically similar to those of mercury, cadmium's excited states are spaced at different energy intervals. One of the energy spacings important to the investigation of the lowest triplet manifold of the element is that between the $^3P_1$ and $^3P_0$ levels (and possibly also that between the $^3P_1$ and $^3P_2$ levels). At the elevated temperatures usually required for the study of atomic cadmium, the $^3P_1$ - $^3P_0$ spacing of 6.48 kJ $mole^{-1}$ is comparable to RT.‡ As a consequence, equilibrium between the two triplet levels is readily established by many buffer gases.

In 1930, Bender[1], while making a qualitative study of the effects of nitrogen, carbon monoxide and hydrogen on the 326.1 nm ($^3P_1$ - $^1S_0$) fluorescence from irradiated cadmium vapour, noted that nitrogen and carbon monoxide have very little effect on the fluorescence intensity and suggested that both probably deactivate the $^3P_1$ level to the metastable $^3P_0$ level. Lipson and Mitchell[2] in their paper of 1935, which reported the first quantitative measurements of the quenching effect of foreign gases on Cd($^3P_1$), also commented on the possibility that nitrogen produces $^3P_0$ atoms from the $^3P_1$ level.

These reports make mention of the deactivation, only, of the $^3P_1$ level, but subsequent papers showed the activation of the $^3P_0$ to the $^3P_1$ level. In a study of the decays of

‡ T = temperature in K,
R = Gas constant = 8.314 JK^{-1} $mole^{-1}$

$Cd(^3P_2)$, $Cd(^3P_1)$ and $Cd(^3P_0)$ in pure cadmium vapour, Penkin and Redko[3] found that $Cd(^3P_2)$ was removed only by diffusion to the walls, but that the $^3P_1$ and $^3P_0$ levels, as well as undergoing removal at the walls and radiative decay, in the case of $Cd(^3P_1)$, were interconverted by collisions with ground-state cadmium atoms.

Young, Greig and Strausz[4] showed the presence of this equilibrium in an experiment on cadmium vapour carried out at room temperature. By the flash photolysis of dimethylcadmium vapour a large concentration of cadmium atoms was created, thus allowing $Cd(^3P_1)$ atoms to be produced for study. The concentrations of atoms in the triplet levels were monitored by the absorption of the atomic lines at 361.1 nm ($5^3D_3 - 5^3P_2$), 346.6 nm ($5^3D_2 - 5^3P_1$) and 340.4 nm ($5^3D_1-5^3P_0$). Although neither a $Cd(^3P_1)$ nor a $Cd(^3P_0)$ population could be detected when carbon monoxide, carbon dioxide or nitrogen were mixed with the dimethylcadmium, faint absorptions by $Cd(^3P_1)$ and $Cd(^3P_0)$ were observed in the presence of rare gases, and intense absorption was observed when methane, iso-butane or neo-pentane were mixed with the substrate.

In a study using the metal vapour obtained at high temperatures, Yamamoto et al.[5] found that the equilibrium is established at rare gas pressures greater than 1 Torr, and that nitrogen is a thousand times more efficient than the rare gases in establishing the equilibrium. More recently, Sato and co-workers,[6,7] using a phase-shift technique, determined the absolute quenching cross sections for the quenching and rates of interconversion of $Cd(^3P_1)$ and $Cd(^3P_0)$

in the presence of methane, nitrogen, carbon monoxide, deuterium, hydrogen, carbon dioxide and nitric oxide. All except the last two quenchers showed a high efficiency for the intramultiplet mixing. They also employed a phase-shift technique to measure the effect of the rare gases on the lifetime of $Cd(^3P_1)$[8]. It was found that although the lifetime is pressure dependent at 534 K, there is scarcely any evidence of the deactivation of the $^3P_1$ level to the $^3P_0$ level at 458 K. One possible explanation presented by them involves the production of an excited complex whose formation introduces an energy barrier to the interconversion of the two levels:

$$Cd(^3P_1) + M \rightleftharpoons CdM^*$$

$$CdM^* \rightleftharpoons Cd(^3P_0) + M$$

[M = rare gas]

As Breckenridge and Broadbent[9] note, the equilibrating action of many of the gases used in earlier studies was unknown, with the result that many values reported as $Cd(^3P_1)$ quenching rate constants are, in fact, combined quenching constants for $Cd(^3P_1)$ and $Cd(^3P_0)$.

(2) Collisional Deactivation of the $Cd(^1P_1)$ State and Reactions Photosensitised by $Cd(^1P_1)$.

Collision-induced intersystem crossing by

$$Cd(^1P_1) + Q \rightarrow Cd(^3P_J) + Q \qquad (1.1)$$

is almost the only channel for the removal of the excited

singlet state for many gases, yet for nearly all quenchers process (1.1) constitutes a violation of the Wigner spin correlation rules.

As quantitative studies of reaction (1.1) have been made only recently, it is in order to first note earlier findings about the interaction of the $^1P_1$ state with added gases. [The case of hydrogen's interaction is dealt with separately in section I-3.]

Steacie and LeRoy, in the late 1930s and early 1940s, conducted experiments on the quenching of $Cd(^1P_1)$ by ethylene[10] and acetylene[11]. The major reaction observed from metal/C_2H_4 mixtures irradiated by 228.8 nm ($^1P_1$ - $^1S_0$) light was polymerization of the alkene. Of the possible primary reactions of ethylene with $Cd(^1P_1)$, the group ruled out all but

$$\left.\begin{aligned} Cd(^1P_1) + C_2H_4 &\rightarrow C_2H_3 + H + Cd \\ \text{or} &\rightarrow C_2H_3 + CdH \end{aligned}\right\} \qquad (1.2)$$

and

$$Cd(^1P_1) + C_2H_4 \rightarrow C_2H_4^* + Cd \qquad (1.3)$$

by consideration of the energy available, and the observation that acetylene is not a major reaction product. Although unable to reject either process, they concluded that free radical processes, after the initial reaction, are required to explain the products of hydrogen, acetylene and some alkenes. LeRoy and Steacie[11] examined the $Cd(^1P_1)$ sensitised reaction of acetylene in the conjunction with the $Cd(^3P_J)$ sensitised reactions. From their study of the

inhibiting effect of nitric oxide on the reactions sensitised by both excited states, they inferred that their observations were consistent with the involvement, to some extent, of a free radical mechanism. (It should be noted though, that quenching of excited cadmium by nitric oxide was assumed to be negligible.) However, a reaction pathway through an excited molecule mechanism could not be ruled out.

Whalley[12], in his paper which discussed previously obtained results of work on the $Cd(^1P_1)/C_2H_4$ system, maintained that experimental evidence was consistent with the production of a vibrationally excited ground-state ethylene molecule by $Cd(^1P_1)$ attack at the molecule's π-bonding system. He considered the excited molecule to be formed in a singlet state, but that as all excited singlet states are too energetic to be reached, the molecule is promoted to a vibrational level of the ground state, so increasing the likelihood of the C-H bond fission that must occur somewhere in the mechanism. Again, the alternative, the direct production of a radical, could not be excluded.

In the early 1970s, Breckenridge and Callear,[13,14] from flash photolysis studies of the quenching of $Cd(^1P_1)$ and $Cd(^3P_J)$ by helium, nitrogen, methane, hydrogen and deuterium, demonstrated that all these quenchers are able to produce $Cd(^3P_J)$ atoms from the $Cd(^1P_1)$ population. Young et al.[4] also found this deactivation in their dimethylcadmium study. Subsequently, Breckenridge and his collaborators published two further papers describing flash photolysis studies of the quenching of $Cd(^1P_1)$.

The first set of experiments[15] showed, through the observation of the nitric oxide $\gamma(0,x)$ bands, that $NO(A^2\Sigma^+ v = 0)$ is formed during the deactivation of $Cd(^1P_1)$ by nitric oxide to give $Cd(^1S_0)$. The over-all quenching rate of $Cd(^1P_1)$ was determined to be twice that predicted by hard-sphere collision theory; long-range interactions were postulated to explain the large value. As well as deactivation to the ground state, it was also suggested that the singlet atoms may be removed by

$$Cd(^1P_1) + NO(X^2\Pi) \rightarrow NO(X^2\Pi)^\dagger + Cd(^3P_J) \ , \qquad (1.4)$$

where the dagger indicates vibrational-rotational excitation.

In the second study[16], the quenching cross sections of $Cd(^1P_1)$ by several gases and the relative yields of triplet atoms produced from $Cd(^1P_1)$ by these quenchers were measured. Except for the rare gases, all the molecules studied showed quenching rates on the order of hard-sphere gas-kinetic rates ($\approx 1 \times 10^{-10}$ cm^3 molecule^{-1} s^{-1}), and, unlike the $Cd(^3P_J)$ quenching rates previously measured by Breckenridge and co-workers[9,18] which showed a marked variation with the quencher, little dependence of the quenching rate on the quencher was found. Production of the ^3P_J levels was noted to occur with reasonable efficiency for a number of gases and with very high efficiency for nitrogen and the alkanes. This behaviour of the alkanes is remarkable considering that exothermic chemical pathways (i.e., reaction (1.5) and the similar reaction giving CdH) are open to these molecules

for removing the singlet state.[19] It is also interesting that, despite the deactivation of $Cd(^1P_1)$ by nitric oxide to $Cd(^3P_J)$ being spin allowed, $Cd(^3P_J)$ atoms were not observed as a major product of the reaction. Cadmium hydride (CdH) was only observed to any appreciable degree in the sensitised decomposition of hydrogen, but there was evidence for some contribution from the reaction

$$Cd(^1P_1) + RH \rightarrow Cd + R + H \qquad (1.5)$$

in the quenching by hydrocarbons. Chemical reaction, with the formation of CdF, was also attributed to collisions between $Cd(^1P_1)$ and sulphur hexafluoride.

A correlation found between the quenching cross sections and the C_6 long-range forces parameter‡ implied the influence of long-range interactions giving efficient coupling between entrance and exit channels when $Cd(^1P_1)$ atoms are in collision with quenching species. For quenchers other than the alkanes, the comparison of experimental measurements and some calculations from model schemes, discussed in detail in the paper, support the concept of the mechanism for the interaction involving the crossing of a charge-transfer complex's ($Cd^+ - Q^-$) potential surface (entrance channel) with the surface of the neutral complex (Cd-Q*) that correlates with the products. For the alkanes, a charge-transfer mechanism seems unlikely because of their

---

‡ The C_6 parameter is the coefficient of the $1/r^6$ term of the intermolecular potential, where r is the internuclear separation.

highly negative electron affinities. Instead, Breckenridge and Renlund proposed the involvement of "golden-rule" coupling[‡] of Cd($^1P_1$) + RH to the product's potential surfaces, or the production of an R-Cd-H intermediate sufficiently long-lived to allow decomposition and curve crossing.

From 1978, Breckenridge's research group conducted experiments to further investigate the mechanisms which lead to the high efficiency of the intersystem crossing from the singlet state to the triplet state. To obtain this information, they developed a pump-probe laser technique that allows newly-formed excited states to be probed before collision with other gaseous species can take place. The technique has been used to determine the initial population distribution in the Cd($^3P_{2,1,0}$) levels created from Cd($^1P_1$).

Two dye laser heads are simultaneously pumped by a single nitrogen laser. The output of one head passes through a frequency doubler to provide the 228.8 nm pump photon, and the second, tuned to one of the $^3S_1$ - ^3P_J transitions, passes through an optical delay line ($\approx$ 20 ns) before entering the cell. In this way the ^3P_J levels are given insufficient time to be collisionally scrambled before they are probed.

---

‡ "Golden-rule" coupling is a scheme by which a discrete entrance channel, n, couples with a continuum (or high density) of exit channels, {m}. The transition rate (k_q) from n to {m} is given by Fermi's "golden-rule":

$$k_q = \frac{2\pi}{\hbar} |V_{mn}|^2 \rho_m$$

where ρ is the density of {m} states and V_{mn} is the operator coupling between n and {m}[20,21].

The Cd/N_2 system was the first to be examined using this technique.[22] The initial distribution of $^3P_2:^3P_1:^3P_0$ proved to be 0.68:0.27:0.05, which could not be fitted to any model distribution as all gave too little $^3P_2$ and too much $^3P_0$. The calculated distribution giving the closest approximation to the experimental values was one in which it was assumed that the surface crossings of CdN_2 molecular states correlating with $Cd(^1P_1) + N_2$, and those correlating with $Cd(^3P_J) + N_2$, are such that each product channel has the same probability of entry. The $^3P_2:^3P_1:^3P_0$ ratios can then be expected to be governed by the degeneracies of the triplet levels (i.e., 5:3:1), thereby giving ratios of 0.56:0.33:0.11. This skewed distribution, arising from the characteristics of the CdN_2^* potential surfaces crossing the $Cd^+N_2^-$ surfaces, leads to a marked preference for the production of $^3P_2$ over $^3P_0$ atoms.

The same apparatus, with a modified technique, was used in 1979[19] to remeasure the quenching cross sections of $Cd(^1P_1)$ by a number of gases and to determine the branching ratios for the production of $Cd(^3P_J)$ (the fraction of collisions with $Cd(^1P_1)$ atoms resulting in the formation of $Cd(^3P_J)$ atoms) by nitrogen, methane and propane. The cross sections measured were in reasonable agreement with those obtained from the flash photolysis experiments,[16] but they could not be reconciled with the values from the phase-shift measurements of Morten et al.[23]. The branching ratios for nitrogen, methane and propane were close to unity, implying deactivation at every hard-sphere gas-kinetic collision.

In the same year, Breckenridge et al.[24] showed that for a series of alkanes, $C_n + H_{2n+2}$, the initial distribution $^3P_2:{}^3P_2:{}^3P_0$ tends from a non-statistical to a statistical distribution (statistical on the basis that the electronic degeneracies govern the distribution) as n increases to 5, with neo-pentane as an exception. In explanation it was proposed that the nature of the $Cd(^3P_J)$-RH potential surfaces gives a greater probability of crossing to the $Cd(^3P_2)$-RH surface from the $Cd(^1P_1)$-RH surface for the simple alkanes, but with the increasing complexity of the alkane the $Cd(^3P_J)$-RH surfaces become increasingly similar, so rendering $^3P_2:{}^3P_1:{}^3P_0$ a better approximation to a statistical distribution. The different result from neo-pentane was considered to be due to the additional influence of a chemical interaction potential arising from the circumstance that all of its C-H bonds are primary, like those of the simple alkanes.

More recently, Breckenridge and Kim Malmin[25] determined the quenching cross sections, branching ratios, and initial $^3P_2:{}^3P_1:{}^3P_0$ distributions for twenty quenching molecules. In agreement with the flash photolysis results[16], all quenchers except helium, argon, and hexafluoroethane yielded cross sections equal to, or greater than, the hard-sphere value, and again a correlation with the C_6 parameter could be demonstrated. Estimates of the branching ratios showed that for nearly all species except those reacting by highly exothermic chemical channels, namely, sulphur hexafluoride, oxygen, carbon dioxide and hydrogen, $Cd(^3P_J)$ atoms are produced with unit, or close to unit, efficiency.

They found that the raw laser data gave an initial distribution of 0.62:0.30:0.08 ($^3P_2$:$^3P_1$:$^3P_0$) for nitrogen, carbon monoxide, the butanes and the butenes. However, they believed systematic errors from two sources to be present in the raw data. First, a review of theoretically and experimentally determined oscillator strengths for the three transitions to the triplet manifold, indicated that the oscillator strengths may differ by as much as 20%; use of the raw data directly assumes these strengths to be equal. Secondly, the natural isotopic abundance of cadmium leads to hyperfine splittings in the ^3P_J - $^3S_1$ lines that are greater than the Doppler line width, and these splittings are more widely spaced for the $^3P_0$ and $^3P_1$ levels than for the $^3P_2$ level. Breckenridge and Kim Malmin thought it possible that some of the more widely spaced $^3P_0$-$^3S_1$ and $^3P_1$-$^3S_1$ lines may have been interpreted as background noise, thus giving $^3P_0$ and $^3P_1$ lower populations with respect to $^3P_2$. As a rational interpretation of the data was possible if the true distribution was electronically statistical (5:3:1), they assumed these two factors skewed the raw data from the true distribution. All other results were therefore scaled by the factors required to bring the population ratios of these quenchers to an electronically statistical distribution.

It was apparent from the widely varying distributions that a number of coupling mechanisms are to be found in the systems studied. Two classes of mechanism, other than that giving a statistical distribution, were distinguished.

(i) That in which the natures of the intersecting potential surfaces correlating on one hand with $Cd(^1P_1) + Q$, and on the other with $Cd(^3P_J) + Q$, result, at a given collision energy, in the preferential crossing to a particular triplet level. This mechanism was identified with distributions favouring $^3P_2$ over $^3P_1$ and $^3P_0$. Argon, for example, gave such a distribution.

(ii) That in which a complex is formed, whose lifetime is of the order of a molecular rotation period. In such a case, a statistical population of the vibrational, rotational, and translational degrees of freedom, in addition to the electronic degrees of freedom, is expected. Approximate calculations showed that this model increasingly favours the production of the $^3P_1$ and $^3P_0$ levels with increasing molecular complexity.

(3) The Photosensitised Formation of Cadmium Hydride

In 1928, Bates and Taylor[26], from a study of the effect of ammonia, and also of a C_2H_4/H_2 mixture, on the 326.1 nm fluorescence from cadmium vapour, suggested that hydrogen in admixture with the vapour was unlikely to affect the fluorescence. Bender[1] showed this prediction to be incorrect, as his results demonstrated that hydrogen is a very effective quencher of $Cd(^3P_J)$ by the sensitised decomposition of hydrogen to give CdH and hydrogen atoms.

The quenching rate of excited cadmium by hydrogen was measured by Lipson and Mitchell[2] in the 1930s and by

Steacie and LeRoy[27] in the 1940s, but it was not until the beginning of the 1970s that interest revived in the formation of CdH. Breckenridge and Callear[13,14] reported that the CdH they observed to be formed in the presence of $Cd(^1P_1)$ was actually formed by the reaction of $Cd(^3P_J)$, formed by the deactivation of $Cd(^1P_1)$, with the hydrogen molecule. Later, Young et al.[28] determined the quenching rates of $Cd(^3P_J)$ by several gases at two temperatures, from which they calculated the Arrhenius parameters A, the pre-exponential factor, and E_a, the activation energy. They concluded from the high alkene quenching rates that $Cd(^3P_1)$, like $Hg(^3P_1)$, acts as an electrophile, and, by analogy with the behaviour of $Hg(^3P_{1,0})$, that decomposition of hydrogen occurs by insertion into the H - H bond (reaction (1.16)):

$$Cd(^3P_J) + H_2 \rightarrow HCdH^* \rightarrow H + CdH \qquad (1.6)$$

The flash photolysis study, by Breckenridge and Renlund,[16] of the quenching of $Cd(^1P_1)$ revealed that little CdH is formed by reaction with the alkanes or ammonia. However, they did find that CdH is produced in varying yields, in some cases as high as that of hydrogen, by the interaction of $Cd(^3P_J)$ and alkanes (except methane)[29].

A detailed study of the quenching of $Cd(^1P_1)$ and $Cd(^3P_J)$ by isotopic hydrogens (H_2, HD and D_2) was published by Breckenridge and Renlund[30] in 1978. They determined the total quantum yield of CdH and CdD in these systems to be about unity for the sensitisation by $Cd(^3P_J)$ atoms, but only

about half this value for sensitisation by the singlet atoms. This is, perhaps, not surprising in view of the 155 kJ $mole^{-1}$ (approx.) released in the reaction

$$Cd(^1P_1) + H_2 \rightarrow CdH + H \quad .$$

However, the phase-space calculations of Callear and McGurk[31] for the production of HgH from $Hg(^3P_{1,0})$ show that the experimental hydride yields are greater than those expected from theory, and Breckenridge and Renlund suggest, by analogy with the mercury system, that this may also be the case for cadmium. It was also found from the study, that when $Cd(^3P_J)$ atoms are quenched by HD the measured ratio of CdD:CdH is closer to two than unity; the isotope effect was scarcely detectable in the case of $Cd(^1P_1)$.

In explanation of the $Cd(^3P_J)$ results, an adiabatic pathway via CdH_2^*, requiring little activation energy (to account for the high yields), was postulated. The intermediate CdH_2^* state is likely to be bent, so favouring side-on attack by the cadmium atom, and thereby presenting an opportunity for bonding differences between Cd-D and Cd-H to become apparent. The preferred explanation of the $^1P_1$ data was the formation of a charge-transfer complex, $Cd^+H_2^-$, whose potential surface crosses that of the neutral complex leading to the products. They considered there to be little variation in the energy of the system in this scheme, therefore giving little isotopic selectivity.

The high exothermicity of the reaction producing CdH from the reaction of hydrogen and $Cd(^1P_1)$ requires the products to be created with a large amount of translational energy, even if the molecule's rotational excitation is as high as it

can tolerate without dissociating. In accord with this expectation, Breckenridge and Oba[32], using the laser technique described in section I-2, recently found the initial rotational energy distribution for the lowest vibrational level of ground-state CdH to give a good fit to a Boltzmann distribution at 5200 K.

(4) The Quenching and Photosensitised Reactions of $Cd(^3P_J)$

(a) Organic Quenchers. The greater part of the literature of excited cadmium quenching and photosensitisation has been concerned with the behaviour of $Cd(^3P_J)$. Although photosensitisation has been known since 1922[33], it was not until 1928 that Bates and Taylor[26] described the first observation of cadmium photosensitised reactions. They found that irradiated mixtures of the metal vapour, hydrogen and ethylene produced polymerization of the alkene. These workers reported only the decomposition of the alkene, but later studies indicated that isomerisation and hydrogen atom rearrangement about the molecule are the predominant reactions from $Cd(^3P_J)$ sensitisation.

Tsunashima et al.[34] found that the quantum yield of the decomposition of dideuteroethylene is three orders of magnitude smaller than that of isomerisation and suggested that a triplet ethylene molecule is formed in the primary process. Their result was confirmed by Hunziker[35] using gas chromatography for product analysis and infrared methods to determine isomer yields. These observations are in contrast with those for $Hg(^3P_1)$ sensitisation where the decomposition of ethylene is the main exit channel. Sato's group's[36] investigation of the $Cd(^3P_1)$ sensitised reactions of cis- and trans-but-2-ene showed that in this system too the major reaction pathway is isomerisation.

Studies, by Sato and his co-workers[37], and Hunziker[38], of mixtures of benzene, but-2-ene and cadmium demonstrated that isomerisation of the alkene is produced directly by collision with the $Cd(^3P_J)$ atoms and by collision with triplet benzene molecules, themselves produced by reaction with $Cd(^3P_J)$. On the groundsof the energy available from the cadmium triplet state, Hunziker identified the $^3B_{1u}$ state as the excited benzene state involved. Both studies reported estimated lifetimes for this benzene state, but the two values differed by about two orders of magnitude. To some extent this difference reflects the choice of the cross section for energy transfer from benzene to butene which is required for the lifetime calculation.

In 1967, Tsunashima and Sato[39] published a short communication describing work on the quenching rates of $Cd(^3P_1)$ by various ethylene derivatives, which used competition with the isomerisation of cis-but-2-ene as a rate indicator. The investigation was undertaken to clarify the reasons for the different behaviour of ethylene derivative reactions sensitised by excited benzene and acetone, and those sensitised by $Hg(^3P_1)$. As $Cd(^3P_1)$ is electronically similar to $Hg(^3P_1)$, but energetically similar to the organic sensitiser, it was hoped an indication could be obtained of which factor, energy or electronic configuration, influences the reaction pathway. The quenching rates were found to be relatively insensitive to the alkene's substitution, in accord with the behaviour found for mercury sensitisation. The electronic character of the sensitiser was therefore taken to be the stronger influence on the choice of the reaction pathway.

In 1980, Umemoto et al.[40] obtained the separate quenching cross sections of $Cd(^3P_1)$ and $Cd(^3P_0)$ by some unsaturated hydrocarbons and fluoroethylenes from phase-shift measurements. The

cross sections for the hydrocarbons were found to be very much larger than those of the fluorine substituted species. The group concluded that formation of a triplet state of the substrate, which is the case for the unsaturated hydrocarbons, was energetically impossible in the case of the fluoroethylenes unless the system's energy can be lowered by twisting the molecule. Complex formation during the interaction, to enable the conformational change, was therefore postulated.

Previous to these studies of the $Cd(^3P_J)$ sensitised reactions of alkenes, experiments by LeRoy and Steacie[41] on the quenching of $Cd(^3P_J)$ by alkanes and alkenes revealed that the excited atoms are quenched rapidly by alkenes but very slowly by alkanes. This was also observed by Breckenridge, Broadbent and Moore[18], who noted that the high quenching rate by the alkenes is consistent with the spin-allowed production of an alkene triplet state.

The quenching of $Cd(^3P_J)$ by some alkanes was further investigated by flash photolysis experiments published in 1979 by Breckenridge and Renlund.[29] In addition to the small quenching values obtained for the alkanes, it was found that the rates increased only slightly for alkanes containing secondary and tertiary C-H bonds. This is in contrast with the equivalent $Hg(^3P_J)$ quenching rates which show a great variation with the C-H bond strength. It was suggested that higher energy pathways, not open to $Cd(^3P_J)$ but accessible to $Hg(^3P_J)$, may account for this difference in behaviour. The slow quenching rates by the alkanes is noteworthy as the greater portion of the encounters resulting in hydrogen atom abstraction produce CdH exothermically; conversely, the quenching rate of $Cd(^3P_J)$ by hydrogen is about four orders

of magnitude faster than those of the alkanes, yet CdH production by this reaction is approximately thermoneutral.

Scheme I-1, in which a low-probability curve crossing from a loosely bound triplet complex to a singlet complex is the rate determining step, was tentatively proposed to explain the observations.

Scheme I-1. $Cd(^3P_1) + H\text{-}R \rightleftharpoons (Cd\text{-}H\text{-}R)^3$

$(Cd\text{-}H\text{-}R)^3 \rightarrow Cd + HR + h\nu$

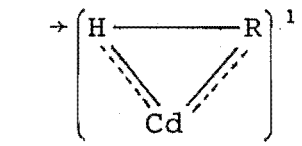

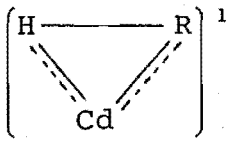

$\rightarrow CdH + R$

$\rightarrow Cd + H + R$

$\rightarrow Cd + RH^*$

Such a mechanism was not considered to make the quenching rate dependent on the C-H bond energy.

As well as the studies of alkane and alkene systems already mentioned, a number of other organic substrate systems have been investigated. The interpretation placed, by LeRoy and Steacie [11], on the results of their experiments into the inhibiting action of nitric oxide on the $Cd(^1P_1)$ and $Cd(^3P_J)$ sensitised reactions of acetylene has already been noted in relation to the reactions of $Cd(^1P_1)$. Subsequently, Sato's group[42] reinvestigated the reaction and, on the grounds of the $Cd(^3P_1)$ atom possessing insufficient

energy to break an acetylenic C-H bond, modelled their results on an excited molecule mechanism.

In the early 1970s, Kalra and Knight conducted experiments on the decomposition of a number of organic molecules sensitised by $Cd(^3P_1)$, using gas chromatography and mass spectroscopy to identify the reaction products. Work on the cyclic alkanes, cyclohexane[43] and cyclopentane[44], was reported. Both substrates were found to undergo primary processes that produce hydrogen atoms and the corresponding alkyl radicals. The over-all reaction in each case gave very similar products to the $Hg(^3P_1)$ sensitised reactions. Although this suggested that the reactions proceed by equivalent pathways, the authors noted that at the experimental temperature of 628 K secondary reactions open to radicals because of the increased energy available may have masked the true mechanism.

Some examinations of systems where cadmium sensitised cleavage of a C-C bond occurs have been made. Sato and co-workers reported work on acetone[45], cyclopentanone[46], and acetaldehyde, propionaldehyde and n-butyraldehyde[47]; Kalra and Knight[48] also studied acetone. The studies reported in references 46 and 48 were comparative examinations of the direct and sensitised decompositions of the substrate aiming to obtain confirmation of the involvement of a triplet ketone state in the direct photolysis, as was believed to be the case in the sensitised reaction. The similarity found in the reaction products of both decompositions was taken as evidence for the presence of a triplet state in both

photolyses. Furthermore, the quenching efficiency of cyclopentanone was found to be much closer to the value characteristic of an alkene than that of an alkane.

The decomposition of the aldehydes to give carbon monoxide and alkanes led Yamamoto et al.[47] to conclude that $Cd(^3P_1)$ attacks the carbonyl π-bond to give an alkane and a (CO-Cd)* complex which subsequently decomposes to carbon monoxide and cadmium.

(b) Inorganic Quenchers. The earlier papers, by Lipson and Mitchell[2], and Steacie and LeRoy[27], reporting classical Stern-Volmer measurements, and the later phase-shift measurements of Morten et al.[23], of excited cadmium quenching were concerned little with the mechanisms of quenching. The series of papers by Breckenridge and his various co-workers, most of which have already been mentioned,[9,13-14,18,29,30] has, with the aid of the quenching data of other excited states, presented detailed mechanistic proposals in addition to quenching rates and quantum yields. Except for the papers describing their laser studies,[19,22,24,25] a flash photolysis technique was employed. For these experiments, the intense pulse of cadmium radiation, tens of microseconds in duration, from a multi-electrode flash lamp coaxially surrounding the reaction cell rapidly created an excited cadmium population ($^1P_1$ or $^3P_1$). The population levels of species in the reaction vessel were monitored by the absorption of radiation from a krypton-filled continuum flash lamp. The output of this lamp passed down the length

of the cell to be dispersed by a spectrometer onto a sodium salicylate-sensitised photographic plate. A digital electronic delay unit controlled the delay between the firing of the photolytic flash and the trigger to the continuum source, thus allowing the populations to be followed from 1 μs to 1 s after the pump flash.

Several of these flash photolysis papers contain results from studies of the quenching of $Cd(^3P_J)$ atoms by various inorganic gases.[9,13,14,18] The results of reference 18 show a quenching efficiency pattern for $Cd(^3P_J)$ which is roughly similar to that for $Hg(^3P_1)$ and/or $Hg(^3P_0)$. Very efficient quenching was observed from sulphur dioxide, nitric oxide, carbon dioxide and the isotopic hydrogens; carbon monoxide and sulphur hexafluoride are moderately efficient; ammonia, nitrogen and the rare gases are inefficient. (Quenching constants, from the literature, for the $Cd(^3P_J)/NH_3$ interaction are given in Table I-1.) The consequence of collision between the excited metal atoms and quenchers varies with the gas: quenching by sulphur dioxide and carbon dioxide was attributed to the involvement of a triplet molecular state; vibrationally excited carbon monoxide was considered to be produced from metal/CO collisions; sulphur hexafluoride reacts chemically; ammonia gives complex formation. The high quenching efficiency of nitric oxide gave some insight into the mechanism of $Hg(^3P_1)$ quenching. It was postulated, before this paper by Breckenridge's group, that $NO(a^4\Pi_i)$ is formed from the quenching of triplet mercury. However, as the cadmium and mercury quenching rates are similar for

Table I-1. Rate constants for the quenching of $Cd(^3P_J)$ by ammonia

k_q/ cm^3 $molecule^{-1}$ s^{-1}	Temperature/K	Reference
1.3×10^{-12}	483	2
1.2×10^{-12}	553	18
1.3×10^{-12}	528	23
1.5×10^{-12}	513	27

nitric oxide, yet production of $NO(a^4\Pi_i)$ from $Cd(^3P_J)$ is not energetically feasible, the formation of $NO(a^4\Pi_i)$ seems unnecessary to explain the quenching of $Hg(^3P_J)$.

The quenching rates for these gases were given as a combined quenching rate of $Cd(^3P_1)$ and $Cd(^3P_0)$ by Breckenridge's group. The individual quenching rates of $Cd(^3P_1)$ and $Cd(^3P_0)$ by a number of gases were reported by Sato and co-workers[6,7]. These phase-shift measurements combined agreed with the flash photolysis results, within the combined experimental uncertainties, for deuterium, carbon monoxide and carbon dioxide.

Although energy transfer from mercury to cadmium has been studied many times, the only studies of energy transfer from cadmium to another metal seem to have been of Cd/Cs mixtures[49,50]. Kartasheva and Kraulinya[50] were interested in the rôle played by $Cd(^3P_0)$ in the sensitisation of the many caesium atomic lines observed in fluorescence from these mixtures irradiated by 326.1 nm light. By the addition of nitrogen to the metal mixture they were able to show that the energy-transfer cross sections of $Cd(^3P_0)$ and $Cd(^3P_1)$ are comparable, and that both levels participate in the sensitisation.

II CADMIUM SYSTEMS FORMING EXCIMERS AND EXCIPLEXES

Lasers are being looked to as a means of producing ultrahigh temperature plasmas for fusion reactors. These lasers will need to be high power, high efficiency systems.

Excimers and exciplexes hold the promise of providing the basis for these lasers because of their intrinsic population inversion (a higher population in the upper state of the transition than the lower) which is a consequence of the unbound nature of the ground-state complex. Already the high peak power outputs of rare gas halide lasers have demonstrated the possibilities of excimer/exciplex systems. This application of the formation of excimers and exciplexes in pure metal vapours, metal vapour mixtures and metal/gas mixtures has provided a stimulus for a revival of interest in their study.

The following review and discussion are arbitrarily divided into those papers dealing with: (1) excimer formation in cadmium vapour; (2) exciplex formation in Cd/metal vapour mixtures; and (3) exciplex formation in cadmium vapour/gas systems.

(1) Excimer Formation in Cadmium Vapour

Fluorescence bands from cadmium vapour, and the emission of cadmium lines and bands from the vapour irradiated by a variety of line sources, were observed by Kapuscinski in 1925[51,52]. A broad blue-green band (500 - 395 nm, λ_{max} = 463 nm) was emitted from the vapour, together with some atomic lines. The $^3S_1-^3P_J$ fluorescence triplet, seen at low cell temperatures and low metal pressures, decreased in intensity as the band intensity grew with increasing metal pressure leading Kapuscinski to speculate on there being a connection between the two observations.

The band observed by Kapuscinski was subsequently attributed to a Cd_2^* molecule, and in the years up until the 1940s the absorption and fluorescence spectra of cadmium vapour were obtained and discussed by a number of researchers (e.g. references 53-56). Prior to the Second World War many European investigators published reports of cadmium vapour experiments in German and Polish journals; these are summarized by Pringsheim.[57]

A qualitative Cd_2^* fluorescence spectrum is given in Fig I-1. With increasing metal pressure the atomic lines at 228.8 nm and 326.1 nm broaden into bands, and the band between 500 nm and 400 nm develops, as do other band systems, some showing "flutings" i.e., vibrational structure, at wavelengths intermediate to these three bands. Winans[53] ascribed the bands in the spectral region around the 228.8 nm band to a radiative transition from a relatively well bound excited state to a very weakly bound ground state. The qualitative potential curves he presented showed the Cd_2 ground state as having a very shallow potential well (as did Cram's[54]), for which he estimated a depth of 0.2eV.‡ He assigned the 228.8 nm band, which appears in absorption and fluorescence, and a 221.2 nm band, only observed in absorption, to transitions between the molecular ground state and an excited molecular state correlating with an atom in the $^1P_1$ state and one in the ground state. The 211.4 nm (fluorescence and absorption) arises, he held, from transitions to and from a

---

‡ 1eV = 96.49 kJ $mole^{-1}$

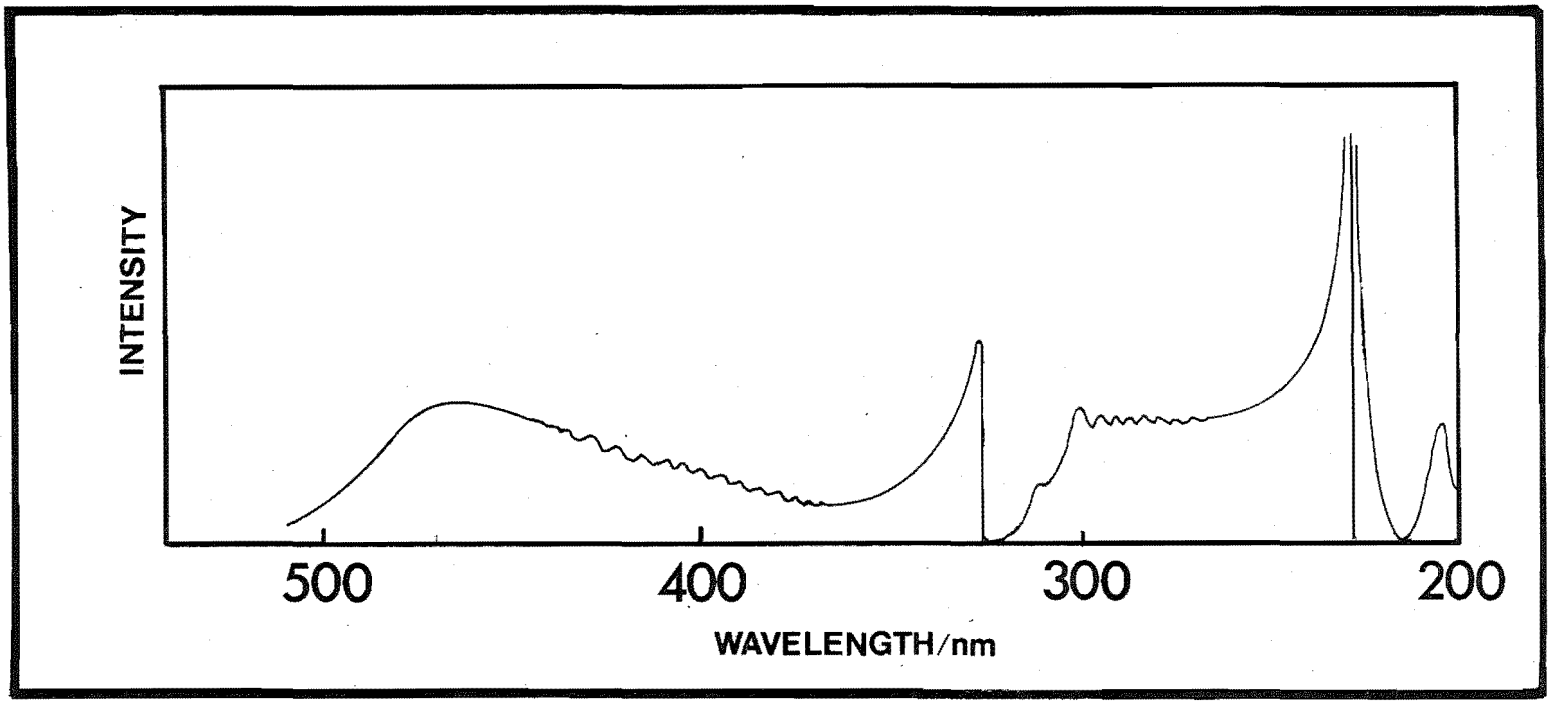

Fig. I-1. A QUALITATIVE CADMIUM EXCIMER FLUORESCENCE SPECTRUM.

This spectrum is based on the spectrum given by Pringsheim from the data of Mrozowski (see reference 57).

Cram gives a summary of the fluorescence bands obtained under differing excitation conditions (reference 54).

molecular state correlating with either the 6^1S or 5^1D atomic states. He attributed the structure observed in some of the bands to the vibrational levels of the excited state.

Two years later, Hamada[55] identified the band extending around the 326.1 nm line with an excited state correlating with the $^3P_1$ atomic level and the broad visible band (seen in fluorescence only) with a Cd_2^* molecule correlating with the $^3P_0$ atomic level. A band spreading from 290 - 308 nm, he suggested, may originate from Cd_3^*. He seems to have believed some form of the ground-state Cd_2 molecule to exist, as he assigned the fine structure he observed in some of the emission bands to transitions from such a molecule's vibrational levels.

By 1949, when Pringsheim published his book[57], the origins of almost all of the cadmium band systems could be qualitatively explained, largely as a result of the work conducted on the mercury bands. The potential curve of ground-state Cd_2 was represented as having virtually no minimum, making vibrational quantization in the state impossible. Although this state is unbound, absorption from it may still be observed at high atom densities as two atoms in collision along the potential curve can absorb a photon to undergo a vertical transition to higher molecular states[57]. Transitions to repulsive upper states will produce absorption bands but no corresponding fluorescence band. Conversely, the absence of an absorption band equivalent to an observed fluorescence band, such as the 500 - 400 nm band, is accounted for by the fluorescence transition terminating on the steeply repulsive wall of the lower potential curve (see Fig.I-2). In these

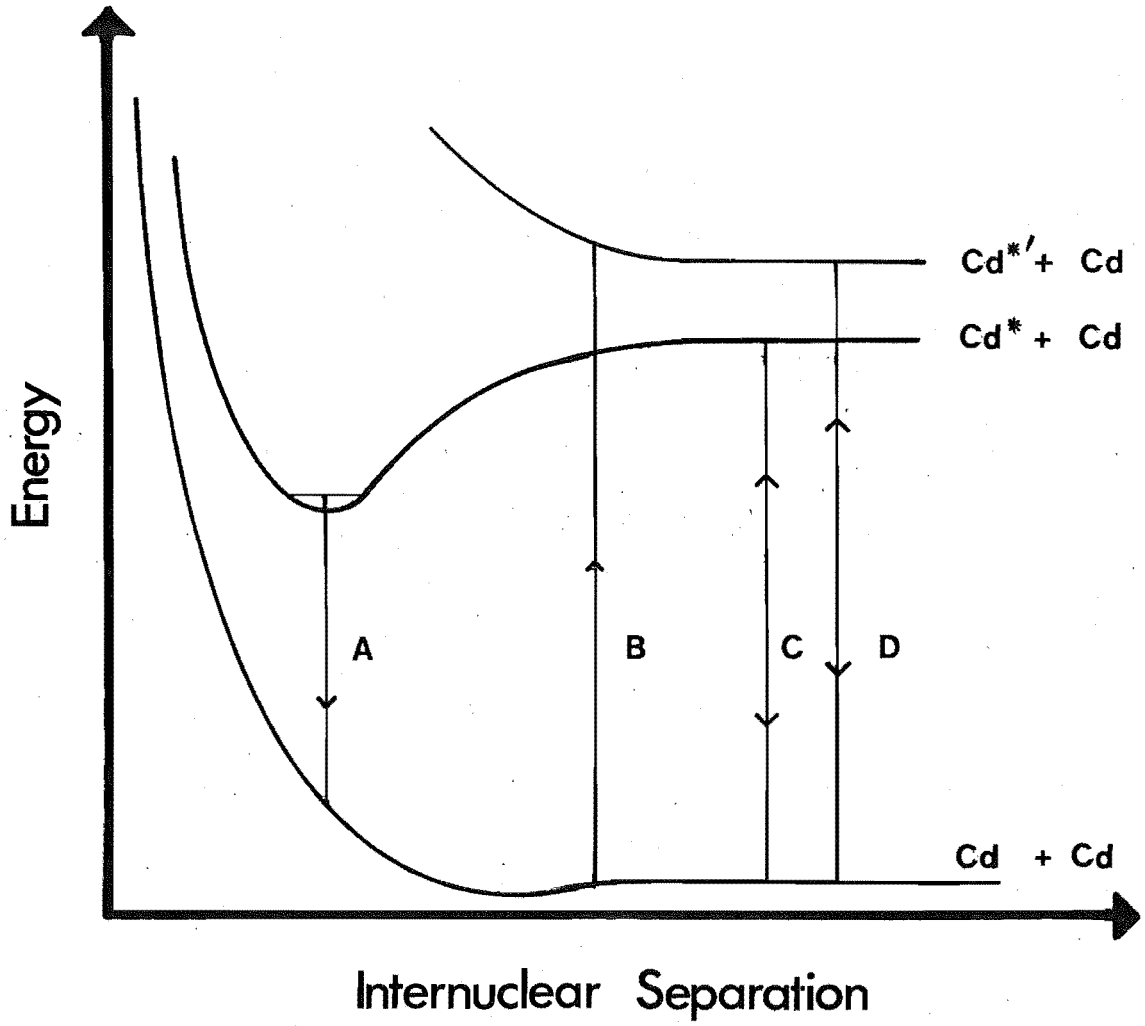

Fig. I-2. GENERALIZED POTENTIAL CURVES FOR DIATOMIC CADMIUM STATES.

Cd* and Cd*' represent two atomic states of cadmium that interact with ground-state cadmium atoms to give a bound and a repulsive excited state respectively.

A band centred around transition A will be seen in fluorescence only, and one about B in absorption only (see text). Transitions C and D, seen in fluorescence and absorption, correspond to atomic lines.

cases, unless the experiment is conducted at high vapour pressure and temperature this region of the lower curve is inaccessible to atoms in collision.

As will be discussed in section II-2, the CdHg* exciplex has received attention because of its possible use as a species for energy storage in laser systems. The modelling of the kinetic behaviour of CdHg* requires rate data for the processes involved in the removal and production of Cd_2^*. This need led to a brief report by Drullinger and Stock[58], which described the only recent kinetic study of any of the cadmium bands. Pringsheim[57] records that Kapuscinski in 1931 studied the kinetics of the afterglow of this visible band. The work revealed that the band possesses a growth period of about 10^{-5} s and decays to half its maximum in 10^{-4} s.

The profile of the visible cadmium band, which Drullinger and Stock determined to have a maximum intensity at about 470 nm, was characterized as a function of temperature and pressure by continuous-wave excitation at 325 nm (He-Cd laser) into the pressure-broadened wings of the 326.1 nm line. No pressure dependence was found in the band profile, but with increasing temperature the band broadens with a shift of intensity into the short wavelength wing of the band. Shallow undulations between 390 nm and 420 nm were observed, and a shoulder at 450 nm was apparent. At the lowest temperatures and highest pressures a very weak emission extending to the red beyond 650 nm was also recorded. As the intensity of this band relative to that of the Cd_2^* band

was found to increase linearly with cadmium pressure, it was attributed to a trimer formed from the dimer. A similar band was observed in fluorescence from a low temperature matrix by Vreede et al.[59].

From a long lifetime of about 700 μs, measured at the lowest pressures and temperatures, the excimer's lifetime fell away rapidly when both experimental parameters were increased. An Arrhenius plot of the decay data gave a slope of about 1 eV, but no interpretation of this datum was offered.

McGeoch[60] returned to these radiative rate measurements to help in his modelling of the CdHg* system. He proposed that two Cd_2^* states are involved in the mechanism, and that the energy measured by Drullinger and Stock from their Arrhenius plot was the activation energy required to produce $Cd(^3P_1)$ atoms from the metastable $Cd_2(^3\Pi_g)$ state (see Fig. I-3). As Fig. I-3 illustrates, the collision of a $Cd(^3P_1)$ atom (produced by thermal excitation of the metastable excimer) with ground-state cadmium can form a $Cd_2(^3\Sigma_u^+)$ molecule which radiates the 470 nm band. The potential curves from which McGeoch worked were those for Zn_2 calculated by Hay et al.[61]; more recently, Bender et al.[62] have produced theoretical curves for Zn_2 and Cd_2.

(2) Exciplex Formation in Cadmium/Metal Vapour Mixtures.

The existence of CdHg* molecules formed in Cd/Hg mixtures was first suggested by Winans in 1929[63] as the explanation for the presence of absorption-band structure

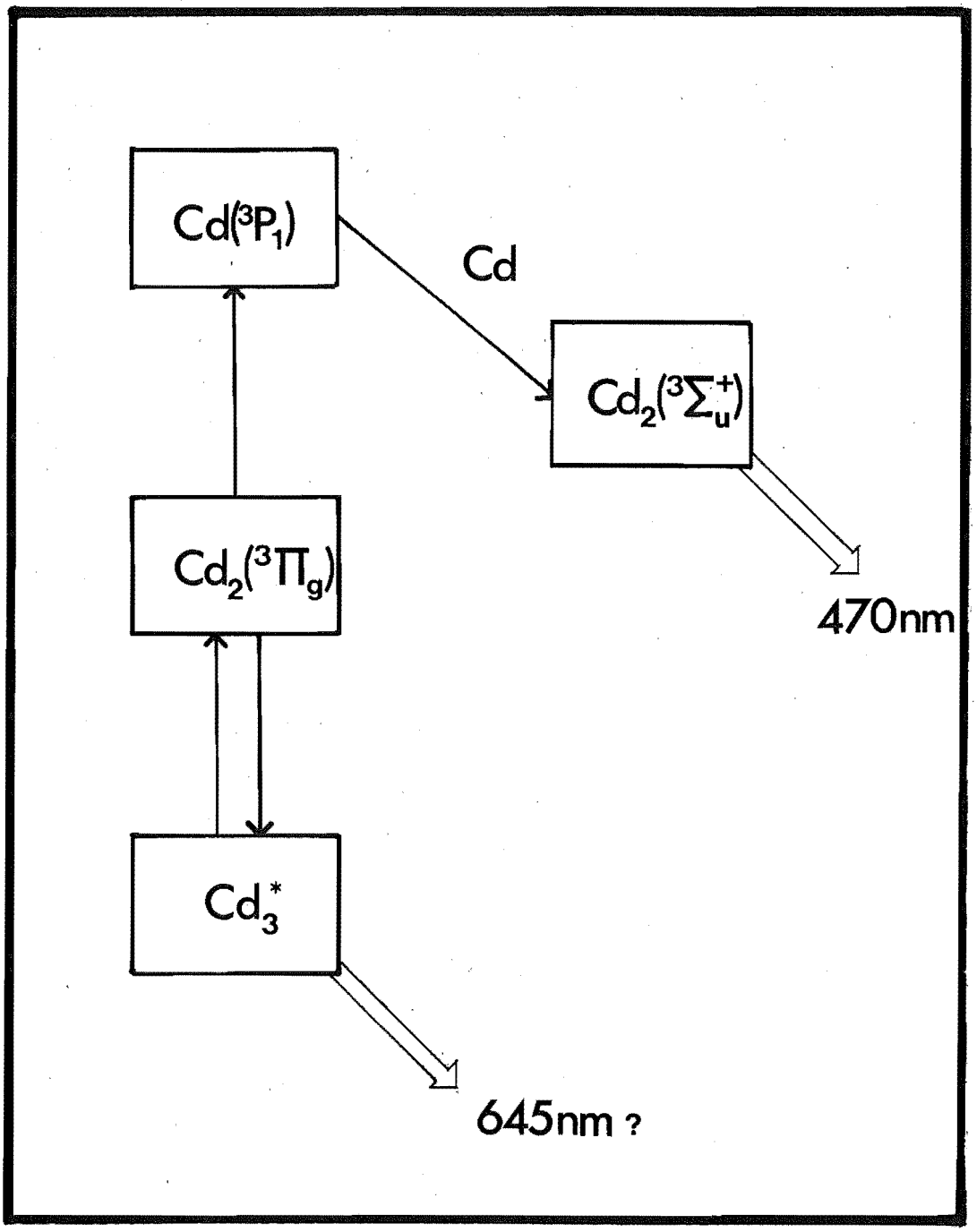

Fig. I-3. McGEOCH'S SCHEME IN EXPLANATION OF THE KINETIC BEHAVIOUR OF THE 470NM CADMIUM EXCIMER BAND.

The band wavelength of Cd_3* is that found by Vreede et al. from their matrix isolation study (reference 59).

that did not originate from Hg_2 or Cd_2. Pringsheim[57] briefly mentions a fluorescence band from Cd/Zn mixtures, not attributable to Cd_2^* or Zn_2^*, observed by Spiewankiewicz in 1932, but since this, it seems the interest in molecular species formed in irradiated Cd/metal mixtures languished until CdHg* was seen as a possible source of laser action.

From 1976, a series of papers by McGeoch and co-workers, heavily orientated towards laser applications, reported a continuing study of exciplexes produced in Cd/Hg mixtures. It was proposed that the CdHg* formation, which occurs at a quantum efficiency of 0.67[64], is by the three-body process,

$$Cd(^3P_J) + Hg + \begin{Bmatrix} Hg \\ Cd \end{Bmatrix} \rightarrow CdHg^* + \begin{Bmatrix} Hg \\ Cd \end{Bmatrix} .$$

An excess of mercury was maintained for these studies to ensure the unwanted process

$$Cd(^3P_J) + Cd + \begin{Bmatrix} Hg \\ Cd \end{Bmatrix} \rightarrow Cd_2^* + \begin{Bmatrix} Hg \\ Cd \end{Bmatrix}$$

was negligible. McGeoch et al.[65] identified two CdHg* species in the vapour mixture by the decay characteristics of the band emission at different temperatures and metal densities. These two states were labelled CdHg(a), having a lifetime of 4.0 μs, and CdHg(b), taken to be collisionally produced from CdHg(a) and possessing a lifetime of 2.8 μs.

By varying the temperature and pressure conditions they also found two emission bands: one whose long wavelength tail stretches down past 600 nm from a maximum at 470 nm, and another, which was predominant at times greater than 1 μs after the initiating pulse[64], whose maximum appears at 460 nm. The band decay characteristics suggested a significant contribution to the removal of the exciplex by the process,[65]

$$CdHg^* + CdHg^* \rightarrow \text{non-radiative products.} \qquad (1.6)$$

McGeoch and co-workers[65] originally proposed that CdHg(b) correlates with a $Cd(^3P_0)$ asymptote, but later found that the radiative transition from this state to the ground state is forbidden, obliging them to substitute $^3P_2$ as the correlating cadmium level.[64]

A few percent of gain from the CdHg* exciplex was reported by McGeoch and Fournier[66], who pumped the metal mixture with a xenon flash lamp filtered to remove wavelengths shorter than 300 nm. It was found that the observation of gain was possible only if a film of cadmium atoms was evaporated from the cell wall and converted to excited atoms, probably $Cd(^3P_1)$, during the lamp flash. Combination with mercury atoms then occurred in this dense phase through

$$Cd(^3P_1) + 2Hg \rightarrow CdHg^* + Hg.$$

In 1980, McGeoch[60] modified the mechanism for CdHg(b) formation after examining the results of Drullinger and Stock (for cadmium excimer decay) and conducting further experimentation of his own. CdHg(a) was taken to be the

emitter of the 470 nm band having a remeasured lifetime of 3.5 μs and the 460 nm band was proposed to originate from CdHg(b) ($\tau \approx 150$ ns). McGeoch was unable to distinguish between CdHg and Cd_2Hg as the identity of CdHg(b), but now held that the molecule's percursor was $Cd_2(^3\Pi_g)$, formed through

$$CdHg(a) + Cd \rightarrow Cd_2(^3\Pi_g) + Hg.$$

Furthermore, through the new scheme there was no evidence for the exciplex-exciplex destruction process (process (1.6)) proposed previously. The paper concluded that CdHg(b)'s potential as a lasing system was reduced because of its rapid radiative decay and the presence of cadmium reservoirs.

Fig. I-4 is McGeoch's model, published in 1980,[67] for the Cd/Hg system. In this work, by increasing the mercury density in the cell, he was able to produce CdHg* by excitation into the $Hg_2(1_u)$ state ($\lambda = 266$ nm). The lifetime of CdHg(a) was re-evaluated to be 2.4 μs. Cd_2Hg was introduced into Fig. I-4 as McGeoch considered its presence to be consistent with his observations that the decay rate of fluorescence from CdHg(a) decreased with increasing cadmium density and increased with temperature.

The likelihood of efficient laser action from this exciplex, too, is decreased by the presence, indicated from absorption measurements across the exciplex's band region, of an absorption intrinsic to CdHg(a). The hopes of laser action from other excimers and exciplexes have also been diminished by a number of recent papers, those concerned with Hg_3[68] and Cd_2[69], for instance.

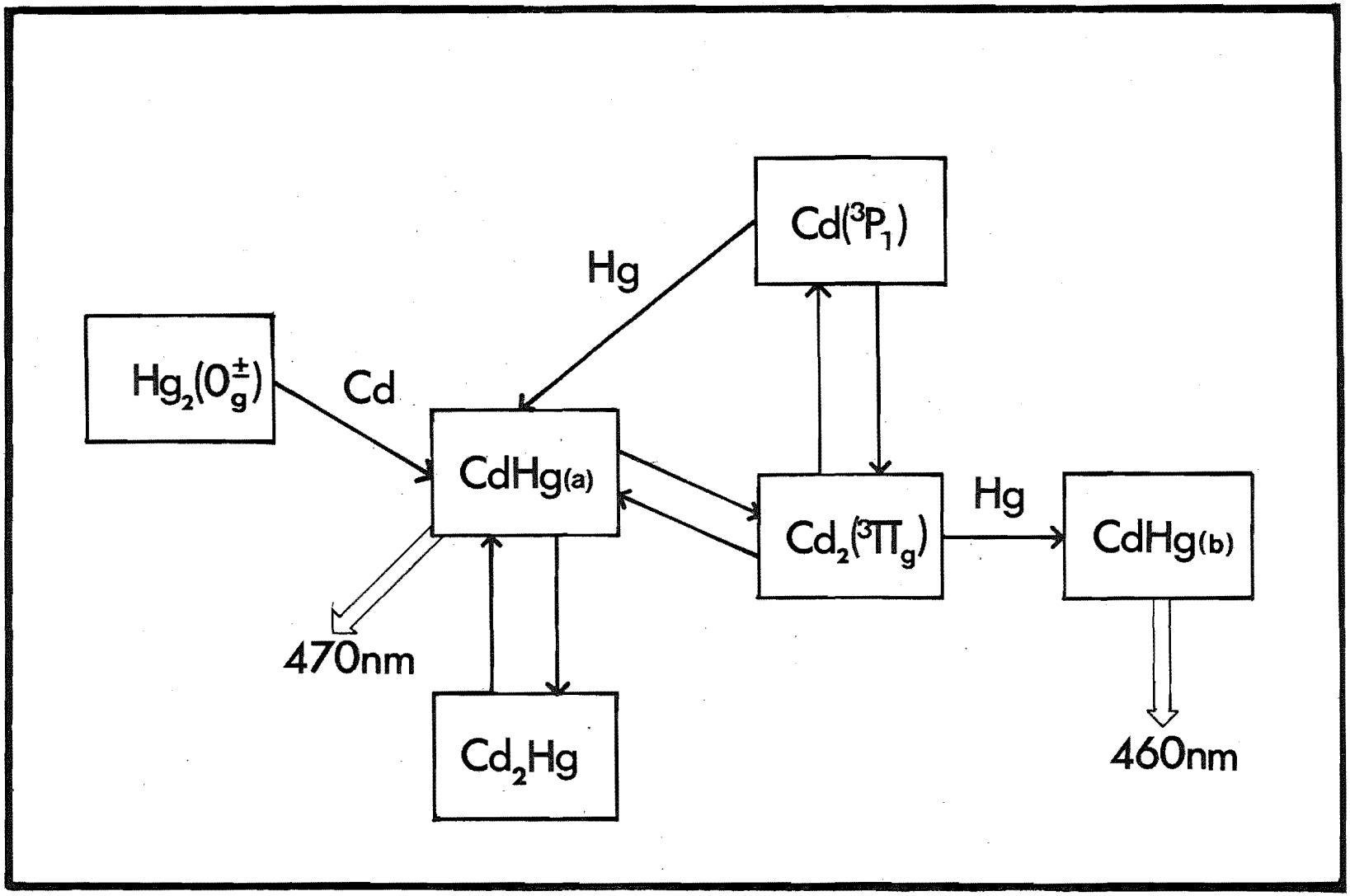

Fig. I-4. McGEOCH'S SCHEME FOR THE CdHg*/Cd_2* SYSTEM.

Not all of the cadmium excimer states are included in this diagram; see Fig. I-3 for the full Cd_2*/Cd_3* system.

(3) Exciplex Formation in Cadmium/Gas Mixtures

Exciplex formation in Hg/NH_3 and Hg/H_2O mixtures was proposed by Gaviola and Wood in 1928[70], to explain the appearance of structureless bands in these systems. Similar exciplex formation in cadmium systems was not reported until the early 1970s.

Not long after a reasonable understanding of the photokinetics of some of the mercury systems had been gained, work on the related Cd/NH_3 system was begun by Morten et al.[71]. The group made measurements of the phase shift between the 326.1 nm fluorescence and the luminescence observed from the mixture (at 560 K) when irradiated by the cadmium intercombination line. A diffuse, structureless band centred at about 430 nm was observed from these mixtures and was attributed to the radiative dissociation of a $CdNH_3^*$ exciplex, analogous to the $HgNH_3^*$ exciplex found in Hg/NH_3 mixtures.

Fig. I-5(a) shows the dependence of the phase lag measured by Phillips and co-workers on the ammonia pressure. As the general characteristics of the plot are similar to the corresponding plots of the Hg/NH_3 system, the mechanism used to describe the system's kinetics (Scheme I-2) was modelled on the Hg/NH_3 system's scheme.

Derivation of the equation describing the dependence of the measured shift on the ammonia pressure demonstrated that the total shift (ϕ) consists of two components. By analogy with the Hg/NH_3 system the first component was assumed to be related to the rate of removal of the $Cd(^3P_0)$

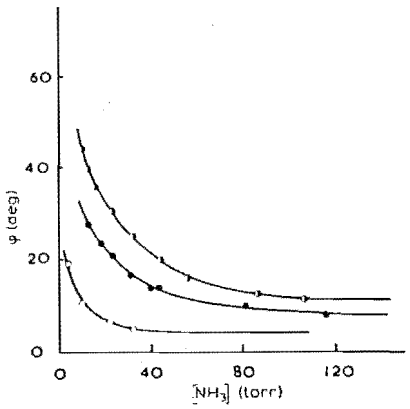

Variation with NH_3 pressure of the phase shift φ between the 326.1 nm and 430 nm emissions. Open circles, f = 10.0 kHz; filled circles, f = 25.5 kHz; half-filled circles, f = 40.0 kHz.

(a) reference 71

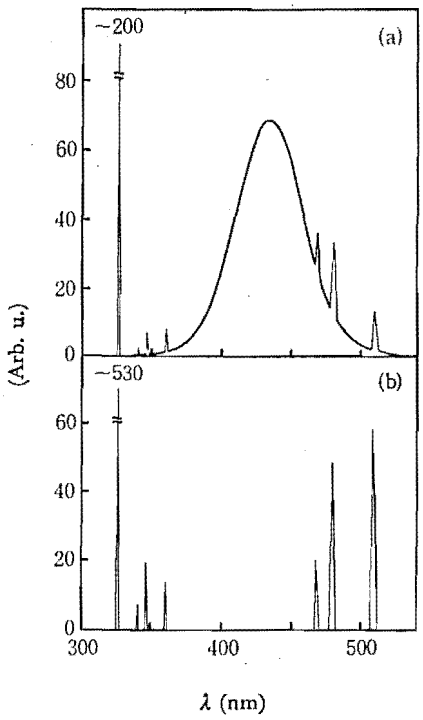

Observed emission intensity distributions in the presence of 31 Torr of NH_3 (a) and in the absence of NH_3 (b); entrance slit is 0.04 mm and the spectra are not corrected for the sensitivity of the photomultiplier.

(b) reference 73

(c) reference 73

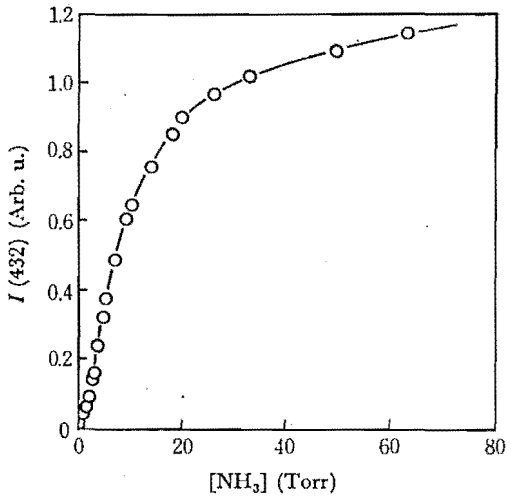

The emission intensity at 432 nm as a function of NH_3 pressure.

Figs. I-5(a),(b) and (c). REPRODUCTIONS OF RELEVANT FIGURES FROM PREVIOUSLY PUBLISHED WORK.

The references from which the figures in Fig. I-5 are taken are given with each diagram.

Scheme I-2

$$Cd + h\nu \rightarrow Cd_1$$

$$Cd_1 \rightarrow Cd + h\nu$$

$$A + Cd_1 \rightarrow Cd_0 + A$$

$$A + Cd_1 \rightarrow Cd + A$$

$$A + Cd_0 \rightarrow CdA^* \qquad (1.7)$$

$$2A + Cd_0 \rightarrow CdA^* + A \qquad (1.8)$$

$$CdA^* \rightarrow Cd + A + h\nu'$$

$[Cd_1 \equiv Cd^3P_1,\ Cd_0 \equiv Cd^3P_0,\ CdA^* \equiv CdNH_3^*,\ A \equiv NH_3]$

level, and the second, the limiting shift at high pressures (ϕ_∞), to the complex's radiative lifetime. From the high pressure shifts the group calculated a value of $(4.9 \pm 0.2) \times 10^{-7}$ s for the complex's lifetime, and through the relationship

$$2\Pi f/[A]\tan(\phi - \phi_\infty) = k_7 + k_8[A] \ ,$$

where f is the modulation frequency and k_j is the rate constant of process (I-j), k_7 was found to be $(1.7 \pm 0.3) \times 10^{-12}$ cm^3 molecule^{-1} s^{-1}. Their data were insufficiently precise to allow evaluation of k_8.

The apparent inability of ammonia to quench the luminescence was explained by the possible formation of higher complexes, such as $Cd(NH_3)_2^*$ (similar to those that had been found in Hg/NH_3 mixtures[72]), that emit at approximately the same wavelength as $CdNH_3^*$.

Further inquiries into the mechanism operating in the Cd/NH_3 system and other cadmium exciplex forming mixtures, were made by Sato and his co-workers,[73-77] and by Yamamato

et al.[78]. Their first $CdNH_3^*$ study, carried out at 523 K, employed a steady-illumination technique[73]. They were led to the acceptance of $CdNH_3^*$ as the emitter of the 430 nm band (Fig. I-5(b)) after the other candidates under consideration, NH, NH_2 and CdH, were ruled out through either energetic considerations, or the incompatibility of the mechanism necessary for their production with the experimental observations. This work also showed that a very weak band at 420 nm could be observed from Cd/CH_4 mixtures.

The behaviour of the intensity of the 430 nm band as a function of the ammonia pressure is illustrated in Fig. I-5(c). To explain the form of this ammonia dependence, they proposed the following mechanism:

Scheme I-3.

$$Cd + h\nu \rightarrow Cd_1$$

$$Cd_1 \rightarrow Cd + h\nu \qquad (1.9)$$

$$A + Cd_1 \rightarrow CdA^\dagger \qquad (1.10)$$

$$\rightarrow \text{other reactions} \qquad (1.11)$$

$$A + CdA^\dagger \rightarrow CdA^* + A \qquad (1.12)$$

$$CdA^\dagger \rightarrow Cd + A \qquad (1.13)$$

$$CdA^* \rightarrow Cd + A + h\nu' \qquad (1.14)$$

$$A + CdA^* \rightarrow Cd + 2A \qquad (1.15)$$

[$CdA^\dagger \equiv CdNH_3^\dagger$, an unstabilised complex]

Should $Cd(^3P_0)$ be the complex precursor, reaction (1.10) was to be replaced by

$$A + Cd_1 \rightarrow Cd_0 + A \qquad (1.16)$$

$$A + Cd_0 \rightarrow CdA^\dagger . \qquad (1.17)$$

Table I-2. Data from the Stern-Volmer Plot of Reference 73.

Quencher	Intercept	Half-Quenching Pressure Torr	Quenching Efficiency
‡Cis-but-2-ene			1
‡H_2			0.8
CO_2	0.55 ± 0.27	0.060 ± 0.030	0.16
CO	0.84 ± 0.22	0.34 ± 0.09	0.03
NH_3	0.85 ± 0.03	29.8 ± 1.4	3.3×10^{-4}
N_2	0.96 ± 0.01	220 ± 3	4.9×10^{-5}

‡From other references (see reference 73), to obtain relative efficiencies for CO_2, CO, NH_3 and N_2.

The information obtained from a Stern-Volmer plot of the quenching of the 326.1 nm fluorescence is given in Table I-2. Although this Stern-Volmer plot was linear, as can be seen from Table I-2 all the intercepts were found to be less than unity. Newman et al.[79] had also found that their Stern-Volmer plots did not possess intercepts of unity and attributed this to the effect of Lorentz broadening, but a calculation by the Japanese group led them to believe that the magnitude of the broadening effect was insufficient to account for the observations in their case. Instead, they ascribed the deviations from Stern-Volmer behaviour to the faster rate of diffusion of cadmium vapour to the cooler parts of the cell at low ammonia pressures, with a resulting drop in the metal's vapour pressure.

A steady-state treatment of Scheme I-3 yielded:

$$1/I = \frac{[1+k_9/(k_{10}+k_{11})[A]][1+k_{13}/k_{12}[A]][1+k_{15}[A]/k_{14}]}{\alpha I_a} \qquad (1.18)$$

where I = total emission intensity from the stabilised complex

α = the fraction of the total quenching of $Cd(^3P_1)$ going by way of reaction (1.10) or (1.16)

I_a = rate of light absorption

To simplify this expression and so obtain the rate constant ratios, two pressure régimes were considered. At high pressures $(1 + k_{13}/k_{12}[A])$ is rendered approximately equal to one, so reducing (1.18) to

$$1/I_{432}(1+k_9/(k_{10}+k_{11})[A]) = (1+k_{15}[A]/k_{14})/\gamma\alpha I_a, \quad (1.19)$$

where I_{432} is the intensity at 432 nm (λ_{max} found by this group), and $I_{432} = \gamma I$, where γ is a proportionality constant.

At low pressures the second approximation, that $(1 + k_{15}[A]/k_{14})$ is approximately equal to one, is valid, allowing (1.18) to be simplified to

$$1/I_{432}(1+k_9/(k_{10}+k_{11})[A]) = (1+k_{13}/k_{12}[A])/\gamma\alpha I_a. \quad (1.20)$$

By assuming $k_9/(k_{10}+k_{11})$ to be equal to the half-quenching pressure given in Table I-2, the left-hand sides of equations (1.19) and (1.20) were evaluated and plotted against the appropriate function of the ammonia concentration. The resulting straight lines yielded $k_{15}/k_{14} = (1.2\pm0.2) \times 10^{-2}$ Torr^{-1} and $k_{13}/k_{12} = (2.8 \pm 0.2)$ Torr.

From this data and the estimation that $k_{12} = k_{15} \approx 1.4 \times 10^{11}$ ℓ mole^{-1} s^{-1} ‡ (the equivalent of a cross section of a 9 Å^2 calculated from atomic radii and bond lengths), lifetimes for the unstabilised and stabilised complexes were determined to be 8.2×10^{-8} s and 2.9×10^{-9} s respectively. The group offered two suggestions to account for the anomalous result of having the unstabilised complex longer lived than the stabilised complex.

The first explanation proposed that through the need for spin conservation the unstabilised complex is produced in a triplet state, while the calculated lifetime of the stabilised complex suggested that it is a singlet species.

---

‡ 1 ℓ mole^{-1} s^{-1} = 1.66×10^{-21} cm^{-3} molecule^{-1} s^{-1}

This, they maintained, accounted for the irregularity, as generally, excited singlet states are shorter lived than excited triplet states.

The other proposal required a modification to the mode by which the stabilised complex was removed, namely,

$$A + CdA^* \rightarrow CdA_2^* \qquad (1.21)$$

$$\rightarrow Cd + 2A \qquad [1.15]$$

$$CdA_2^* \rightarrow CdA^* + A \quad .$$

If this is to be the case, it was reasoned that k_{15} would be smaller than k_{12}, and consequently with the reduction in k_{15} the stabilised complex lifetime would be increased. If k_{21}/k_{15} is greater than thirty the stabilised complex's lifetime would be greater than that of the unstabilised complex.

In this study some consideration was also given to the photosensitised decomposition of ammonia, because of the finding that the intensities of both the 326.1 nm fluorescence and the 430 nm luminescence diminished with irradiation time (both were reduced to about 37% of their initial intensity after 14 minutes, in about 64 Torr of ammonia.)

Scheme I-4.

$$Cd + h\nu \rightarrow Cd_1$$

$$Cd_1 \rightarrow Cd + h\nu$$

$$NH_3 + Cd_1 \rightarrow CdH + NH_2 \qquad (1.22)$$

$$CdH \rightarrow Cd + H$$

$$H + NH_3 \rightarrow H_2 + NH_2$$

$$2NH_2 \rightarrow NH + NH_3$$

$$2NH \rightarrow H_2 + N_2$$

Scheme I-4 sets out the way in which the photosensitised decomposition products were believed to form. Reaction (1.22) was estimated to contribute only 2% of the triplet quenching, but the high efficiency of

$$H_2 + Cd_1 \rightarrow CdH + H$$

was thought to explain the way in which the increasing quantum yield of hydrogen and nitrogen with time paralleled the decreasing emission intensities.

This group's second study of the Cd/NH_3 system[74] (at 493 K) used the same steady-illumination method. However, work they had done on the rôle of the $Cd(^3P_0)$ level in the quenching of the 326.1 nm fluorescence by nitrogen, carbon monoxide and carbon dioxide[5] had indicated that Lorentz broadening probably was responsible for the low intercepts they had obtained in the Stern-Volmer plots of their 1973 paper. Accordingly, all mixtures in this second study were made up to a constant total pressure with argon to ensure the degree of absorption of the 326.1 nm radiation was independent of the ammonia pressure.

As Fig. I-5(d) shows, the Stern-Volmer plot for the quenching of the 326.1 nm fluorescence in this investigation gave the expected intercept of unity, but curvature of the plot, especially at lower pressures (Fig. I-5(f)), was also found. To accommodate this observation the mechanism proposed in the previous work was modified to that given in Scheme I-5.

Scheme I-5.

$$Cd + h\nu \rightarrow Cd$$

$$Cd \rightarrow Cd + h\nu$$

$$M + Cd_1 \rightarrow Cd_0 + M$$

$$M + Cd_0 \rightarrow Cd_1 + M$$

$$A + Cd_1 \rightarrow \text{Products} \qquad (1.23)$$

$$A + Cd_0 \rightarrow \text{Products} \qquad (1.24)$$

$$A + Cd^* \rightarrow CdA^\dagger \qquad (1.25)$$

$$CdA^\dagger \rightarrow Cd^* + A \qquad (1.26)$$

$$A + CdA^\dagger \rightarrow CdA^* + A \qquad [1.12]$$

$$Ar + CdA^\dagger \rightarrow CdA^* + Ar \qquad (1.27)$$

$$CdA^* \rightarrow Cd + A + h\nu' \qquad [1.14]$$

$$A + CdA^* \rightarrow Cd + 2A \qquad [1.15]$$

$$Ar + CdA^* \rightarrow Cd + A + Ar \qquad (1.28)$$

[$Cd^* \equiv Cd(^3P_1)$ or $Cd(^3P_0)$, M is a second body, either Ar or A]

It was assumed that the unstabilised complex does not fluoresce, as the luminescence profile did not alter with a change in the ammonia or argon pressure. The band intensity as a function of ammonia pressure, at various total pressures, is shown in Fig. I-5(e). The form of the plot is similar to that found earlier.

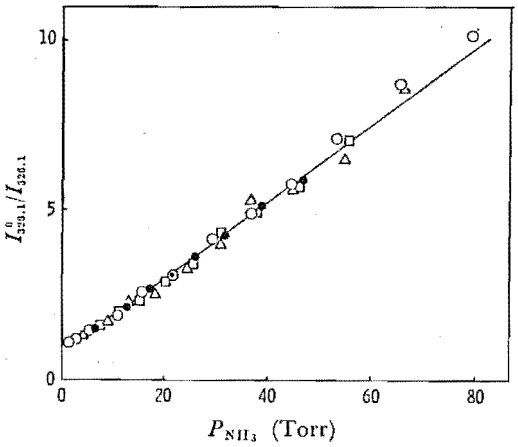

Stern-Volmer plots for the quenching of the resonance radiation at 326.1 nm by ammonia diluted with argon. The total pressures are 208 (○), 175 (△), 147 (□), and 123 (●) in Torr. Solid line shows the values calculated according to Eq. (1).

(d) reference 74

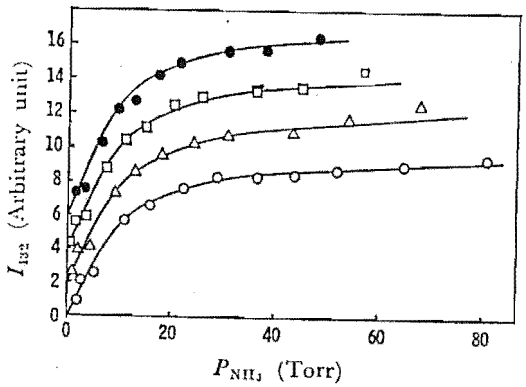

The emission intensity at 432 nm as a function of the partial pressure of ammonia. The total pressures are 208 (○), 175 (△), 147 (□), and 123 (●) in Torr. Solid lines show the values calculated according to Eq. (2). The plots are displaced upwards by 2 units of I_{432} for clarity in the above order of the total pressure.

(e) reference 74

(f) reference 74

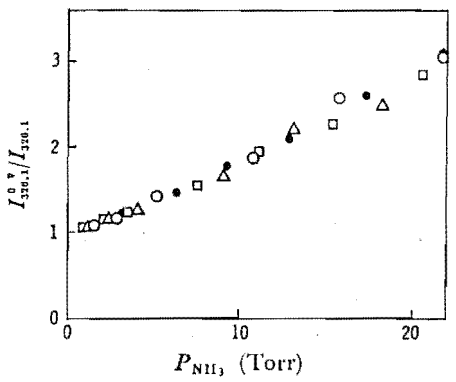

Stern-Volmer plots in the low pressure region. The total pressures are 208 (○), 175 (△), 147 (□), and 123 (●) in Torr.

Figs. I-5(d),(e) and (f). REPRODUCTIONS OF RELEVANT FIGURES FROM PREVIOUSLY PUBLISHED WORK.

Their steady-state analysis of Scheme I-5, assuming that equilibration between the $^3P_1$ and $^3P_0$ levels is fast and that either of these levels could be the precursor of the emitting species, gave the following relationships:

$$I^0_{326.1}/I_{326.1} = 1 + a[A] + \frac{b[A]}{1 + \frac{1}{c+d[A]}}$$

$$\left(\begin{array}{l} I^0_{326.1} = 326.1 \text{ nm fluorescence intensity at } [A] = 0 \\ I_{326.1} = 326.1 \text{ nm fluorescence intensity at the} \\ \qquad \text{corresponding } [A] \end{array} \right)$$

and

$$I_{326.1}[A]/I_{432} = \gamma(e + f[A])\left(1 + \frac{g}{h + [A]}\right)$$

The constants a to h are dependent upon the reaction rate constants and total foreign gas pressure only. The full expressions for b,e and f are slightly different depending on whether Cd* is taken to be Cd($^3P_1$) or Cd($^3P_0$).

The values of a,b,c and d were obtained by a trial and error method from the Stern-Volmer data. The constants γe and γf were found from high pressure data where

$$I_{326.1}[A]/I_{432} \approx \gamma e + \gamma f[A] \quad .$$

Estimates of g and h were then obtained and a re-evaluation of γe and γf carried out. This process was repeated until a self-consistent set of values was obtained. From the constants a to h and a previously reported lifetime for the Cd($^3P_1$) level, the values presented in Table I-3 were

Table I-3. Rate Constants and Ratios of Rate Constants from Reference 74.

$k_{23} + 1.68\ k_{24}$	$= (2.1 \pm 0.4) \times 10^{-13}$ cm^3 molecule^{-1}s^{-1}
k_{25} or $1.68\ k_{25}$	$= (2.2 \pm 0.4) \times 10^{-12}$ cm^3 molecule^{-1}s^{-1}
k_{12}/k_{26}	$= 0.336 \pm 0.012$ Torr^{-1}
k_{12}/k_{27}	$= 139$
k_{15}/k_{14}	$= (4.9 \pm 0.2) \times 10^{-3}$ Torr^{-1}
k_{15}/k_{28}	$= 1$

determined. From this information the half-quenching pressure for the 326.1 nm line was redetermined as 12.6 Torr, a value less than half the previous determination of 29.8 Torr. Of the two, the value determined latterly was considered the more reliable because of the measurements being influenced by pressure broadening during the earlier work.

From their values for a and b, it was also possible for Yamamoto et al. to calculate a value of 2.4×10^{-12} cm^3 $molecule^{-1}s^{-1}$ for a rate constant equivalent to the k_7 of Morten et al.. Also, by again estimating the cross section of reaction (1.12), a lower limit of 7.4×10^{-8} s was calculated for the unstabilised complex. From this they predicted that if other substrates, more complex than ammonia, were found to form exciplexes, and if the back reaction from the unstabilised complex (reaction (1.26)) was unimportant in these cases, the curvature in the Stern-Volmer plot would not be observed. Note was also made that examination of the rate constant ratios revealed that while the efficiencies of quenching the stabilised complex were about equal for ammonia and argon, ammonia was considerably more efficient than argon in quenching the unstabilised complex.

Soon after this study, Sato and his co-workers made a study of some Cd/amine, Cd/H_2O, Cd/alcohol and Cd/ether mixtures[75,76] using the same experimental system and under the same conditions of temperature and constant total pressure as the work of reference 74. As can be seen from Table I-4, the luminescence quantum yields for these mixtures, calculated by intensity comparisons with the Cd/NH_3 system luminescence

Table I-4 Exciplex Data from References 73,75,76 and 78

Substrate	$\lambda_{(max)}$/nm	Quantum Yield	Reference
NH_3	432 ± 2	0.67 ± 0.1	75
Methane	≈ 420		73
Methylamine	449 ± 5	0.58 ± 0.1	75
Ethylamine	452 ± 5	0.26 ± 0.09	75
Propylamine	452 ± 5	0.20 ± 0.09	75
n-Butylamine	453 ± 5	0.18 ± 0.05	75
sec-Butylamine	453 ± 5	0.12 ± 0.05	75
tert-Butylamine	454 ± 5	0.04 ± 0.02	75
Dimethylamine	450	-	78
Diethylamine	454		78
Triethylamine	longer than 460		76
Pyrrolidine	442	0.18	78
Piperidine	450	0.20	78
Morpholine	442	0.18	78
H_2O	385	1.2×10^{-3}	76
D_2O	385	5.7×10^{-3}	76
Methanol	395	3.1×10^{-3}	76
Ethanol	400	1.5×10^{-3}	76
Dimethylether	390	4.8×10^{-3}	76
Diethylether	398	1.1×10^{-3}	76
Tetrahydronfuran	398	8.5×10^{-3}	76

and its quantum yield (which was the average of twenty-five determinations in the range 5-50 Torr of gas), were all less than that of the ammonia system; markedly so for the water, alcohol and ether substrates. All these mixtures showed the decrease in emission intensities with time that had been noted with the Cd/NH_3 system.

The luminescence band maxima are tabulated with the quantum yields (Table I-4). The band shapes from all mixtures were found to be the same as the $CdNH_3^*$ band although the oxygen containing substrate mixtures emitted slightly narrower bands. Plots of these band intensities as a function of substrate pressure are shown in Figs. I-5(g) and (h). They demonstrate that while the intensity from the water, alcohol and ether mixtures increased monotonously with increasing substrate pressure, the intensity from the amine mixtures passed through a maximum value. Except for the case of the sec-butylamine mixture, this maximum value was achieved at lower pressures with increasing molecular complexity.

The Stern-Volmer plots for the quenching of the cadmium fluorescence by all substrates were linear and possessed unit intercepts. The same mechanism as that proposed in the 1975 paper on the Cd/NH_3 system (Scheme I-5) was used to interpret the observations; consequently the steady-state analyses revealed the same relationships between the observed quantities and the mechanism's rate constants as have been given above. The results from these analyses provide the data for Tables I-5 and I-6. The Stern-Volmer plots also enabled the half-quenching pressures

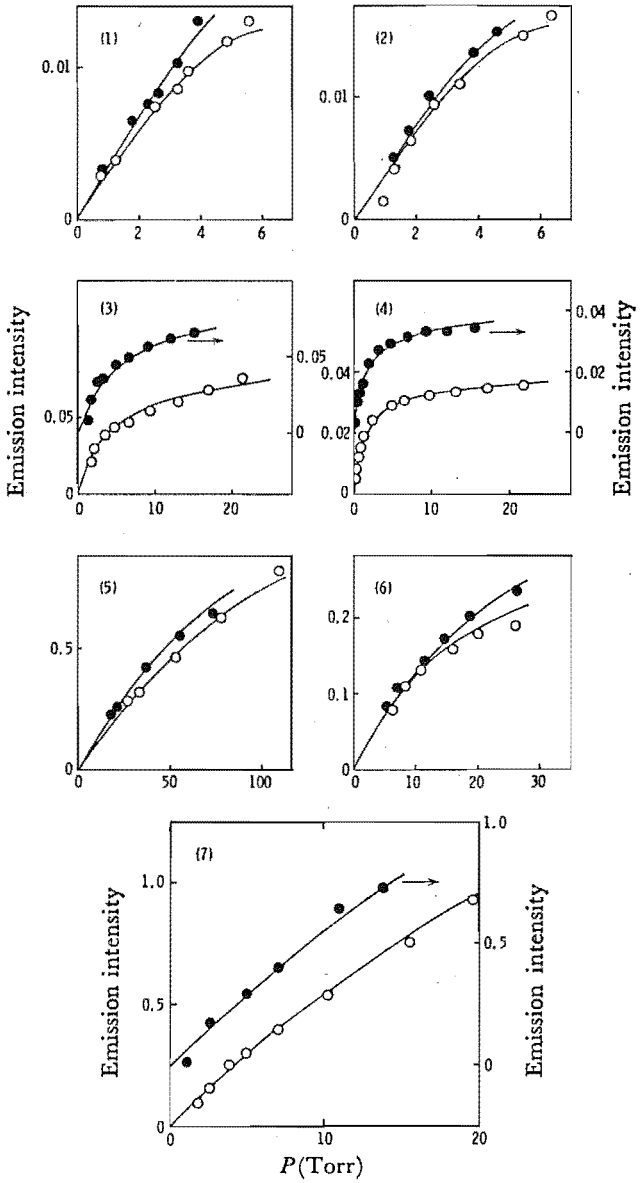

The intensity at the peak of the emission band from the complex as a function of the partial pressure of substrates. The total pressures are 80(○) and 56(●) in Torr, except for dimethylether, and those for dimethylether are 210(○) and 148(●) in Torr. The plots for 48 Torr in the cases of methanol, ethanol, and tetrahydrofuran are displaced upwards for clearity. 1) H_2O; 2) D_2O; 3) methanol; 4) ethanol; 5) dimethylether; (6) diethylether; 7) tetrahydrofuran.

(g) reference 76

Fig. I-5(g). REPRODUCTIONS OF RELEVANT FIGURES FROM PREVIOUSLY PUBLISHED WORK.

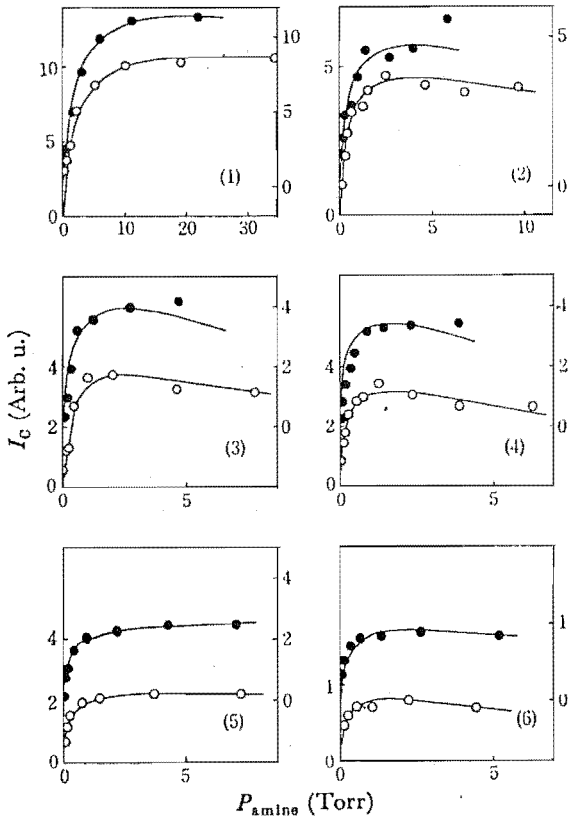

The intensity at the peak of the emission band from the complex as a function of the partial pressure of amines. The total pressures are 80 (○) and 48 (●) in Torr. The plots for 48 Torr are displaced upwards for clarity. 1) methylamine; 2) ethylamine; 3) *n*-propylamine; 4) *n*-butylamine; 5) *sec*-butylamine; 6) *tert*-butylamine.

(h) reference 75

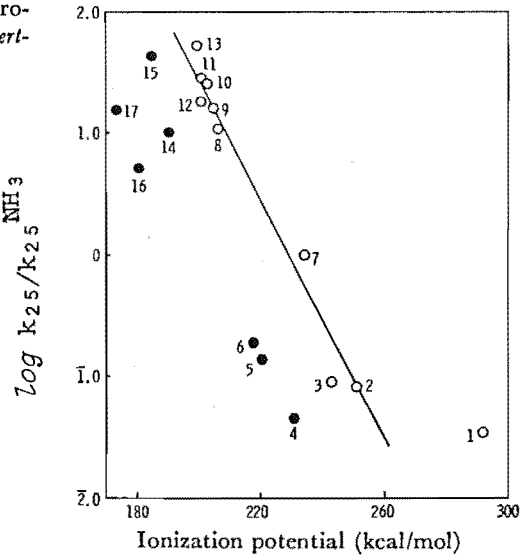

(i) reference 76

Relationship between the relative rate constants for the formation of the excited complex and the ionization potential of substrates.
1) H_2O; 2) methanol; 3) ethanol; 4) dimethylether; 5) diethylether; 6) tetrahydrofuran; 7) ammonia; 8) methylamine; 9) ethylamine; 10) *n*-propylamine; 11) *n*-butylamine; 12) *sec*-butylamine; 13) *tert*-butylamine; 14) dimethylamine; 15) diethylamine; 16) trimethylamine; 17) triethylamine.
The plots for *s*- and *t*-amines and ether are shown as filled circles.

Figs. I-5(h) and (i). REPRODUCTIONS OF RELEVANT FIGURES FROM PREVIOUSLY PUBLISHED WORK.

The rate constant ratio of Fig. I-5(i) is labelled in accordance with the labelling of Scheme I-5.

Table I-5. Rate Constants and Rate Constant Ratios from References 74,75,76 and 78

Substrate	$k_{23}+1.68k_{24}+k_{25}$ or $k_{23}+1.68(k_{24}+k_{25})$ / (cm^3 $molecule^{-1}s^{-1}$)	$\frac{k_{25}}{k_{25}^{NH_3}}$	Reference
NH_3	$(2.4 \pm 0.4) \times 10^{-12}$	1.0	74
Methylamine	$(2.4 \pm 0.2) \times 10^{-11}$	10.7	75
Ethylamine	$(6.1 \pm 0.1) \times 10^{-11}$	15.8	75
n-Propylamine	$(9.9 \pm 0.2) \times 10^{-11}$	24.9	75
n-Butylamine	$(1.2 \pm 0.1) \times 10^{-10}$	28.0	75
sec-Butylamine	$(2.0 \pm 0.1) \times 10^{-10}$	17.8	75
tert-Butylamine	$(7.4 \pm 0.4) \times 10^{-10}$	53.3	75
Dimethylamine	2.9×10^{-11}	10.0	76
Trimethylamine	1.9×10^{-11}	5.1	76
Diethylamine	1.7×10^{-10}	43.1‡	76
Triethylamine	1.1×10^{-10}	15.3‡	76
Propylenimine	$(2.83 \pm 0.04) \times 10^{-10}$	-	78
Azetidine	$(4.33 \pm 0.09) \times 10^{-10}$	-	78
Pyrrolidine	$(7.7 \pm 0.06) \times 10^{-11}$	14.0	78
3-Pyrroline	$(1.03 \pm 0.06) \times 10^{-9}$	-	78
Pyrrole	$(1.23 \pm 0.06) \times 10^{-9}$	-	78
Piperidine	$(7.0 \pm 0.2) \times 10^{-11}$	14.0	78
Morpholine	$(3.2 \pm 0.04) \times 10^{-11}$	5.6	78
Pyridine	$(1.01 \pm 0.02) \times 10^{-9}$	-	78
H_2O	3.9×10^{-12}	0.035	76
D_2O	6.7×10^{-13}	0.038	76
Methanol	7.2×10^{-12}	0.081	76
Ethanol	2.6×10^{-11}	0.091	76
Dimethylether	2.3×10^{-13}	0.044	76
Diethylether	1.9×10^{-12}	0.139	76
Ethylene oxide	1.6×10^{-10}	-	76
Tetrahydrofuran	7.8×10^{-13}	0.189	76

‡These values may be slightly smaller than the true values as they were not obtained at the peak wavelength because of interference from the lamp.

Table I-6. Rate constant Ratios from References 74, 75 and 78

Substrate	$\frac{k_{27}}{k_{26}}$ / (Torr^{-1})	$\frac{k_{12}}{k_{26}}$ / (Torr^{-1})	$\frac{k_{15} \times 10^3}{k_{14}}$ / (Torr^{-1})	$\frac{k_{15}}{k_{28}}$	Reference
NH_3	0.0024 ‡	0.336 ± 0.012	4.9 ± 0.2	1.0	74
Methylamine	0.0059	0.813	10.8	1.8	75
Ethylamine	0.0275	3.80	77.6	8.0	75
n-Propylamine	0.0253	3.48	153.7	12.2	75
n-Butylamine	0.0649	8.93	259.0	16.4	75
sec-Butylamine	0.0195	7.81	7.0	1.0	75
tert-Butylamine	0.0058	2.30	347.9	20.8	75
Pyrrolidine			171		78
Piperidine			230		78
Morpholine			105		78

‡ From Reference 75.

given in Table I-7 to be determined and the accompanying relative quenching efficiencies to be calculated.

The general trend for an increase in the k_{12}/k_{26} and k_{27}/k_{26} ratios with increasing amine complexity was interpreted as resulting from a decrease in the rate of the back reaction of the unstabilised complex returning to its precursors. The decrease in the significance of reaction (1.26) is evident in the linear Stern-Volmer plots of these mixtures. The straight lines of the Stern-Volmer plots of the oxygen-containing substrates were also explained by the decreased part played by the back reaction.

Except for the sec-butylamine system, the increase in the $k_{25}/k_{25}^{NH_3}$‡ ratios paralleled the quenching efficiency of the amines, and this was taken as an indication that the main channel for the quenching of the 326.1 nm fluorescence is exciplex formation. Although the luminescence quantum yields of the amine mixtures did not follow the $k_{25}/k_{25}^{NH_3}$ trend, this was explained by examination of the k_{15}/k_{14} ratios. By assuming that the rate of radiative decay of the complex (k_{14}) is approximately independent of the nature of the substrate, it is seen that the quenching rate of the complex by the substrate (k_{15}) increases as the complex production rate (k_{25}) and molecular complexity increase. This decrease in the luminescence quantum yield with increasing amine complexity is in contrast with the Hg/primary amine systems studied[80] in which the luminescence yield is governed by the competition between the production of the exciplex and α-hydrogen atom abstraction, so that the luminescence yield increases with increasing alkyl substitution.

---

‡ $k_{25}^{NH_3}$ = k_{25} for the Cd/NH_3 system.

Table I-7. Data from the Stern-Volmer Plots of References 74,75,76 and 78.

Quencher	Half Quenching Pressure/(Torr)	Relative Quenching Efficiencies	Reference
NH_3	12.6	1	74
Methylamine	0.885	14.2	75
Ethylamine	0.350	36.0	75
n-Propylamine	0.215	58.6	75
n-Butylamine	0.177	71.2	75
sec-Butylamine	0.108	116.7	75
tert-Butylamine	0.029	434.5	75
Diethylamine	0.181	69.6	76
Triethylamine	0.191	66.0	76
Propylenimine	0.078 $\pm$ 0.001	161	78
Azetidine	0.051 $\pm$ 0.001	247	78
Pyrrolidine	0.288 $\pm$ 0.002	43.8	78
3-Pyrroline	0.022 $\pm$ 0.001	573	78
Pyrrole	0.018 $\pm$ 0.001	700	78
Piperidine	0.317 $\pm$ 0.008	39.7	78
Morpholine	0.690 $\pm$ 0.009	18.3	78
Pyridine	0.022 $\pm$ 0.001	573	78
H_2O	5.38	2.3	76
D_2O	31.5	0.40	76
Methanol	2.95	4.3	76
Ethanol	0.82	15.4	76
Dimethylether	92.6	0.14	76
Diethylether	11.2	1.1	76
Ethylene oxide	0.13	96.9	76
Tetrahydrofuran	26.8	0.47	76

An investigation into the nature of the mercury-amine complexes had shown a correspondence between the rate of exciplex formation and the substrate's ionization potential.[80] The relationship is consistent with the exciplex being of the charge-transfer type. Fig. I-5(i), taken from Sato and co-worker's paper[76], shows a similar relationship which suggests that the cadmium-amine exciplexes are also charge-transfer in nature. This evidence is reinforced by the shift in the emission's peak intensity to longer wavelengths with a decrease in the complexed amine's ionization potential. The relationship illustrated in Fig. I-5(i) was taken to indicate that the complex production efficiency is dependent upon the electron-donating ability of the nitrogen atom alone.

Although they found that k_{15} increased with increasing molecular complexity, Sato and his collaborators did not consider the size of this increase could be explained in terms of the increasing cross section alone. The other contribution they proposed arises from the possibility of a substrate molecule colliding with the exciplex to form a complex containing two substrate molecules; the complex would behave in the way described by Phillips and co-workers.[71] This, it was argued, would mean that the increasing bulk of the amines would progressively inhibit the extent to which they could form the higher complexes.

The data from the Japanese group's paper concerned with Cd/H_2O, Cd/alcohol and Cd/ether mixtures are presented in Table I-5. The values of $k_{23} + 1.68\ k_{24} + k_{25}$ show that the alcohols and water are more efficient at quenching the

triplet cadmium atoms than are the ethers. However, the small $k_{25}/k_{25}^{NH_3}$ ratios indicate that the formation of the exciplex is not the major channel by which the triplet cadmium species is removed, as is the case in Cd/amine mixtures. The group concluded that vibrational excitation of the substrate molecule is the main quenching pathway as cleavage of the O-H could be dismissed on energetic grounds.

As had been found with the Cd/amine mixtures, the k_{25} value of the mixtures of oxygen atom containing substrates (except for dimethylether mixtures) increased with decreasing substrate ionization potential. However, while the alcohol and water mixtures possessed $k_{25}/k_{25}^{NH_3}$ values and ionization potentials that gave a plot approximately the same as had been obtained from the amine mixtures (Fig. I-5(i)), the $k_{25}/k_{25}^{NH_3}$ values of the ether mixtures fell below the line straddled by the other points. To determine whether this behaviour accompanied the replacement of the second hydrogen atom bonded to the central oxygen by another alkyl group, experiments were carried out to provide the data (in Table I-5) on secondary and tertiary amines. As Fig. I-5(i) shows, mixtures with these substrates were also found to yield $k_{25}/k_{25}^{NH_3}$ values lower than predicted by the primary amine plots. It was inferred from this that the reactivity of amines, alcohols, ethers and water could be explained mainly, but not completely, in terms of the electron-donating ability of the central oxygen or nitrogen atom. An additional factor suppressing the complex formation with ethers and secondary and tertiary amines was postulated,

but left unidentified. Furthermore, the relative positions of the band maxima could not be explained fully by trends in the ionization potentials of water, the alcohols or the ethers.

Using the same method, and basing their analysis on the mechanism Sato and his co-workers developed, Yamamoto et al.[78] investigated the behaviour of some cyclic amines in admixture with cadmium vapour. As with the open-chain amines, the Stern-Volmer plots for the quenching of the 326.1 nm line were linear. On the basis of the quenching constants shown in Table I-5 the cyclic amines were divided into three groups.

The first group showed large quenching rates which they attributed to the formation of triplet amine states after the fashion of substrates like benzene. No indication was given as to where this excited state leads, for no luminescence was observed from these mixtures. The second group possesses intermediate quenching rates and its members do not form emitting complexes. Two consequences of the collisions between these substrates and the excited metal atoms were suggested: the formation of an excited molecule, followed by decomposition; or a ring-opening reaction. The latter possibility was supported by the high exothermicity to be expected from such a reaction by the strained, three and four-membered cyclic compounds in comparison with the slight endothermicity of the equivalent reactions of the five and six-membered systems.

The third group contained those compounds with a low quenching rate. These mixtures exhibited luminescence,

(quantum yields and emission maxima are given in Table I-4), so behaving in the manner of the acyclic amines. An examination of the correlation between the $k_{25}/k_{25}^{NH_3}$ values (Table I-5) and the ionization potentials of these substrates, revealed that like the secondary amines, the $k_{25}/k_{25}^{NH_3}$ values fall well away from the line upon which the data of the primary amines and ammonia fall. In addition, their emission maxima do not show the correlation with their ionization potentials shown by the primary amines. Yamamoto et al. believed that the correlations that were obtained could be explained by the reactivity of the amines being governed mainly by the electron-donating ability of the nitrogen atom. They also suggested that the steric effects of the amine substituents in the cyclic and secondary amines are probably partly responsible for this behaviour. The k_{15}/k_{14} values for these cyclic amines, presented in Table I-6, are seen to be approximately the same as those of n-proplylamine and n-butylamine.

The report by Sato and co-workers on their last examination of the Cd/NH_3 and Cd/amine systems appeared in 1978[77]. This study was a phase-shift investigation at a system temperature of 525 K. Like the earlier work of Phillips' group, their measurements showed a decrease in the phase lag of the 430 nm luminescence behind the 326.1 nm fluorescence with increasing ammonia pressure (Fig. I-5(j)), although at a given ammonia pressure the shifts obtained by the Japanese group were somewhat larger than those found by Morten et al.. The equivalent plots of Fig. I-5(j) for the Cd/amine systems were of the same form. Unlike the

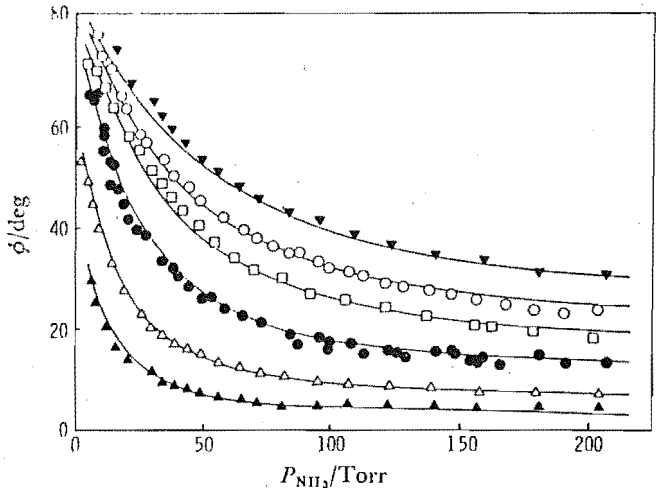

Phase difference between the resonance fluorescence at 326.1 nm and the luminescence from $CdNH_3$* at 432 nm as a function of NH_3 pressure.
▲: 10 kHz, △: 20 kHz, ●: 40 kHz, □: 60 kHz, ○: 78 kHz, ▼: 99 kHz.
Solid lines show the values calculated according to Eq. 12.

(j) reference 77

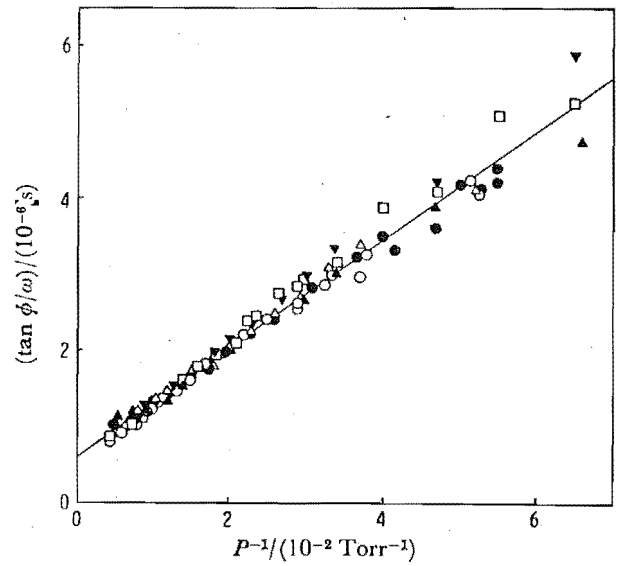

Values of $\tan \phi/\omega$ as a function of the reciprocal of the NH_3 pressure.
▲: 10 kHz, △: 20 kHz, ●: 40 kHz, □: 60 kHz, ○: 78 kHz, ▼: 99 kHz.

(k) reference 77

Figs. I-5(j) and (k). REPRODUCTIONS OF RELEVANT FIGURES FROM PREVIOUSLY PUBLISHED WORK.

study they had made of the Hg/NH_3 system[81], in which the phase difference between the complex emission and the intercombination line was dependent upon the wavelength within the band at which the measurement was made (taken as evidence of two emitting species being present in the system), there was no such dependence in the Cd/NH_3 system. This supported the idea that if an unstabilised exciplex is an intermediate in the system, it does not contribute to the observed luminescence.

In the pressure range from 15-200 Torr of added gas, a linear relationship between $\tan \phi/\omega$ [$\omega = 2\pi f$] and the inverse of the gas pressure was found (Fig. I-5(k)). This was explained by the following mechanism:

Scheme I-6.

$$Cd + h\nu \rightarrow Cd_1$$

$$Cd_1 \rightarrow Cd + h\nu$$

$$A + Cd_1 \rightarrow \text{products}$$

$$A + Cd_1 \rightarrow CdA^{\dagger} \qquad [1.10]$$

$$CdA^{\dagger} \rightarrow Cd_1 + A \qquad (1.29)$$

$$CdA^{\dagger} \rightarrow Cd_0 + A \qquad (1.30)$$

$$A + Cd_0 \rightarrow CdA^{\dagger} \qquad (1.31)$$

$$A + CdA^{\dagger} \rightarrow CdA^{*} + A \qquad [1.12]$$

$$CdA^{*} \rightarrow Cd + A + h\nu' \qquad [1.14]$$

Consideration of this scheme showed that the measured phase shift, like that of Morten et al., could be broken down into two components. The first component was associated with the rates of removal of $Cd(^3P_0)$ and $CdA^{\dagger}$, and the second, which was taken to be the limiting shift at high pressure (ϕ_{∞}), was related simply to the complex lifetime.

Although this mechanism explained the linear relationship between tan ϕ/ω and $1/[A]$ it was incapable of predicting a second linear relationship found between $\omega/\tan(\phi-\phi_\infty)$ and [A]. (The intercept and slope of this plot were frequency dependent.) Accordingly, a second, simpler model was devised (Scheme I-7).

Scheme I-7.

$$Cd + h\nu \rightarrow Cd_1$$

$$Cd_1 \rightarrow Cd + h\nu$$

$$A + Cd_1 \rightarrow \text{products}$$

$$A + Cd_1 \rightarrow CdA^*$$

$$CdA^* \rightarrow Cd_1 + A$$

$$CdA^* \rightarrow Cd_0 + A$$

$$A + Cd_0 \rightarrow CdA^*$$

$$CdA^* \rightarrow Cd + A + h\nu'$$

Both linear relationships noted above could be derived from this scheme once the exact expression for the observed phase shift was reduced in complexity by some simplifying assumptions regarding the relative magnitude of some rate constant terms in the phase equation. However, the non-linearity found in the Stern-Volmer plots for the quenching of the 326.1 nm fluorescence by ammonia could not be accounted for.

Nevertheless, by the inclusion of the reverse of reaction (1.12) in Scheme I-6,

$$A + CdA^* \rightarrow CdA^{\dagger} + A \quad , \tag{1.32}$$

a mechanism was found that was capable of explaining all observations. A complicated equation, describing the phase

Table I-8. Slope and Intercept Values from the Plots of tan ϕ/ω v. 1/[substrate] of Reference 77.

Substrate	$\frac{k_{29}k_{31}+k_{30}k_{12}}{k_{31}(k_{29}k_{32}+k_{12}k_{14})}$ 10^{-5}(s Torr)	$\frac{k_{12}+k_{32}}{k_{29}k_{32}+k_{12}k_{14}}$ 10^{-7} s
NH_3	7.1 ± 0.1	6.0 ± 0.3
Methylamine	4.2 ± 0.1	9.6 ± 0.2
Dimethylamine	1.8 ± 0.2	2.9 ± 0.8
Trimethylamine	1.4 ± 0.1	5.7 ± 0.2

Table I-9. Rate Constants Evaluated numerically in Reference 77.

$k_{29} = 5.5 \times 10^{6}\ s^{-1}$
$k_{30} = 3.8 \times 10^{8}\ s^{-1}$
$k_{31} = 9.1 \times 10^{5}\ s^{-1}\ Torr^{-1}$
$k_{12} = 2.2 \times 10^{7}\ s^{-1}\ Torr^{-1}$
$k_{32} = 8.6 \times 10^{6}\ s^{-1}\ Torr^{-1}$
$k_{14} = 1.7 \times 10^{5}\ s^{-1}$

lag's dependence on the rate constants, the frequency and the substrate concentration, resulted from the analysis of the modified Scheme I-6, but a set of assumptions similar to those mentioned above allowed the equation to be reduced to:

$$\frac{\tan \phi}{\omega} = \frac{k_{29}k_{31}+k_{30}k_{12}}{k_{31}(k_{29}k_{32}+k_{12}k_{14})} \cdot \frac{1}{[A]} + \frac{k_{12}+k_{32}}{k_{29}k_{32}+k_{12}k_{14}}$$

From the plot in Fig. I-5(k), and the equivalent amine plots, the group determined the values listed in Table I-8. While this model was so complex as to render analytical evaluation of the exciplex's radiative lifetime impossible, the set of values listed in Table I-9, which were used to fit the curves to the data of Fig. I-5(j), were determined numerically. It was noted that these values may not be unique because the phase readings for two species only could be obtained. However, they do indicate that the assumptions made in the simplifications above are self-consistent.

Chapter III of this thesis will show that although these results are self-consistent, they cannot be related to the results of the present study because of the reinterpretation of the phase data that the additional information available from this work requires.

III INTRODUCTION TO THE PRESENT STUDY

A number of studies of the Hg/NH_3 system have clearly defined the rôle of $Hg(^3P_0)$ in the formation of the $HgNH_3^*$ exciplex[82,83]. From the review of section II-3 it can be

seen that the part played by $Cd(^3P_0)$ in the photochemistry of the Cd/NH_3 system is not so well defined, mainly because of the equilibrium established between the two lower triplet levels. The studies reported here returned to the Cd/NH_3 system to measure the rates of processes involving $Cd(^3P_0)$ to obtain a better understanding of its importance in the formation of $CdNH_3^*$.

Two methods were used to make measurements of the phase shifts between some of the species in the system. The first employed a lock-in amplifier after the fashion of many other studies that have used electronic phase-shifting networks to obtain such measurements. Through this method the phase shift of the emitter of the 430 nm band could be measured with respect to the $Cd(^3P_1)$ level.

Initially it was thought that the decay of the $Cd(^3P_0)$ population might be measured directly by a laser-induced fluorescence (hereafter LIF) technique. This technique, used to study the Hg/N_2 system[84], relies on the very short radiative lifetime ($\approx$ 10 ns) of the $Cd(^3S_1)$ state to provide an instantaneous probe of the $Cd(^3P_0)$ population. By laser excitation of the $^3P_0$-$^3S_1$ transition (467.8 nm), and subsequent observation of fluorescence from the upper state (see Fig. I-6), changes in the metastable atom population can be followed.

However, to measure a decay time directly, an excitation pulse with a short fall time is required. Examination of the fall time of the exciting 326.1 nm radiation from the lamp showed the decay rate of the exciting light to be of similar magnitude to the expected decay rate of the $Cd(^3P_0)$

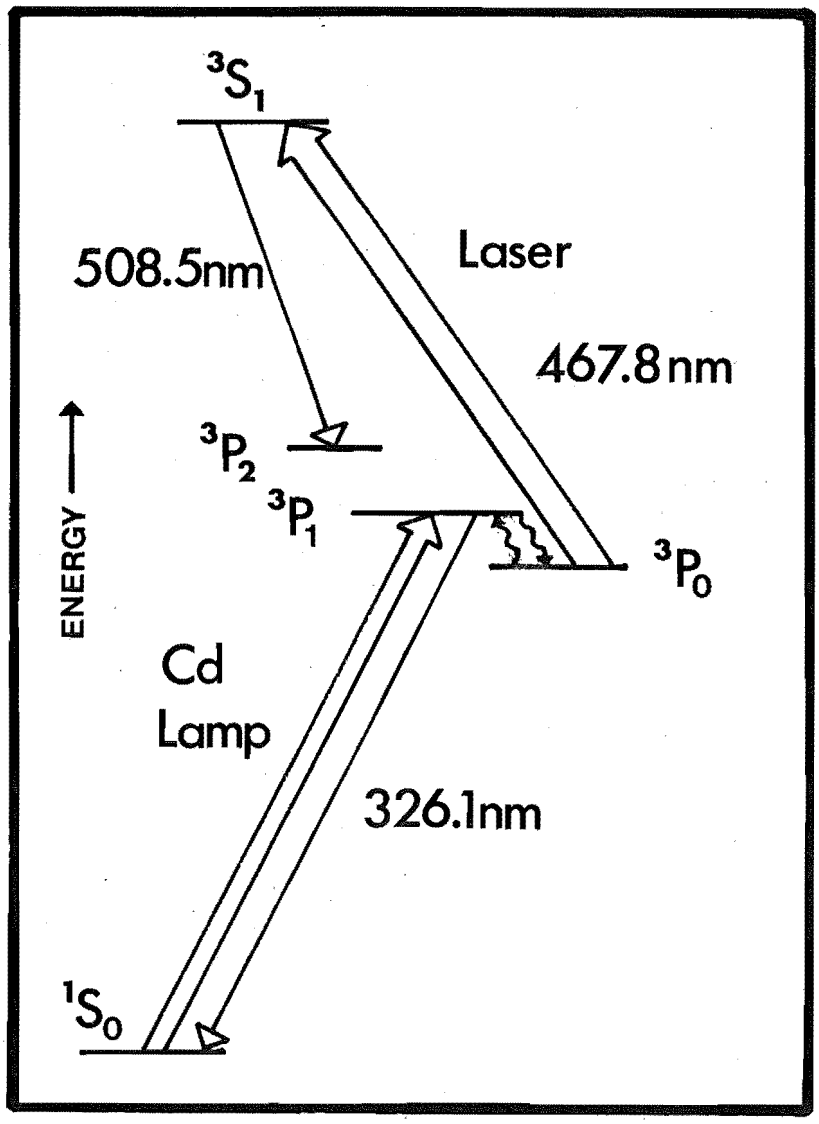

Fig. I-6. EXCITATION AND FLUORESCENCE SCHEME FOR THE PRESENT WORK.

For clarity, the energy spacings are not to scale. The wavy lines denote the collisional deactivation and activation of the $^3P_1$ and $^3P_0$ levels.

population. Because of the resulting distortion of the decay data, it was decided instead to use the LIF technique to measure the phase shift of the $Cd(^3P_0)$ species with respect to the $Cd(^3P_1)$ level. Complete waveforms of the modulated emission signal of $Cd(^3P_1)$, $Cd(^3P_0)$ or $CdNH_3^*$, as detected by a photomultiplier, were scanned by a boxcar integrator and the averaged signals passed via an analog to digital interface to a microcomputer for storage on disk and subsequent Fourier analysis. Thus, from the modulated waveforms of all three species their relative phase shifts have been obtained.

In addition to the phase-shift data, this work has measured: the spectral band profile of the exciplex; the intensity of the exciplex band as a function of the ammonia pressure; the ratio of I_{430} (the exciplex emission intensity) to $I_{326.1}$ (the $Cd(^3P_1)$ fluorescence intensity) as a function of the cadmium pressure.

From the phase-shift and steady-illumination data, conclusions about the mechanism operating in the Cd/NH_3 system have been drawn and the rate constants for some processes determined.

CHAPTER II

EXPERIMENTAL

I. APPARATUS

(1) The Metal Vacuum Line

The fluorescence cell used for these studies was a modified VARIAN stainless steel 1½ in. cross. Into the centre of the cross, perpendicular to both existing sets of arms, two ¾ in. holes were drilled to accommodate two extra VARIAN Mini-ConFlat Flanges. The first Mini-ConFlat Flange was argon arc welded directly to the cross while the second was joined to a 5 cm length of ¾ in. O.D. stainless steel tubing which in turn was welded into the remaining hole in the cross. The cross was orientated to position these two smaller flanges and two of the larger (2¾ in.) flanges horizontally.

VARIAN sapphire windows were bolted to the uppermost 2¾ in. flange and to one of the horizontal 2¾ in. flanges to act as excitation ports, and a VARIAN Mini-Hardware sapphire window was bolted to the cross to serve as an observation port. The other large horizontal cross arm was blanked off. In positioning the observation window as closely as possible to the cell's excitation region, the exit path length of the 326.1 nm line in fluorescence was reduced and consequently, so was the degree of re-absorption of the line.

Bolted to the lower vertical cross arm, in an inverted position, was a VARIAN bakable stainless steel 1½ in. valve

which led via; a VARIAN stainless steel bellows, an adaptor section, an EDWARDS model 2L1B isolation/baffle valve and an EDWARDS cold trap, to an EDWARDS model E01 oil diffusion pump backed by a WELCH Duo-seal model 1402 rotary pump. The adaptor section served to mate the ConFlat Flange system of the VARIAN components to the O-ring sealing system of the EDWARDS components. It also provided the mounting for a VEECO RG-75P ionization gauge head , through a greaseless glass valve (ACE Glass Inc.), and supplied the take-off for the reference port of an MKS BARATRON 315 BH (0.001-1000 Torr) differential bakable sensor. When necessary, the manometer's reference port could be isolated from the rest of the metal vacuum line by a VEECO forged brass "L" type valve situated between the sensor port and the isolation valve.

Bolted in series to the second of the two Mini-ConFlat Flanges were two VARIAN Mini-Tees. The side-arm of the Mini-Tee closest to the cell ran to a VARIAN Mini-Valve placed in an upright position so that the metal reservoir, to which it led, extended down through the oven base. The reservoir tube was an 18 cm length of $\frac{3}{8}$ in. O.D. stainless steel tubing which flared out at one end to a Mini-ConFlat Flange and was stoppered at the other by a welded plug into which a thermo-couple well was let. The end farthest from the cell of the second Mini-Tee was blanked off and a VARIAN bakable leak valve was bolted, through an adaptor, to the Mini-Tee's vertically standing arm. Two elevations of the metal vacuum line are given in Fig. II-1.

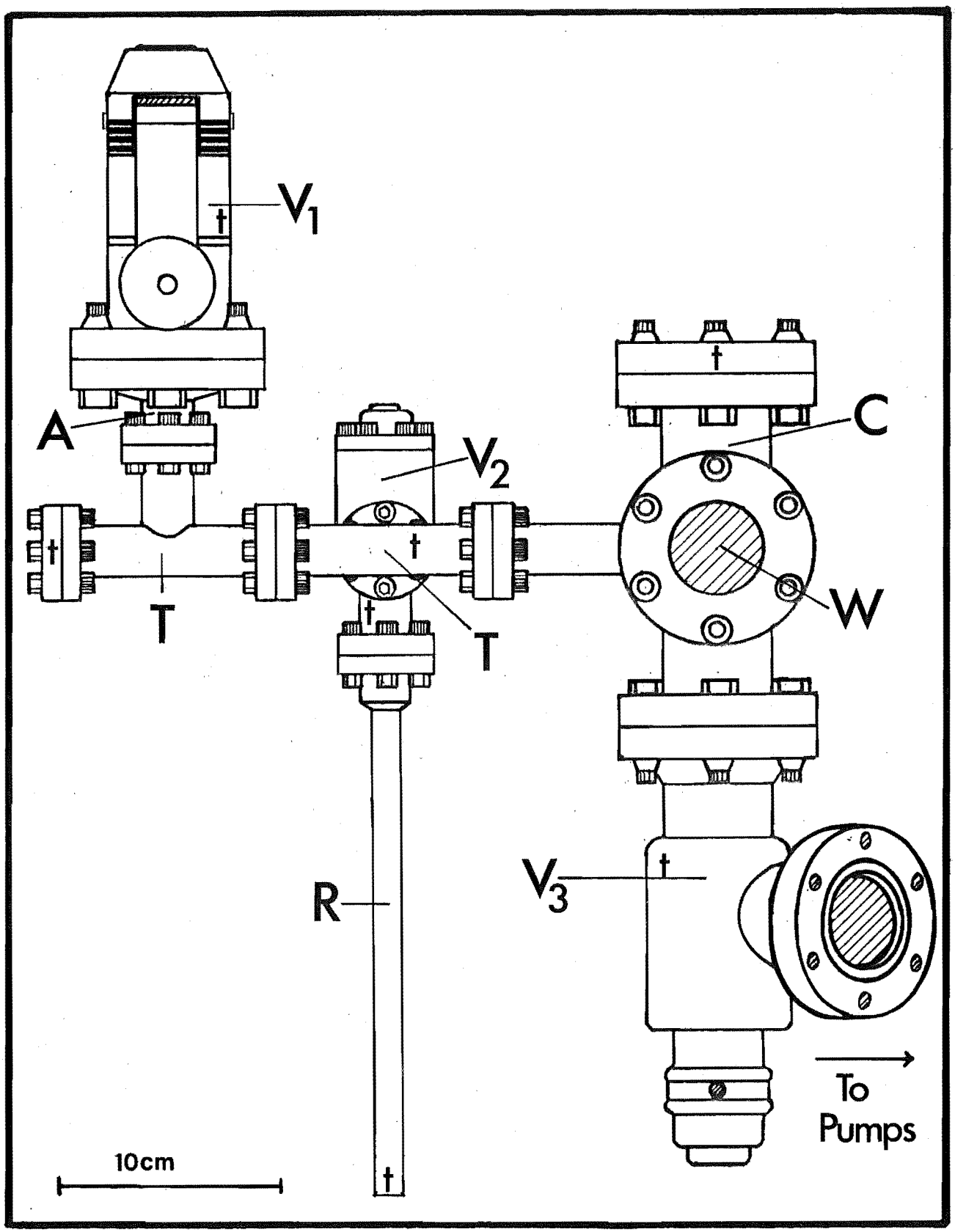

Fig. II-1(a). ELEVATION OF THE STAINLESS STEEL VACUUM LINE.

(See over page for the Key.)

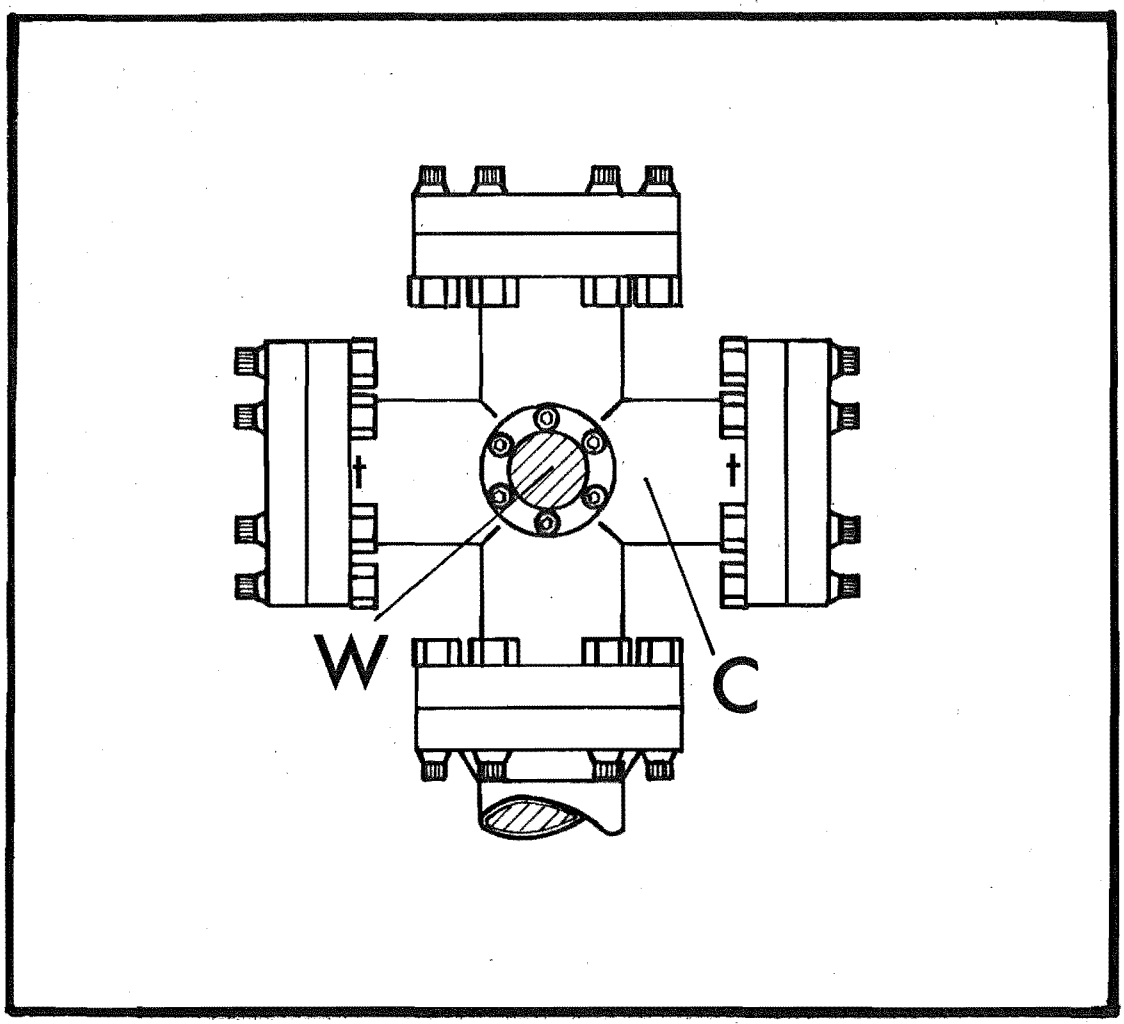

Fig. II-1(b). ELEVATION OF THE STAINLESS STEEL VACUUM LINE.

This second elevation is of the cross only, viewed at right angles to the elevation of Fig. II-1(a).

Lower case "t"s indicate thermocouple positions.

KEY:
- A = Adaptor section
- C = Cell cross
- R = Reservoir finger
- T = Mini-Tee
- V_1 = Leak valve(leading to glass line)
- V_2 = Mini-Valve
- V_3 = 1½ in. valve
- W = Sapphire window.

The stainless steel vacuum line was clamped to a DEXION framework. Four aluminium alloy clamps supported the vacuum line: two grasped the horizontal arms of the cross, one held the far Mini-Tee, and the last was clamped to the Mini-Valve to reduce the strain on the system when this valve was sealed or opened. Asbestos webbing was packed between the clamps and the metal line to stop thermal conduction away from the line at the point of contact. Because of the large closing torque required to seal the 1½ in. valve, a steel bracing sleeve was made to fit over the end of the valve as shown in Fig. II-2. Three holes around the valve body allowed the positioning of pins that slid into locating slits in the sleeve so that when the sleeve was clamped to a bracing bar running diagonally across the framework, very little of the movement during closure or opening was transmitted to the vacuum line.

The reflective surfaces presented to exciting light by the internal walls of the steel cell created a considerable problem. Attempts to collimate the light before it entered the cell, by lens systems, blackened glass tubing, or discs, were unable to reduce the amount of light scattered about the cell, to an acceptable extent, without crippling the total amount of light incident upon the central region of the cell. Accordingly, an internal baffle system was arranged in three of the cross's large arms.

To collimate light passing vertically into the cell through the uppermost window, three discs whose diameters were just less than the internal diameter of the cell tubing

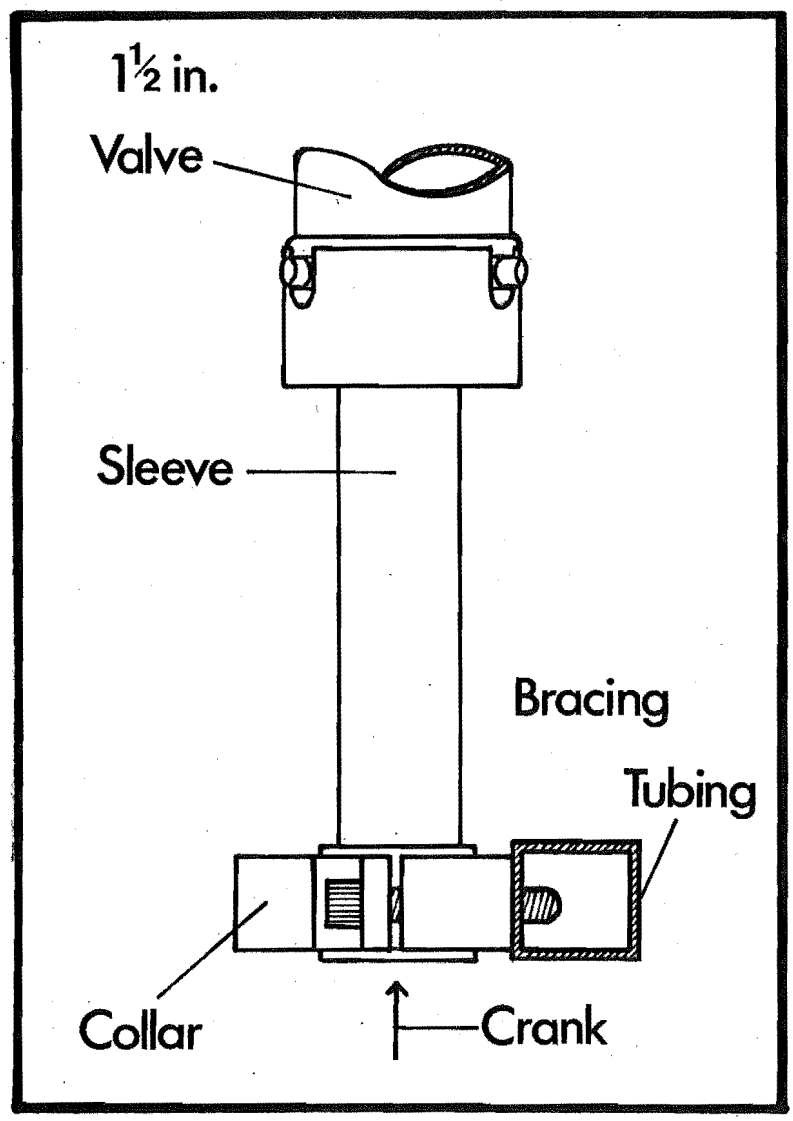

Fig. II-2. THE 1½ IN. VALVE BRACING SYSTEM.

The drive-shaft of the crank ran up the inside of the sleeve to engage the valve's drive socket.

were cut from 1.3 mm thick aluminium alloy sheet. The centre of each disc was bored out to a 12 mm diameter bevelled hole. The discs were equally spaced by two sections of aluminium alloy tubing of the same outer diameter as the discs, and the whole assemblage was kept from slipping down the cell arm by an internal circlip at the bottom of the stack. A similar collimating system was mounted in the horizontal arm behind the other excitation window. This assemblage differed from the first in having one more disc and having all discs bored out to 17.8 mm diameter holes. In addition, a light trap, as shown in Fig. II-3, was cut from pure aluminium sheet and placed in the lower vertical arm that led to the vacuum take-off. All baffle system surfaces, except the outer surfaces of the spacers, were given a light coating of colloidal carbon (AQUADAG-Acheson Colloids Co.). Measurements of the amount of 326.1 nm exciting light scattered into the observation optics when the cell was evacuated indicated that this baffle system reduced the scatter component to less than 2% of the total 326.1 nm signal when only cadmium vapour was present in the cell. With about 60 Torr of ammonia in admixture with the metal the scatter component was about 5% of the total signal at 326.1 nm.

(2) The Main Oven

The steel vacuum line was encased in a fire-brick oven measuring approximately 58 cm x 46 cm x 34 cm. The fire-bricks chosen for the construction were KAMO GREEN 26

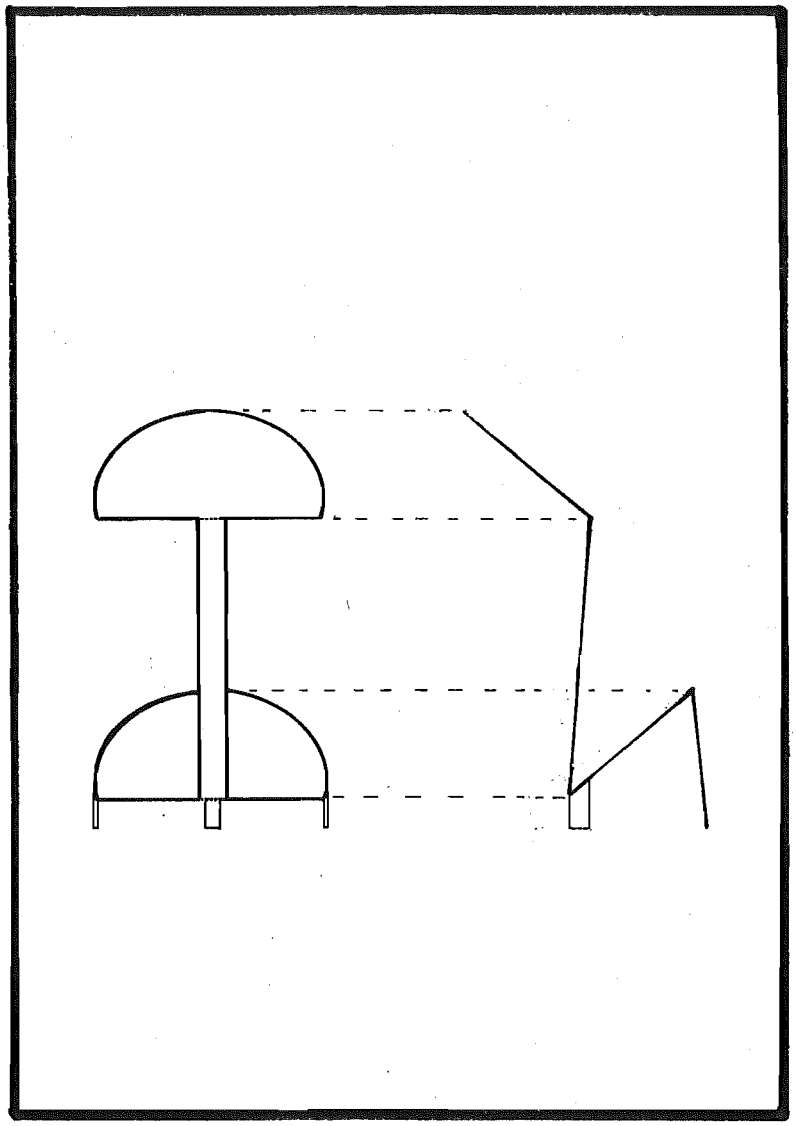

Fig. II-3. THE LIGHT TRAP.

The trap sat in the 1½ in. valve (see text).

insulating fire-bricks (Kamo Green Refractories Ltd.) which provided adequate insulation for the temperatures to which the oven was run. Unlike ordinary fire-bricks, they are sufficiently friable to make the fashioning of the bricks to accommodate the vacuum line a relatively easy task. To reduce heat losses from the oven through gaps between the bricks, the crevices were plugged with asbestos string. Where it was unlikely that the bricks would have to be removed for cell maintainence the asbestos plug was sealed with a sodium silicate and talc mixture that hardened to a smooth cement. Also, to reduce any hinderance caused by the rough brick surfaces to the hot air flow, these surfaces were sealed and smoothed by a coating of a slightly more dilute solution of the same mixture.

Stainless steel's low co-efficient of thermal conductivity coupled with the irregular shape of the vacuum line, created problems in obtaining an acceptable temperature distribution over the vacuum line. Numerous combinations of internal oven arrangement and air circulation methods were tried while a design, capable of giving a good temperature uniformity over the cell, was sought. Axial-flow fans run at various speeds and orientations were tested, but they could not provide a sufficiently fast flow of air for the task. Experiments were conducted with a compressed air line of perforated copper tubing that first passed over the heaters then coiled around the vacuum line to carry hot air to the parts of the cell in oven corners sheltered from the airflow, but this arrangement gave little improvement over the

axial-flow fan results. The possibility of wrapping the heating coils around the metal line was examined, but the irregular shape of the system made the preparation of an electrically insulating layer between the coils and the steel vacuum line extremely difficult. Together with the various air circulation methods investigated, brick "islands" and deflectors of steel sheet were positioned in the oven to direct the airflow. The alteration of their positioning showed that the temperature of the vacuum line extremities could be altered by several degrees through small changes in the orientation of these deflectors. Eventually it became apparent that a much greater fan speed than had been used initially, and an internal design that would channel the airflow over the line in one direction, rather than randomly mixing the air, were required.

The internal design that was found to give the best uniformity of vacuum line temperature is illustrated in Fig. II-4 and required the division of the oven into two compartments. The first compartment housed the vacuum line; the second, which was separated from the first by a brick partition, contained electric heating elements capable of dissipating a maximum of 2.2 kW, and a centrifugal circulation fan whose steel cowling directed the heated air into the first compartment.

The fan drum was driven by a 0.3A/240 V shaded-pole induction motor (Pacific Electric Co. Pty. Ltd. type MF041) by way of an O-ring pulley system which converted the 1440 rpm provided directly by the motor to about 4300 rpm (Fig. II-5).

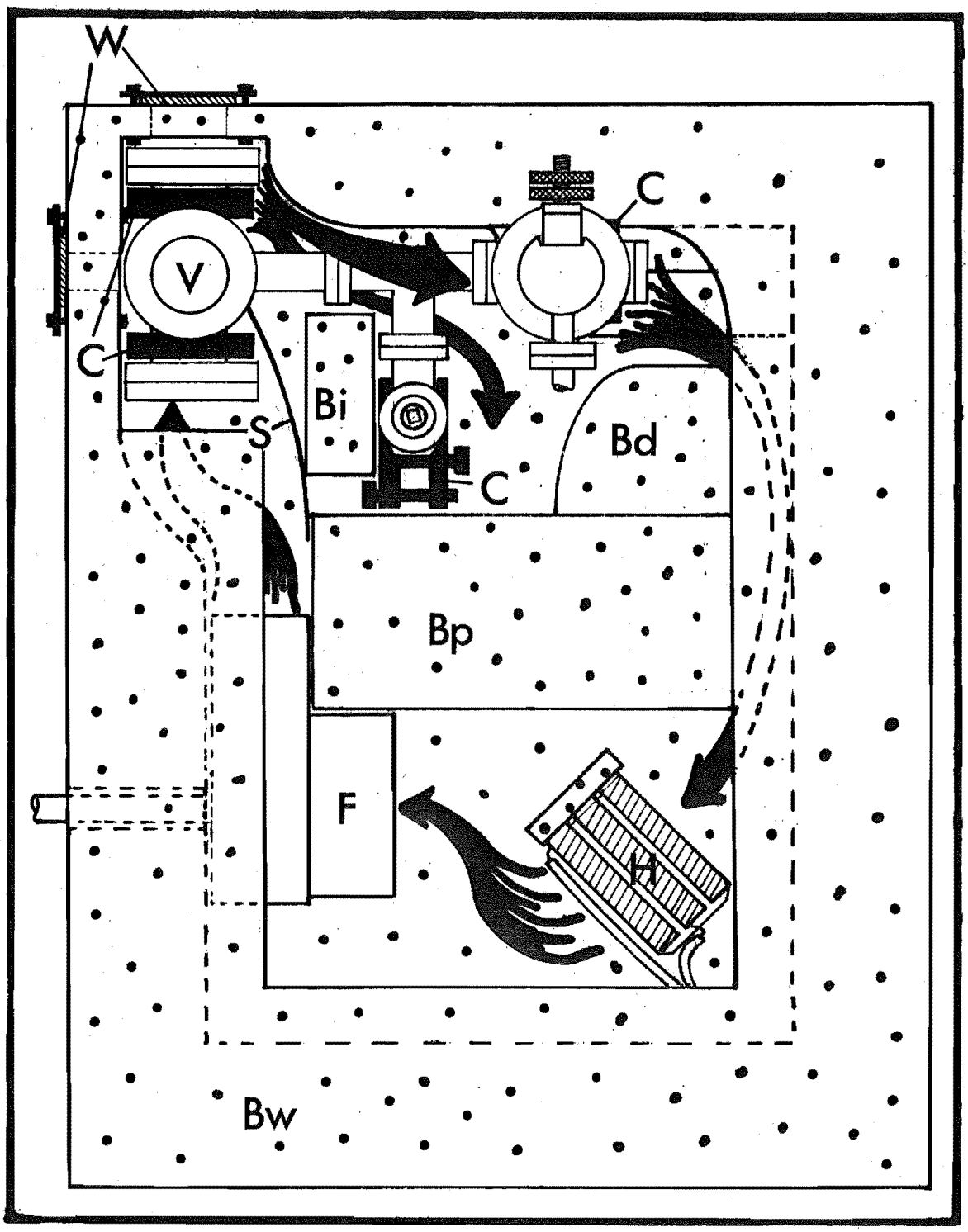

Fig. II-4. THE INTERNAL DESIGN OF THE OVEN.
(plan view, brick roof removed)

The airflow is indicated by the arrows.
Dashes indicate detail under the brick ledge.

Key: Bd = brick deflector; Bi = brick island; Bp = brick partition(see text); Bw = brick wall; C = clamps; F = fan cowling; H = heaters; S = steel deflector; V = vacuum line; W = Supracil oven windows.

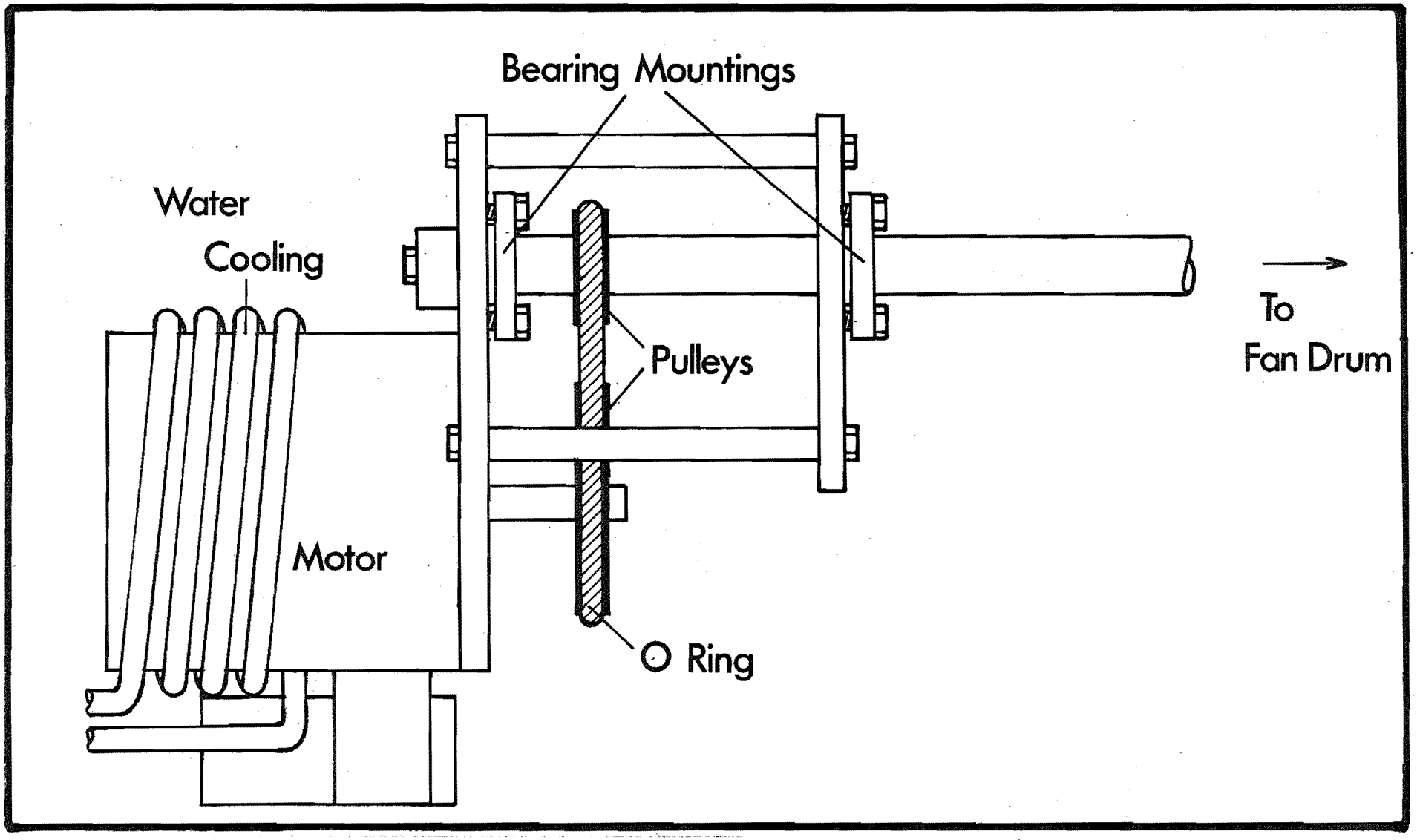

Fig. II-5. THE CENTRIFUGAL FAN DRIVE SYSTEM.

This fan speed was about the minimum that gave an acceptable temperature uniformity, as the distribution deteriorated rapidly with decreasing fan speed. If the pulley diameter ratio was changed to increase the speed much beyond 4300 rpm however, difficulties arose, as the O-ring drive tended to slip under the increased load. The use of a faster brush-type motor was ruled out because of the possibility of increased levels of electrical noise being generated by this type of unit. Because of the gearing of the electric motor (which increased its loading) and its proximity to the oven, it was found necessary to wind the motor casing with copper tubing to provide water cooling.

The position of the vacuum line in the other oven compartment was dictated by the need to have the cell windows as close to the outside of the oven as was consistent with maintaining a reasonable temperature uniformity over the cell. To this end the cross was situated in the corner of the oven, and the insulation bricks in this region were carved to provide a wall thickness of about 1.5 cm close to the windows. Holes were drilled through this thin section of the wall to allow the passage of light to and from the cell by way of the horizontally orientated excitation window and the observation window respectively. SUPRACIL windows (2 in. square) were held in place over these holes by aluminium alloy plates painted matt black. The plates were bolted to the brick-work by small diameter threaded rods that passed through the brick and plate to be secured by nuts and washers at each end. To provide a

better air seal between the brick and windows small strips of teflon sheet were sandwiched between the two surfaces; this also aided in protecting the window from the brick.

The fan cowling was orientated to first direct the air from the heaters to the bottom of the oven corner in which the cell cross was positioned. To a degree, this compensated for the heat losses from the cell that resulted from its closeness to the thin walls, combined with the 1½ in. valve's protrusion through the oven floor. To achieve the flow indicated in Fig. II-4, a brick "island", together with a steel deflector, were placed by the outlet of the fan to force hot air around the parts of the cell closest to the oven walls. Thus, the hot air passed around the observation port, horizontal excitation port and the 1½ in. valve before flowing over the Mini-Tees to return to the heating region through the passage cut in the dividing wall. Below the blanked end of the Mini-Valve farthest from the cross, the brick-work was built up to direct the hot air over this portion of the vacuum line. Without this brick-work, the airstream flowed below the level of the vacuum line, thereby dropping the Mini-Tee's temperature.

The main oven heaters were powered through a variable transformer (10 A/230 V VARIAC) which ran at about 160 V to maintain a cell temperature of 550 K. Satisfactory regulation of the system's temperature was achieved by the adjustment of the transformer setting, until, after thermal equilibration, the required operating temperature was reached. Without major air currents passing through the room and with

adequate equilibration time, this method allowed the average cell temperature to be kept within $\pm$ 1 K for several hours. When runs requiring the use of the boxcar integrator, the TRS-80 microcomputer and the laser were being carried out, the airflow through the room was increased somewhat to avoid the deterioration in performance that all sometimes suffered at an increased ambient temperature. During such runs a watch was kept on the temperature readings, and manual adjustment made to the heater voltage if it became necessary.

The leak valve, through which ammonia from the gas handling line was conducted to the cell, could not be totally contained within the main oven, so a small heating system was arranged to heat the upper portion of the valve. The design of the system is given in Fig II-6. A single insulating brick was carved to allow it to sit over the protruding top of the valve, and in a recess next to this cavity a heat-gun's ceramic former, wound with a nichrome spring capable of operating at 230 V, was positioned. This heater was powered through a variable transformer (8 A/230 V VARIAC) operated at approximately 140 V during experimental runs.

The vacuum line's temperature was monitored in nine places, marked on Fig. II-1, by chromel-alumel thermocouples. The welded junctions of these thermocouples were insulated from the stainless steel of the vacuum components by a thin coating of sodium silicate/talc cement. After the sheath of cement had dried on the junction it was cemented into thermal contact with the vacuum line using the same type of

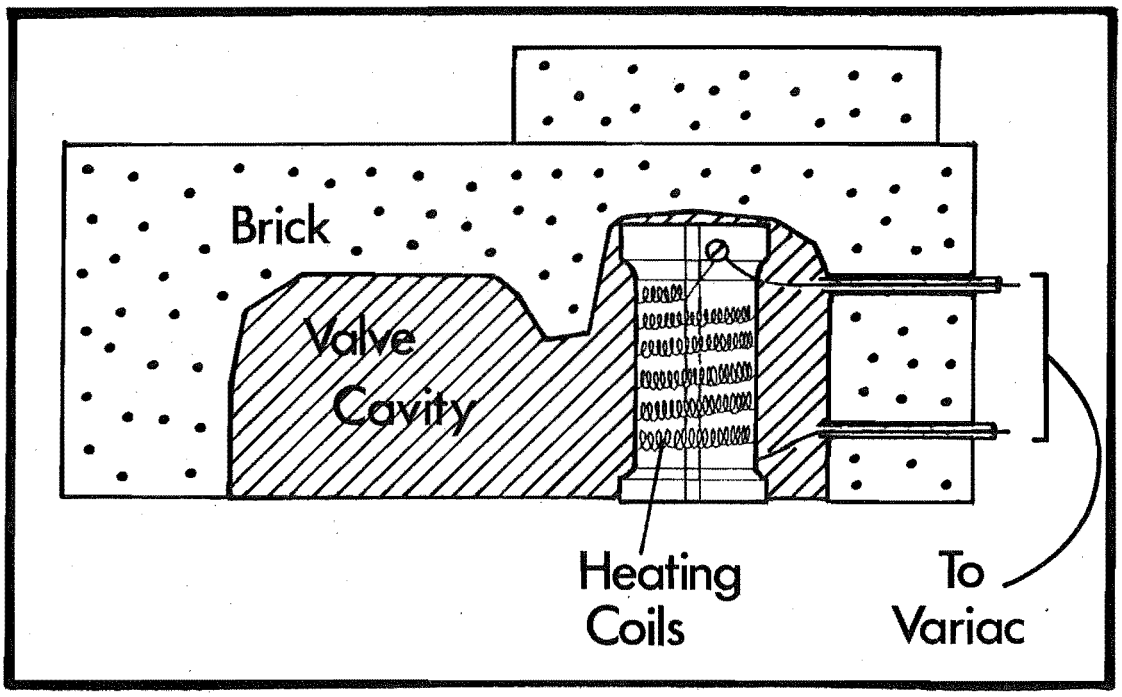

Fig. II-6. THE LEAK VALVE HEATING SYSTEM.

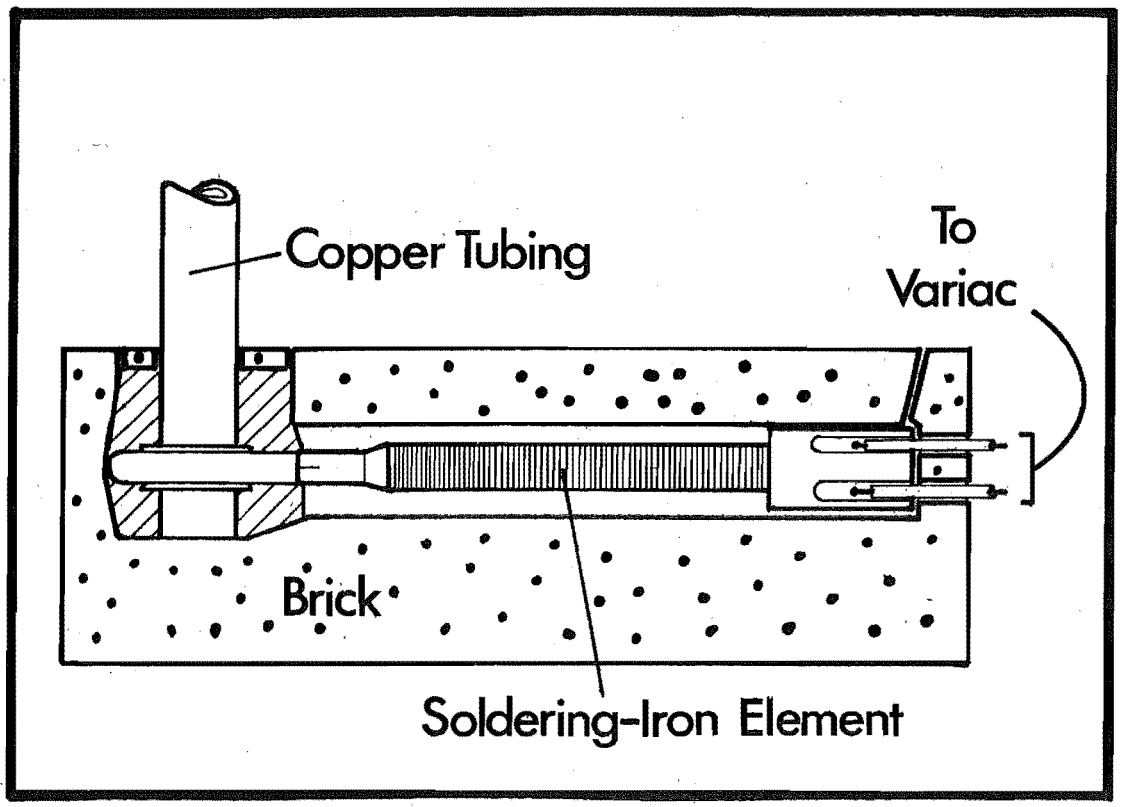

Fig. II-7. THE RESERVOIR OVEN.

(See text for description.)

cement; some junctions were further secured by a wire binding. All thermocouples were referenced to a common cold junction emersed in a melting ice/water mixture; a simple switching system allowed any thermocouple reading to be readily displayed. The digital monitoring unit for the thermocouples was constructed in the department's electronics workshop from an INTERSIL IC L7107 3½ digit single chip digital panel meter wired for a thermocouple probe. By using the temperature/voltage table for the chromel-alumel alloy pair, contained in reference 85 , and a FLUKE 895A d.c. differential voltmeter, the unit's reading in the temperature range 473 K to 573 K was adjusted to give the temperature in degrees Celsius.

Because of problems experienced with the metal to sapphire window seals fracturing, during the early part of the work, it was decided to run the oven at elevated temperatures for an extended period to reduce the strain placed on the window seals by cooling the system at the end of a day's work. The oven was therefore kept above 510 K for five days at a time, after which it was cooled and the valves relubricated.

(3) The Reservoir Oven

The stainless steel finger that served as the metal reservoir extended down through the base of the main oven to the reservoir oven. This oven, too, was carved from a single insulating brick and is illustrated in Fig. II-7.

A length of copper tubing, sheathing the reservoir finger, extended from the reservoir oven up into the main oven to ensure that sufficient heat was conducted along the finger to give it a continuously decreasing temperature from the main oven to the end of the reservoir. Silver soldered around the lower end of this tubing was a "U" shaped piece of copper tubing whose ends fitted into the bit recesses of two 30 W/230 V soldering iron elements. These elements were coupled in parallel to a variable transformer (2 A/230 V VARIAC) and during experiments were operated at about 140 V to maintain 543 K.

(4) The Glass Vacuum Line

The glass vacuum line consisted of two sections; a diagram is given in Fig. II-8. The diffusion pump and associated traps, a main and a small storage bulb, a demountable trap and the gas inlet, constituted the first section. The stop-cocks in this section were the grease-less type (J. Young Scientific Glass-ware Ltd.). A calibrated section of line ran from the manifold of the first section to the metal line. Compartment volumes in this section were calibrated to allow the cell pressure to be determined by an indirect means, for although the BARATRON sensor could be baked to 523 K this temperature fell short of the 550 K that was found to be a suitable experimental temperature.

The section of line between V_1, V_2 and V_3 (see diagram) was uncalibrated but all remaining compartment volumes from

Fig. II-8. THE GLASS VACUUM LINE.

To the left of the discontinuity at X lies the calibrated part of the vacuum line in plan view; to the right is an elevation of the vacuum manifold, small and large storage bulbs, traps, and pumps.

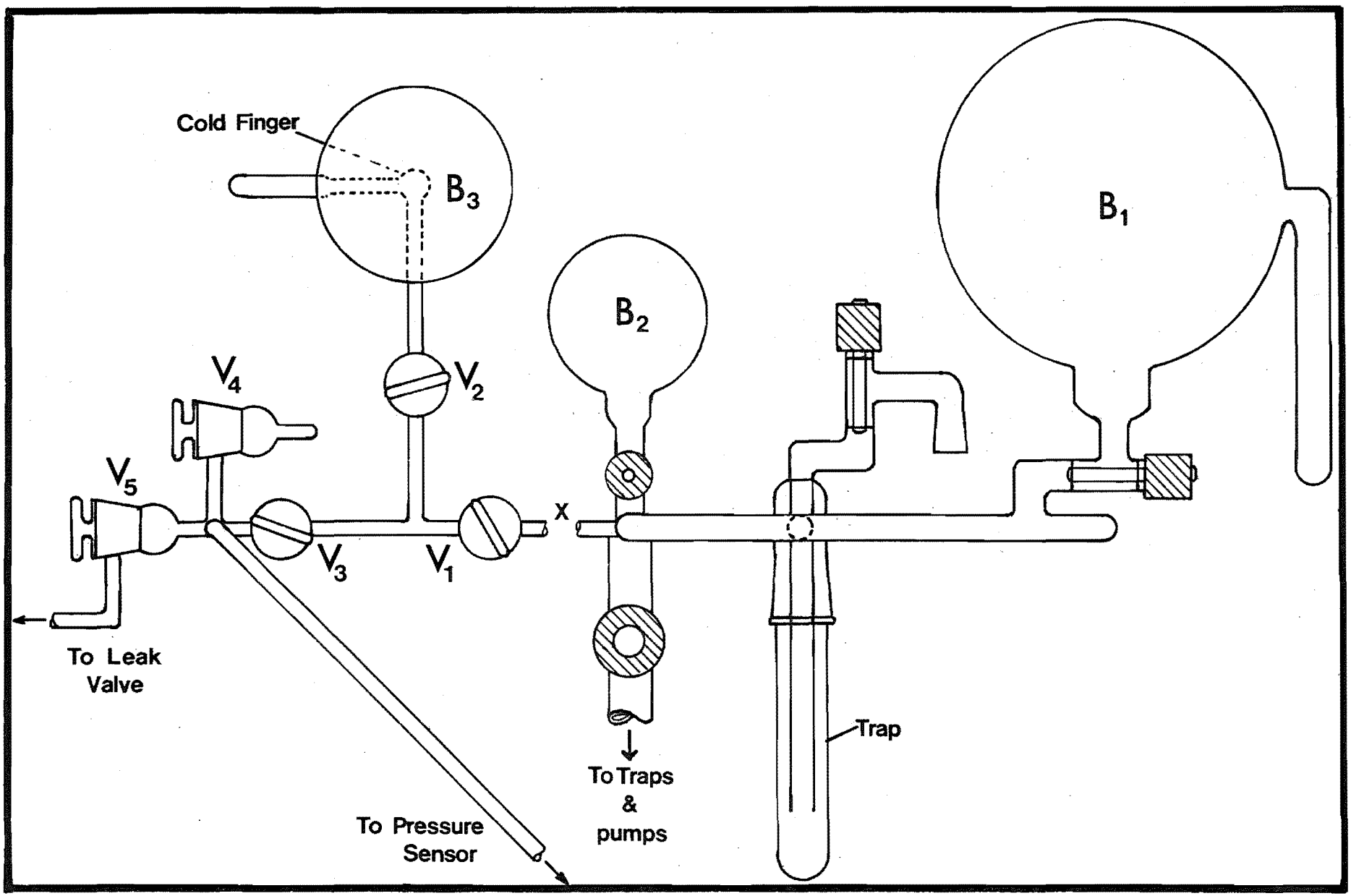

(Caption on facing page.)

V_3 to the leak valve, and the metal cell, were known. The line volumes were determined by expansion of dry nitrogen from the line section defined by V_3, V_4 and V_5 into the known volume contained by V_4. The gas aliquot was then expanded to the leak valve by opening V_5 and finally released into the cell through the leak valve. The determined volumes are given in Appendix A. At each stage in the series of expansions the pressure and temperature were noted. Before it was blown onto the system, the blank section sealed by V_4 was weighed empty, then when filled with water, to allow its volume to be determined.

During some of the early phase measurements greaseless stop-cocks were used in the calibrated section of the vacuum line. However, anomalously small phase-shift measurements were obtained at this time, so, to ensure atmospheric leaks into the ammonia through the valves' teflon sealing rings were not responsible, these stop-cocks were replaced by greased stop-cocks (VAC-SEAL-Jencons Ltd.). Although a layer of fibre-glass insulation was placed on the brick roof of the oven below the calibrated section, the temperature of this part of the glass line could climb to 305 K; the stop-cocks were therefore lubricated with APIEZON "H" grease. Small amounts of ammonia dissolve in stop-cock grease, but the methods of pressure measurement used during the admission of gas to the cell, to be described in section III-1(b), minimized any errors in pressure calculation from this source.

The line pressure, in torr, was read from an MKS BARATRON type 170 M - 27 C Digital Readout Unit used in

conjunction with an MKS type 170 M - 6B Electronics Unit. The differential pressure sensor was encased in the heater shells of an MKS BARATRON 170 M - 39 Temperature Controller which, although designed for operation at temperatures greater than ambient, was set to keep the sensor temperature as close as possible to the calibrated line temperature. When necessary, corrections were made to the direct pressure reading using the manufacturer's calibration data.

The ideal gas equation was used to calculate the compartment volumes from the expansion data, as trial calculations using Berthelot's real gas equation,

$$PV = nRT\left[1 + \frac{9}{128}\frac{PT_C}{TP_C}\left(1 - \frac{6T_C^2}{T^2}\right)\right] \quad , \qquad (2.1)$$

[where P_C = critical pressure, T_C = critical temperature and P,V,n,R and T have their usual meanings] showed that the two equations gave values that agreed within the experimental uncertainties of the pressure measurements. A mercury glass thermometer, graduated in 0.1 K intervals, was used to measure the temperature of the calibrated line.

The indirect method of pressure determination required all temperatures and volumes to be known; both were known for all necessary sections of both vacuum lines except for the section that ran between V_5 and the leak valve. When the oven was heated above the ambient temperature, a thermal gradient existed along this section. To minimize the errors in pressure calculation brought about by this gradient, the volume of this compartment was made as small as possible.

Initially, glass capillary tubing was used for this section but as there was a slight movement in the metal line when the 1½ in. metal valve was closed or opened, in spite of its bracing, the capillary tubing sometimes fractured. Ample flexibility was attained by using stainless steel syringe tubing for this rôle (Fig. II-9). A copper blank was machined to act as the ConFlat gasket for the leak valve; into this blank a hole was bored. Four lengths of the stainless steel capillary tubing were cut, and a brass collar was passed over each end of the bundle. At one end, the capillaries were silver soldered into the collar, which in turn was silver soldered into the gasket blank. At the other end, the capillaries were soft soldered into the collar before it was soft soldered into the ¼ in. Kovar tubing of a Kovar/pyrex adaptor joined to V_5.

(5) The Microwave Lamp

An electrodeless microwave powered lamp was chosen as the light source for this work because of its low self-absorption and simplicity of construction. The final lamp design was a simple sealed length of 13 mm O.D. silica tubing having a silica window fused into one end and a silica rod fused onto the other to allow mounting of the lamp. A flowing lamp was tested, but its performance was below that of the sealed lamp. Moreover, in comparison with the sealed lamp which was easily moved to allow

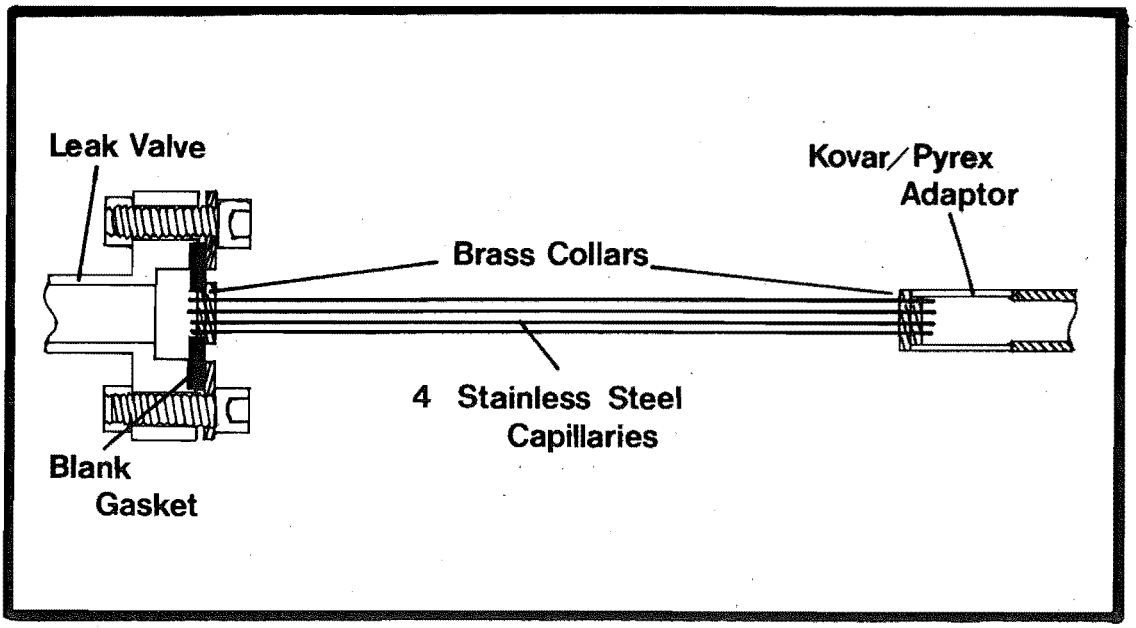

Fig. II-9. THE FLEXIBLE ADAPTOR LINKING THE GLASS VACUUM LINE TO THE LEAK VALVE.

disassembly of the oven, the flowing lamp was cumbersome. The output of the flowing lamp deteriorated with time, partly because of the window "fogging" with condensing metal and partly because of the formation of either a brown cadmium oxide deposit or a cadmium mirror, or both, round the inside of the lamp. The cause of the formation of the cadmium oxide deposit is unclear, but seems to have been peculiar to the flowing lamp, as, except for a very light brown discolouration which probably resulted from the "clean-up" of trace oxygen impurities trapped in the lamp, the sealed lamp showed no sign of this deposit. A sealed cadmium iodide lamp was also tested, but was found to have an intensity inferior to that of the metal lamp.

Fig. II-10 depicts the sealed-lamp blank. The lamp was prepared in a way that loosely followed that given by Gleason and Pertell.[86]

(i) The blank was washed with a mixture of approximately 50% HNO_3 and 50% HCl then rinsed with distilled water and a few pieces of metal were placed in the reservoir finger.

(ii) The blank was blown onto the glass line manifold and flamed (under vacuum) to a dull red colour.

(iii) Several torr of argon was admitted to the line, and the blank "scrubbed" with a Tesla coil for 5 minutes.

(iv) A microwave discharge was run in the lamp at an argon pressure of 7-8 Torr for about 2 hours.

(v) Step (iii) was repeated and the blank evacuated.

(vi) Step (ii) was repeated.

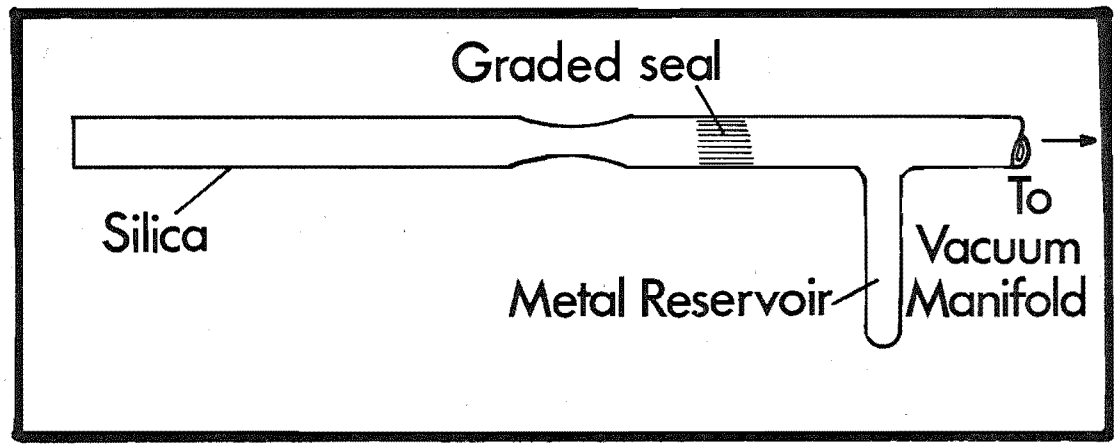

Fig. II-10. THE ELECTRODELESS LAMP BLANK.

(vii) A microwave discharge was run in the lamp, containing 11 Torr of argon, for 2 hours.

(viii) More argon was admitted to the lamp to give a pressure of approximately 23 Torr, and the blank was "scrubbed" again with the Tesla coil while the gas was slowly pumped away.

(ix) The line was opened to the diffusion pump, and the blank pumped on for 30 minutes.

(x) Sufficient cadmium was flamed from the reservoir into the silica tubing to deposit a mirror 2 cm long around the tubing.

(xi) The line was pumped on by the diffusion pump for about 10 minutes.

(xii) Step (iii) was repeated, and the line evacuated.

(xiii) Approximately 6 Torr of argon was admitted to the blank, and the lamp sealed at the constriction.

The lamp's output was a little unstable initially, but after a few hours of operation the intensity fluctuations settled to a level too low to adversely affect the measurements to be made.

To aid in keeping the lamp window hot, and therefore free of condensing metal, a hole to contain the lamp, approximately the same diameter as the lamp, was cut in the brick above the uppermost window of the cell. This arrangement enhanced the light intensity reaching the cell in two further ways. First, cadmium vapour migrating away from the lamp's discharge region tended to be driven back into the microwave field by the high temperature around the

lamp's window, thereby maintaining the metal concentration in the discharge. Secondly, because the lamp window served as the oven's excitation window, the surface losses associated with a window between the lamp and the cell were eliminated.

The microwave generator used to power the lamp was a RAYTHEON CMD-13 unit, modified to enable its output to be modulated. This modification is described by Phillips.[87] The unit's waveguide was mounted in a water-cooled aluminium alloy block (Fig. II-11) to avoid the waveguide overheating during operation because of the lamp's proximity to the oven.

(6) The Laser

For these studies an AVCO Model 4000 dye laser was pumped by an AVCO Model C5000 nitrogen laser (maximum average power output = 500 mW). Because of the relatively high repartition rate (188 Hz) at which the laser was pulsed, a flowing dye cassette was used to circulate the dye.

EXCITON Coumarin 460 dye, which lases over a range from 440 nm - 478 nm (when pumped by a nitrogen laser), was dissolved in ethanol to give a 10^{-2} molar solution for use in the cassette. To extend the dye's life, oxygen was purged from the solution by bubbling nitrogen through it before and after the dye was fed into the cassette.

The spectral bandwidth of the dye-laser output was reduced to about 0.1 nm (nominally) by the use of a telescope consisting of a quartz rod, to give lateral

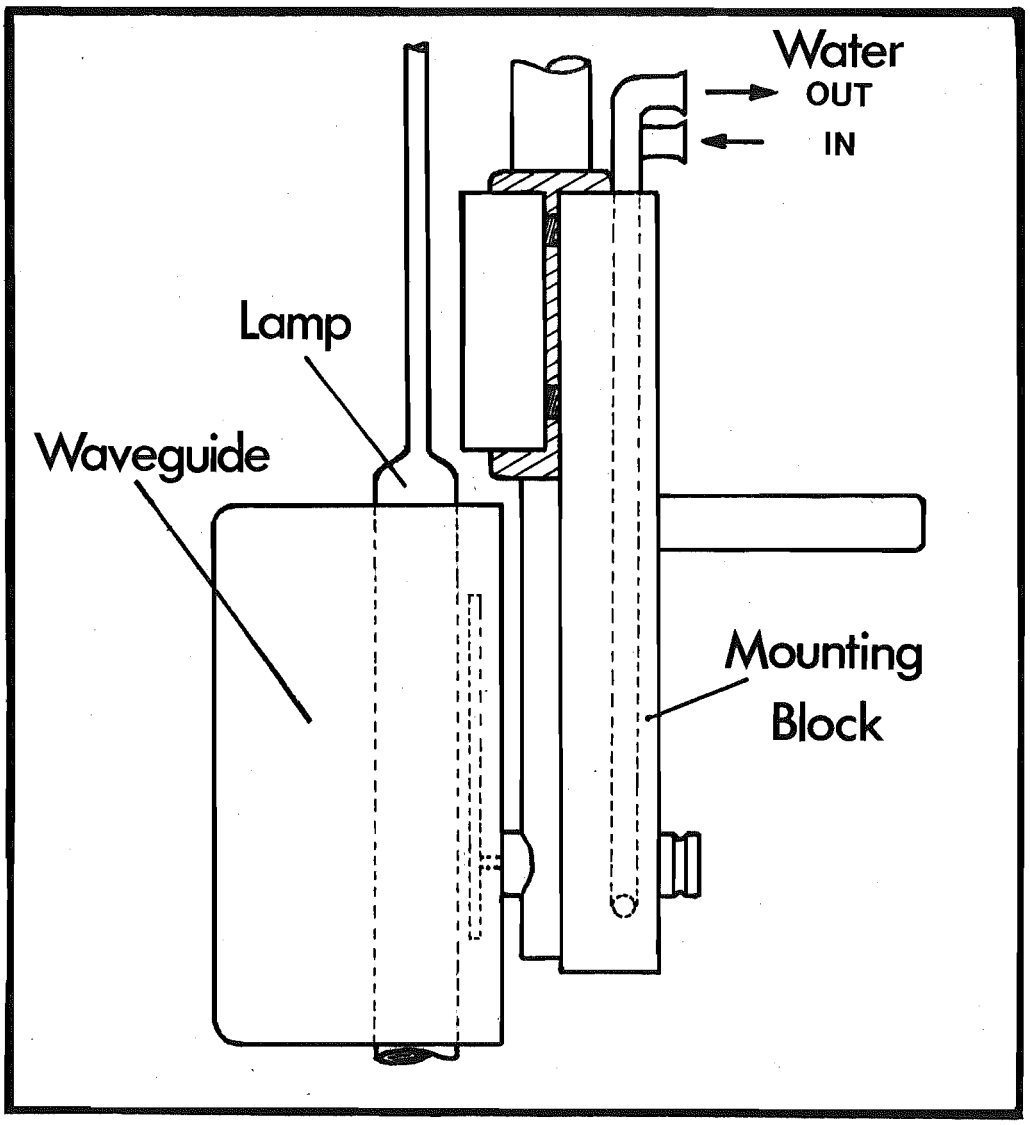

Fig. II-11. THE WATER-COOLED MOUNTING FOR THE MICROWAVE ANTENNA (waveguide).

dispersion of the beam, and a plano-convex collimating lens, to collect and focus the dispersed beam onto the diffraction grating. The effective pulse width of the dye laser was less than 10 ns.

(7) The Microcomputer System

The microcomputer system that collected, stored, and analysed some of the experimental data, was built around a RADIO SHACK TRS-80 microcomputer. Interfaced to the microcomputer were a visual display unit, a print-out unit, and two RADIO SHACK 5¼ in. diameter disk drives. During data storage and analysis, drive "zero" held the Disk Operating System software and the source program, and drive "one" held the disk to which the data was written, or from which the data was read.

Also peripheral to the system was an analog to digital (hereafter A/D) interface designed by Professor L.F. Phillips and constructed in the department's workshops. The 16 channel multiplex A/D converter used in this device was a DATEL MDAS-16 giving 12 bit data resolution and a throughput rate of 50 kHz. The voltage input range was 0 to 10 V.

The software, which will be described in section III-2(b), was written in RADIO SHACK Level II BASIC. The program listings may be found in Appendix D.

II PURIFICATION OF CHEMICALS

(1) Cadmium

The metal used was 99.9998% pure cadmium shot purchased from Kock-Light Laboratories Ltd. (Batch No. 69379) and was used without further purification.

(2) Ammonia

The ammonia used was commercially available gas (Christchurch Gas, Coal and Coke Co. Ltd.). Before being stored in the bulb on the calibrated vacuum line (B_3) the gas was purified in the following way:

(i) The ammonia was frozen into the trap (see Fig. II-8) as the gas was admitted to the vacuum line, then pumped on while the trap was kept immersed in liquid air. Impurities were baked from the walls of the storage bulb B_3 and pumped away.

(ii)(a) The liquid air around the trap was replaced by a dry ice/acetone slush (194 K), and the first fraction of vapour pumped away.

(b) The stop-cock to the storage bulb B_3 was opened and the middle fraction of ammonia distilled into the bulb's cold finger (at liquid air temperature).

(c) The calibrated section of the vacuum line was sealed at V_2 before the last fraction of gas was distilled; this fraction was then pumped away. (If a large amount of gas was left in the trap after B_3 was filled, the remainder was stored in B_1).

(iii) The ammonia was transferred back to the trap and steps (i) and (ii) repeated.

To remove any remaining water or oxygen impurities in the gas stored in B_3, a sodium mirror was deposited in the side-arm extending from this storage bulb. A diagram of the glass-ware used to prepare this mirror is given in Fig. II-12. Sodium metal was washed in heptane to remove adhering paraffin, dried on tissue, cut into pieces, and dropped into the open glass tubing above constriction (1). The end of the tubing was then sealed and the side-arm pumped on to remove the solvent and atmospheric contaminants. By gentle heating with a gas torch the sodium could then be melted and run down into the next compartment leaving behind the crusty oxide. Further pump-down followed, after which, the first constriction was sealed and the upper section drawn off.

This process was repeated until the metal lay in the bottom of the vertical tubing and constriction (3) had been sealed. The metal was then heated while the side-arm was pumped on, until a thin mirror developed along the side-arm walls. Once the mirror was deposited the last constriction was closed, and the compartment containing the residue drawn off.

As small amounts of hydrogen may have formed by reaction between the mirror and ammonia during storage, the gas was frozen in the bulb's cold finger, pumped on, thawed, and this process repeated before each set of experiments.

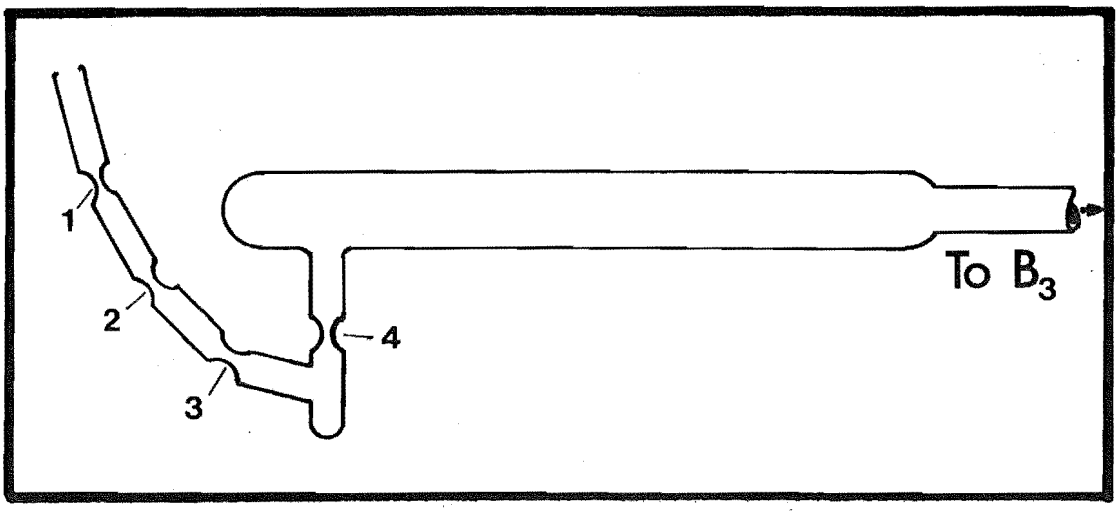

Fig. II-12. THE GLASS-WARE USED TO PREPARE THE SODIUM MIRROR FOR THE STORAGE BULB B_3.

(See Fig. II-8.)

III MEASUREMENT TECHNIQUES AND EXPERIMENTAL PROCEDURES

(1) Lock-in Amplifier Measurements

(a) Light Detection and Instrumentation. Except for a few lock-in amplifier measurements made at the pressure extremes (using the same light detection system as the boxcar measurements), no attempt was made to isolate the 326.1 nm line from the lamp during experiments with the PAR HR-8 lock-in amplifier (Princeton Applied Research Corporation). The emission from the cell was viewed at the small sapphire window through a SPEX MINIMATE monochromator (grating blazed at 500.0 nm with 1200 grooves/mm), set on its side for reasons of vacuum line geometry, by a dry-ice-cooled EMI 6255 photomultiplier. The spectral sensitivity of this monochromator/photomultiplier combination was determined, as described in section III-4(b), and is presented graphically in Fig. II-13.

Before the photomultiplier signal was taken to the lock-in amplifier it was amplified by a low noise FET preamplifier (Fig. II-14) designed by Mr R. Hooper. The preamplifier's output was fed to the "A" input (10 MΩ) of the lock-in amplifier's A-type differential preamplifier, and a dummy cable was connected to the "B" input to act as an aerial equivalent to the signal cable. The same earthed shielding enclosed both cables from the photomultiplier housing to the input jacks. With the preamplifier set to subtract the input at "B" from the input at "A", this arrangement minimized the distortion of the signal by aerial pick-up emanating from the microwave generator's waveguide.

Fig. II-13. LOG OF THE MONOCHROMATOR/PHOTOMULTIPLIER RELATIVE SENSITIVITY AS A FUNCTION OF WAVELENGTH.

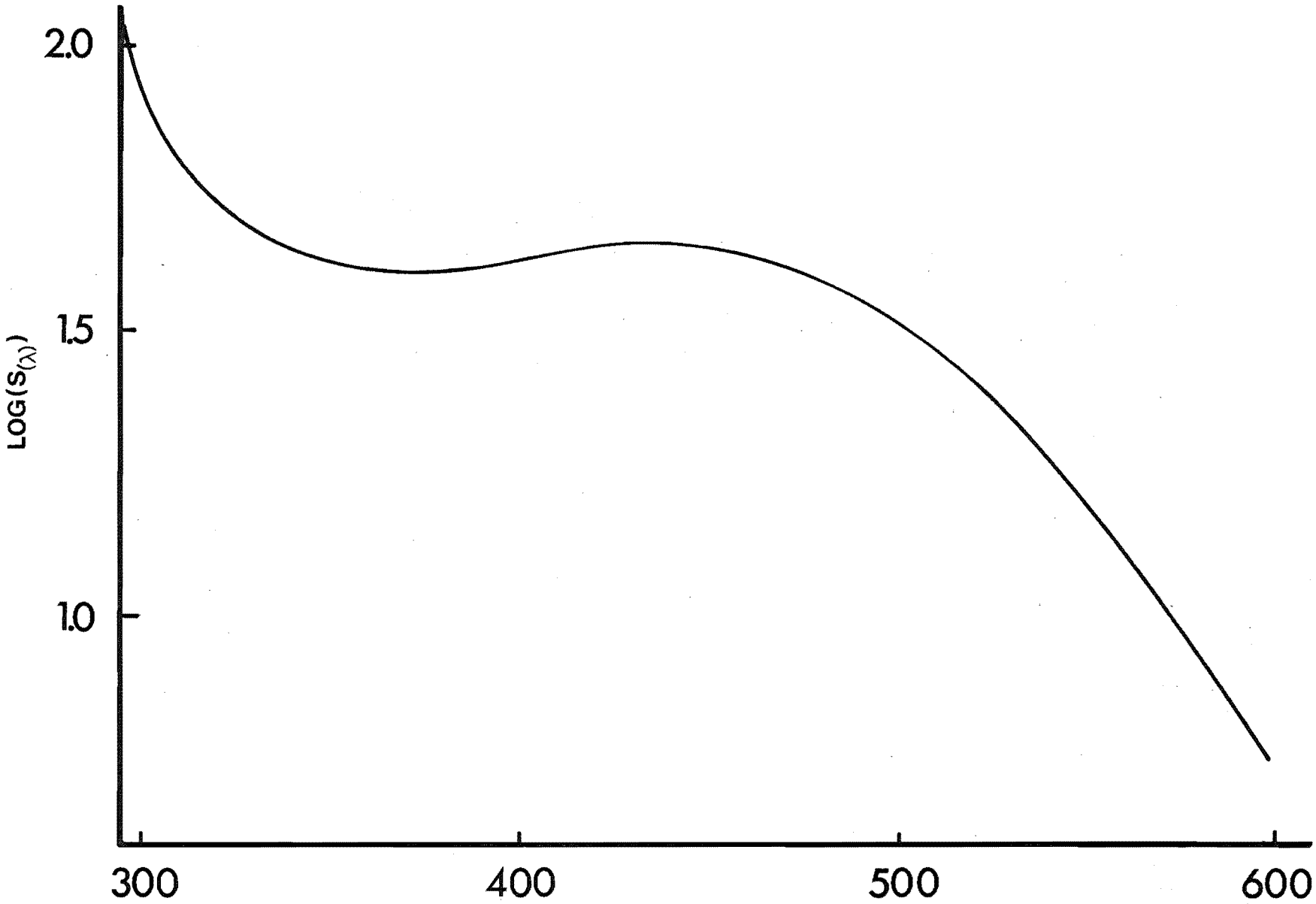

(Caption on the facing page.)

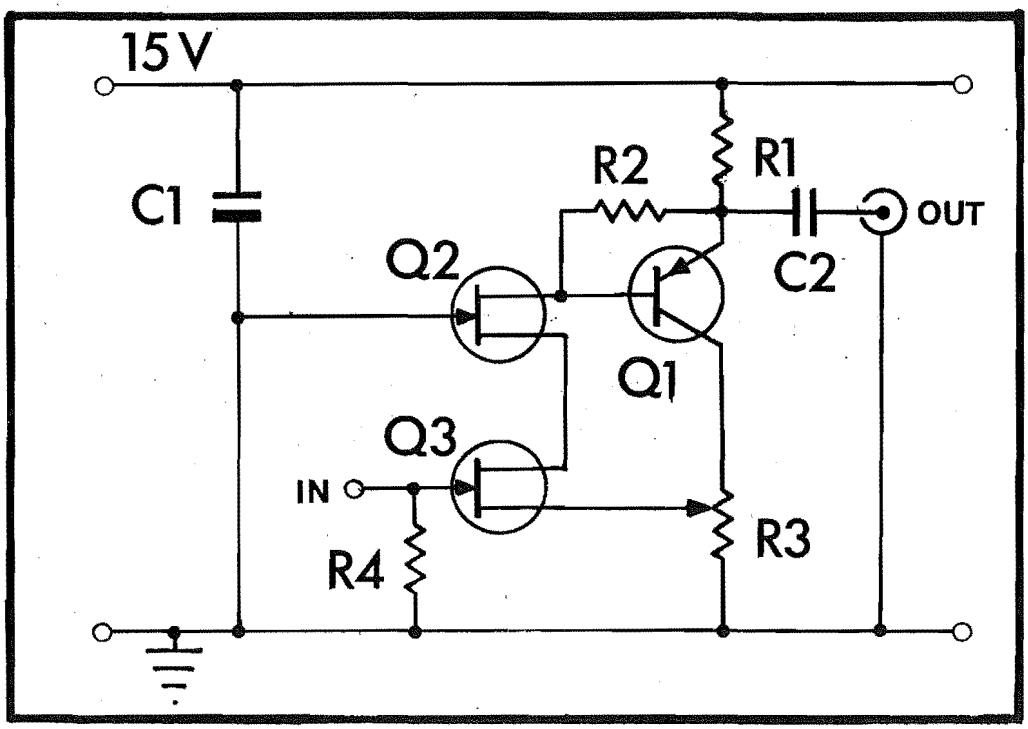

Fig. II-14. FET LOW-NOISE PREAMPLIFIER CIRCUIT (Lock-in amplifier measurements).

R1 = 1.5 kΩ R2 = 2.7 kΩ R3 = 500Ω

R4 = 100 kΩ C1 = 10 μF C2 = 10 kpF

Q1 = 2N5227 Q2 = 2N4221 Q3 = 2N4220A

Input impedance up to 1000 MΩ depending on the gate leakage of Q3.
Voltage gain = 5.

Within the lock-in amplifier, the signal and any accompanying noise, having been amplified, passed to a tuned amplifier. This amplifier rejected any components of the incoming signal that did not occur at its tuning frequency. The amplifier's resonant frequency, which was the experiment's modulation frequency, and its "Q" factor, which determined the rate at which signal harmonics, mains pick-up and white noise outside the amplifier's band width were attenuated, were set at the instrument's front panel. An intermediate "Q" value of 10 was chosen for these studies.

After this stage the signal passed to the mixer, or phase-sensitive detector, where its phase was compared with that of a phase-shifting network. The mixer's output is given by,

$$\text{Signal}_{(\text{Out})} = \text{Signal}_{(\text{In})} . \text{Cos}\ \phi \qquad (2.2)$$

where ϕ is the phase shift between the instrument's reference signal and the experimental signal. Therefore, as the phase of the phase-shifting network is adjusted to compensate for phase delays in the experiment, and ϕ tends to zero, the instrument's meter reading is maximized. In consequence of this relationship, the most sensitive condition under which the phase relationship between the reference and the experiment can be determined, is with the two in quadrature (i.e. 90° out of phase), as the change in cos ϕ with ϕ is most rapid at this point.

The last stage of the instrument, from where the signal is passed to the meter, is an integrator (having a variable time constant) whose function is to minimize noise

spikes that have passed through the preceding circuitry.

To modulate the lamp, the lock-in amplifier's internally generated reference signal was taken to a Schmitt trigger (Fig. II-15) where the sine wave was squared, amplified, and fed to the microwave generator. A potentiometer in the Schmitt trigger provided a means of adjusting the mark/space ratio of the output square wave, which was otherwise asymmetric, so that a symmetric wave could be passed to the generator's modulation circuitry. The modulation frequency for each experiment was set while monitoring the frequency driving the Schmitt trigger with a HEWLETT-PACKARD HP 5318A digital frequency counter.

(b) Experimental Procedure. After the ammonia had been purified as set out in section II-2, a set of phase measurements was conducted in the following manner.

The metal vacuum line was heated to run temperature and pumped on as it came to thermal equilibrium. When the system was heated from room temperature this process took about 4 hours; if the oven had been maintained at an elevated temperature overnight the equilibration time was correspondingly reduced. If the cell had been open to the atmosphere before an experiment, it was found necessary to thoroughly bake the metal line for about 6 hours at a temperature of 640 - 660 K. Failure to do this resulted in anomalously small phase shifts being obtained because of adsorbed contaminants on the cell walls being released into the gas mixture during measurements. As a precaution, this high temperature bake-out was also conducted after the pumping and heating systems had been

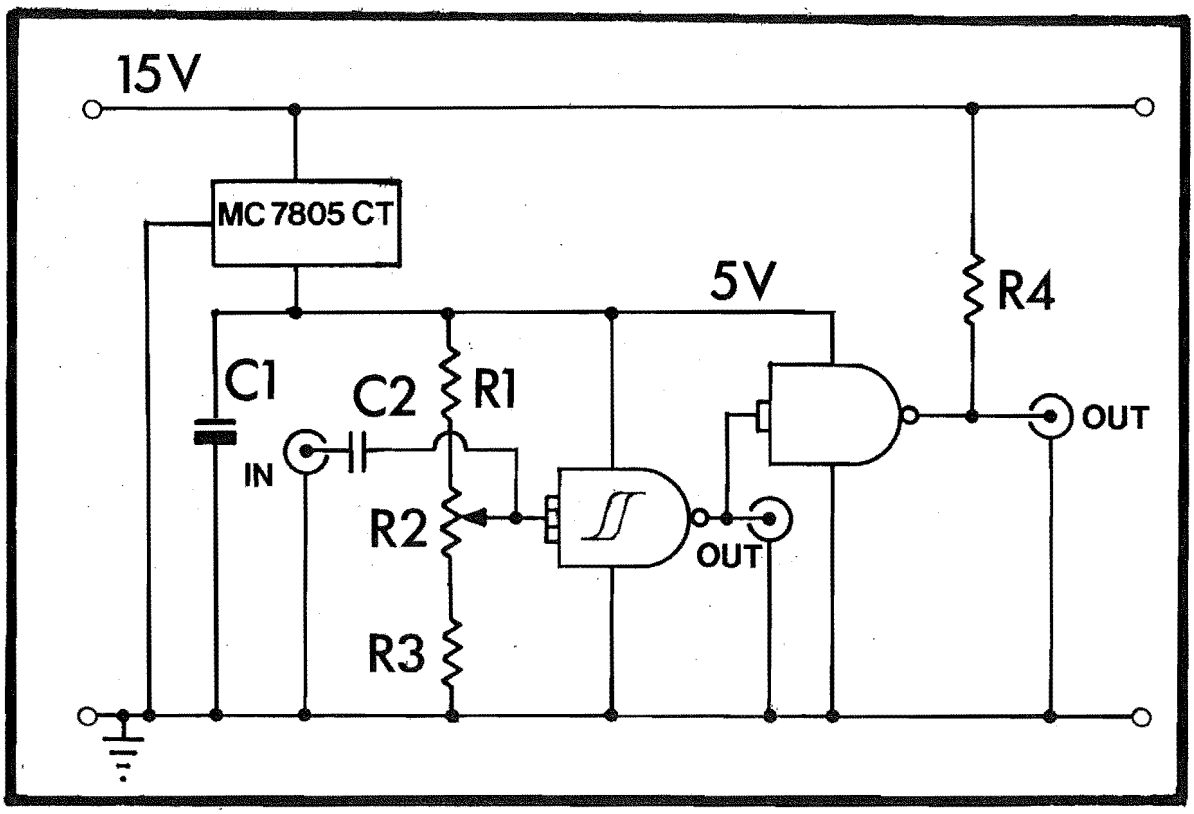

Fig. II-15. SCHMITT TRIGGER CIRCUIT.

R1 = 2.2 kΩ R2 = 10 kΩ R3 = 1 kΩ

R4 = 470 Ω C1 = 6.4 μF C2 = 1.5 μF

Schmitt trigger = 7413 NAND gate = 7407

Output from the Schmitt trigger = 5 V pk-pk.
Output beyond NAND gate ≃ 10 V.
Max. input voltage = 5 V.

closed down for an extended period. Between high temperature bake-outs, a pump-down of the system as it came to thermal equilibrium was sufficient to prepare the cell for an experiment. Once the reservoir temperature reached 500 K during the bake-out, the Mini-Valve was closed to avoid pumping away too much of the metal. The residual pressure in the cell (at 550 K), after preparation, was usually $2\text{-}4 \times 10^{-6}$ Torr.

After the thermal equilibration of the system, the thermocouple readings were noted, the pressure gauge zeroed, the leak valve closed and the Mini-Valve opened eight turns (the number provided for in the volume calibration). Following this, the cell was sealed at the 1½ in. valve, V_1 in the glass vacuum line was closed (V_4 and V_5 were already closed), and ammonia was bled from the storage bulb through V_2.

If the change in the gas pressure in the calibrated line, for the required pressure rise in the cell, was estimated to be less than 80 Torr, the BARATRON gauge was operated on its 0.01 - 100 Torr range, allowing a pressure of up to 109.99 Torr to be measured to a precision of $\pm$ 0.02 Torr. The 0.1 - 1000 Torr range (uncertainty, $\pm$ 0.1 Torr) was used if a greater pressure change was required. Whichever the case was, V_3 and V_2 were then closed, and the pressure was allowed to equilibrate; adsorption of ammonia onto the glass walls and the loss of gas into the stop-cock grease resulted in an initial pressure drop.

To admit an aliquot of gas to the cell, the pressure in the compartment V_5-V_4-V_3 was noted, the leak valve opened,

and ammonia bled through V_5 until the required pressure change was reached. V_5 was then closed, rapidly followed by the leak valve, and the new pressure in the calibrated line and the line's temperature were noted.

Next, with the microwave lamp operating, the monochromator setting was adjusted to pass the 326.1 nm intercombination line, or the luminescence at 430 nm, and a number of readings, in quadrature, of the angle between the emission signal and the instrument's reference signal were made. The number of readings depended on their reproducibility; usually measurements were noted until three consecutive values, differing by 0.3° or less, were obtained. The other wavelength was then moved to, and phase measurements were made in the same way. At times, a second set of readings were taken at the first wavelength to ascertain whether there was a drift in the phase readings. If a significant change was found, the two sets were averaged. Pairs of measurements were made in this way at 20, 30, 40, 50 and 60 kHz before a further aliquot of gas was admitted to the cell, and the next set of phase readings taken. When it became necessary to recharge the volume contained by V_3, V_4 and V_5, V_1 and V_3 were opened, and the whole section evacuated before fresh gas was admitted.

Using Berthelot's equation for real gases (see section I-4)[‡] the increase in cell pressure was calculated from the moles of gas lost from the calibrated line. For this calculation it was assumed that the gas did not reach

---

‡ For NH_3 $P_C = 8.474 \times 10^4$ Torr
$T_C = 405.6$ K

thermal equilibrium before the leak valve was closed, and therefore, that the gas lost from the calibrated line was approximately evenly distributed throughout the cell and the volume between the leak valve and V_5. The error involved in this assumption is indeterminable, but small, because of the small volume contained between V_5 and the leak valve.

When more than one aliquot had to be admitted to the cell, the cell pressure was calculated from the summed contributions of the moles of gas from each aliquot. (The cell pressure could also have been calculated by subtracting the pressure reading of the calibrated line, after the final aliquot was admitted, from the reading before the admission of the first aliquot. This would have reduced the random uncertainty in the calculation. However, the chosen method was employed, because the possibility of a drift in the calibrated line temperature, and the effects of ammonia dissolving into the grease and adsorbing onto, or desorbing from, the glass walls, would have introduced into the second method of calculation a systematic uncertainty of unknown magnitude.)

(2) Boxcar Integrator Measurements

(a) Light Detection and Instrumentation. Detection of the $^3P_0$ level required at least one of the atomic lines resulting from a transition from the $^3S_1$ state to one of the ^3P_J levels (467.8 nm, 480.0 nm, 508.5 nm) to be detectable after the laser probe photon at 467.8 nm ($^3P_0$ - $^3S_1$) had

been absorbed. In principle, the fluorescence at 467.8 nm was as suitable as the other two lines, but in practice, as the lifetime of the upper level of the transition was of the same order of magnitude as the laser pulse duration, the fluorescence became buried in scattered laser light.

Attempts to observe the LIF on either of the other two transitions, using the monochromator, were unsuccessful for two reasons. First, the already low intensity of the LIF was drastically attenuated by the monochromator. When the slits were widened to increase the light incident on the photomultiplier, a signal associated with the laser output that was not the LIF (possibly the dye's fluorescence band) was also passed by the monochromator, making distinguishing between the presence and absence of the LIF signal extremely difficult. Secondly, because the accuracy of the laser's tuning could only be judged by the presence or absence of the fluorescence signal from the $^3S_1$ state, it was impossible to tell whether the laser's tuning, or the monochromator's orientation or setting, was to be held responsible for the lack of LIF signal. This applied especially when narrow slit pairs were in use.

The failure to observe the fluorescence from the $^3S_1$ state using the monochromator led to a system of filters being used to isolate the required wavelengths. The mounting for the filter and photomultiplier is illustrated in Fig. II-16.

The exciting light from the lamp was filtered using a disc of CORNING CS 7-54 glass filter cut to fit into the recess above the excitation sapphire window seal so not to disturb the hot air flow pattern around the cell. At 326.1 nm

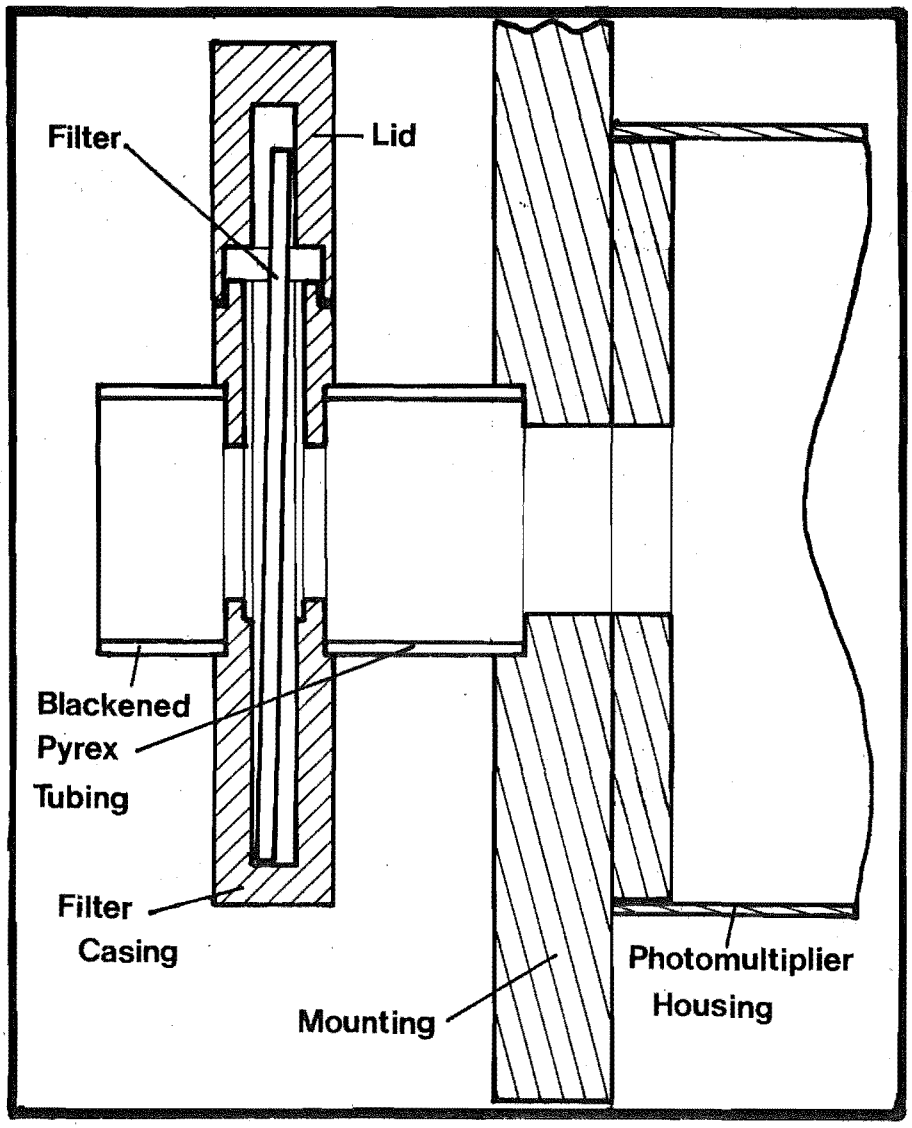

Fig. II-16 THE FILTER AND PHOTOMULTIPLIER MOUNTING.

this filter has an 85-90% transmittance. Three filters were used to isolate the three emission wavelengths. An interference filter, with a transmittance of about 10% at 326.1 nm, was employed to isolate the intercombination line; the exciplex luminescence was viewed through a CORNING CS 3-74 glass filter, and the $^3P_2$ - $^3S_1$ transition fluorescence was passed by a CORNING CS 3-70 glass filter (20-25% transmittance at 508.5 nm).

The photomultiplier viewing the emission from the cell was the same EMI 6255 tube (dry-ice-cooled) used in the lock-in amplifier work, but the preamplifier used in conjunction with it had a shorter response time than that first used. The circuit diagram of this fast preamplifier, designed by Mr J. Sherriff, is given in Fig. II-17. From the photomultiplier's preamplifier the signal was taken to the 100 kΩ input jack of the PAR model 160 boxcar integrator. Briefly, the boxcar operates as follows.

After an external trigger is applied to the instrument a time base voltage ramp is generated; typically there is a delay of about 150 ns between the trigger and the initiation of the ramp. Trigger pulses with risetimes as short as 10 ns and at frequencies up to 250 kHz are accepted. The time base can range in duration from 2 μs to 20 s, and at some predetermined point along it, from 5% to 100% of the time base the input circuitry is gated open and the experimental signal is sampled. The duration of the gate (the aperture time) can be set at any value ranging from 10 ns to 0.55 s, and to allow the recovery of the full experimental waveform, the gate can also be scanned across the time base at a rate

Fig. II-17. FAST PREAMPLIFIER CIRCUIT (Boxcar measurements).

R1 = R2 = R5 = 47 Ω

R3 = 3.9 kΩ R4 = 470Ω

R6 = 2.2 kΩ R7 = 100 Ω

R8 = 220 Ω R9 = 10 Ω C1 = 220 µF

C2 = 0.22 µF C3 = 0.022 µF

C4 = 1 µF Q1 = Q2 = Q3 = BFX 89

Zener diode = 4.7 V

Input impedance = 1 kΩ
Max. input impedance = -0.3 V
Voltage gain = 6
N.B. Input power supply must be constant current not constant voltage.

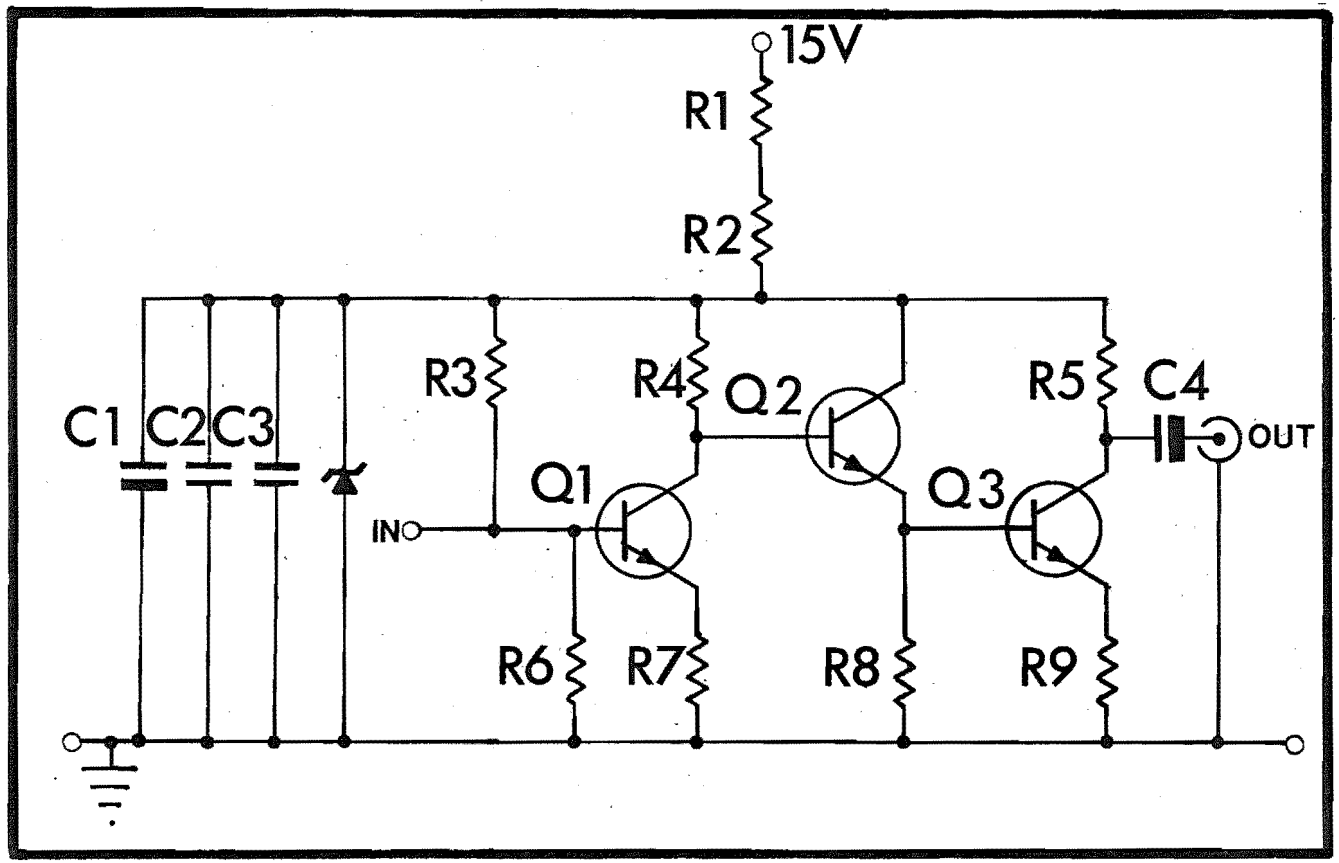

of from 1 to 1000 minutes per scan. After the instrument's circuitry is gated open the input signal passes to an integrating operational amplifier whose storage characteristics are determined by the time constant setting.

A trigger output jack allows an experiment to be triggered from the instrument at some fixed interval after the boxcar is triggered, or for the trigger to be scanned synchronously with the gate along the time base. The latter mode was used to retrieve the waveforms for this study.

Usually it is difficult to simultaneously attain the optimum settings for all of the boxcar's parameters, so, if a waveform is to be scanned and recorded faithfully, a compromise between these settings must be reached. Often the particular experimental conditions will dictate the settings of one or two parameters, leaving the experimenter with a limited choice of the others if he is to obtain the best results from the instrument. The settings for this work are given, and the reasons for their choice discussed, in section III-2(c).

As Fig. II-18 shows, the experiment's trigger signal originated from the lock-in amplifier (its internal reference signal) from where it passed through the Schmitt trigger to the microwave generator and the boxcar. To trigger the boxcar, the squared sine wave was taken from the Schmitt trigger, before the signal was amplified for the microwave unit (see Fig. II-15), through a frequency divider (Fig. II-19) to the boxcar's trigger input jack. The frequency divider was necessary because although the boxcar could be operated at frequencies up to 250 kHz, the laser's maximum operating

Fig. II-18. BLOCK DIAGRAM OF THE INSTRUMENTATION USED FOR WAVEFORM RETRIEVAL EMPLOYING THE BOXCAR INTEGRATOR.

The arrows indicate the direction of triggering signals and information flow. Waveforms on the diagram give a qualitative indication of the transformation in the signal passing through the various stages.

Key: A = amplifier to laser; AD = A/D interface; BI = boxcar integrator; C = fluorescence cell; D = disk drives; DL = dye laser; FD = frequency divider; HV = photomultiplier high voltage supply; L = microwave powered lamp; LA = lock-in amplifier; MC = TRS-80 microcomputer; MG = microwave generator; NL = nitogen laser; PM = photomultiplier; O = oscilloscope; R = X-Y recorder; ST = Schmitt trigger; V = 15 V supply.

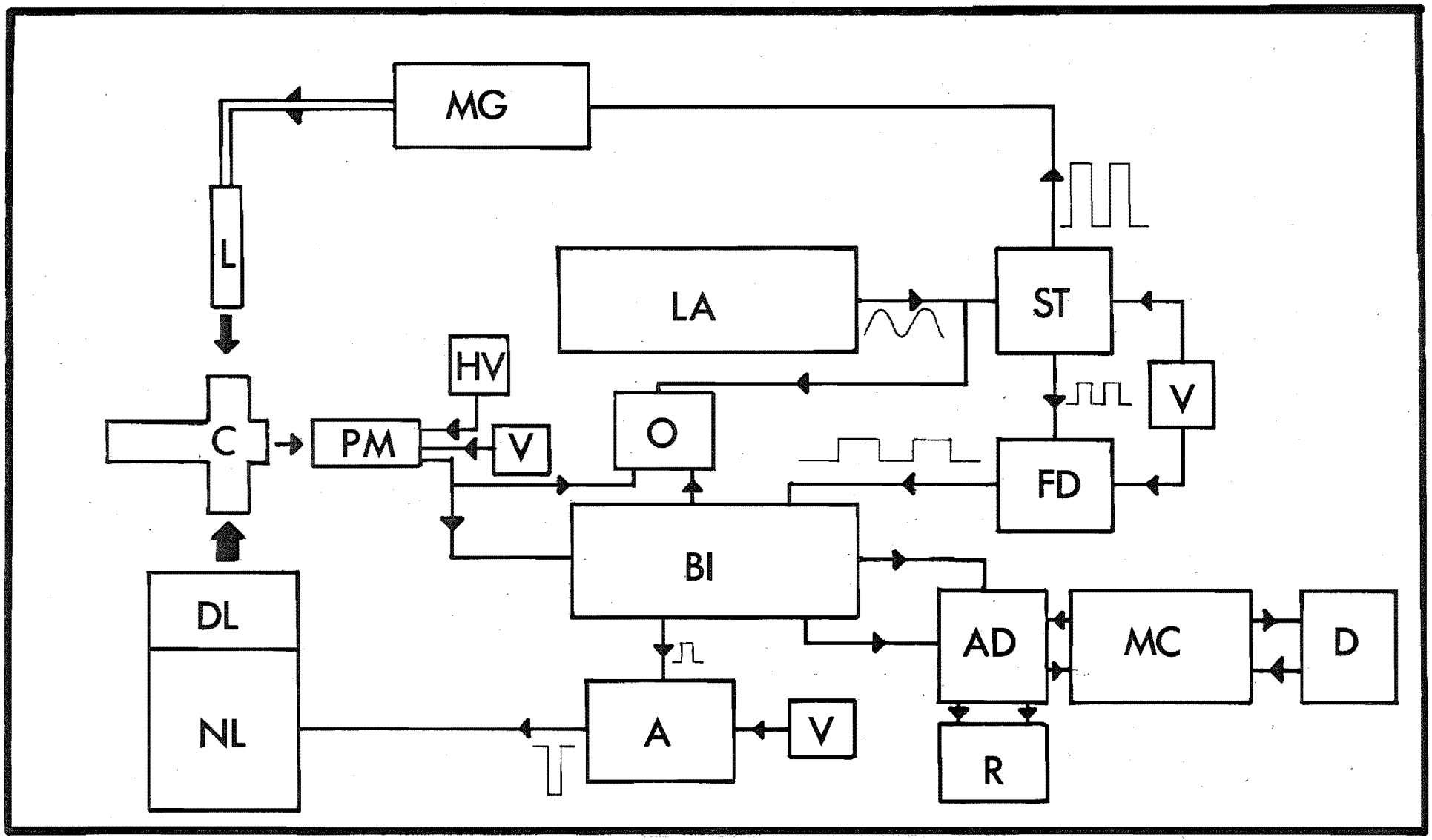

(Caption on facing page.)

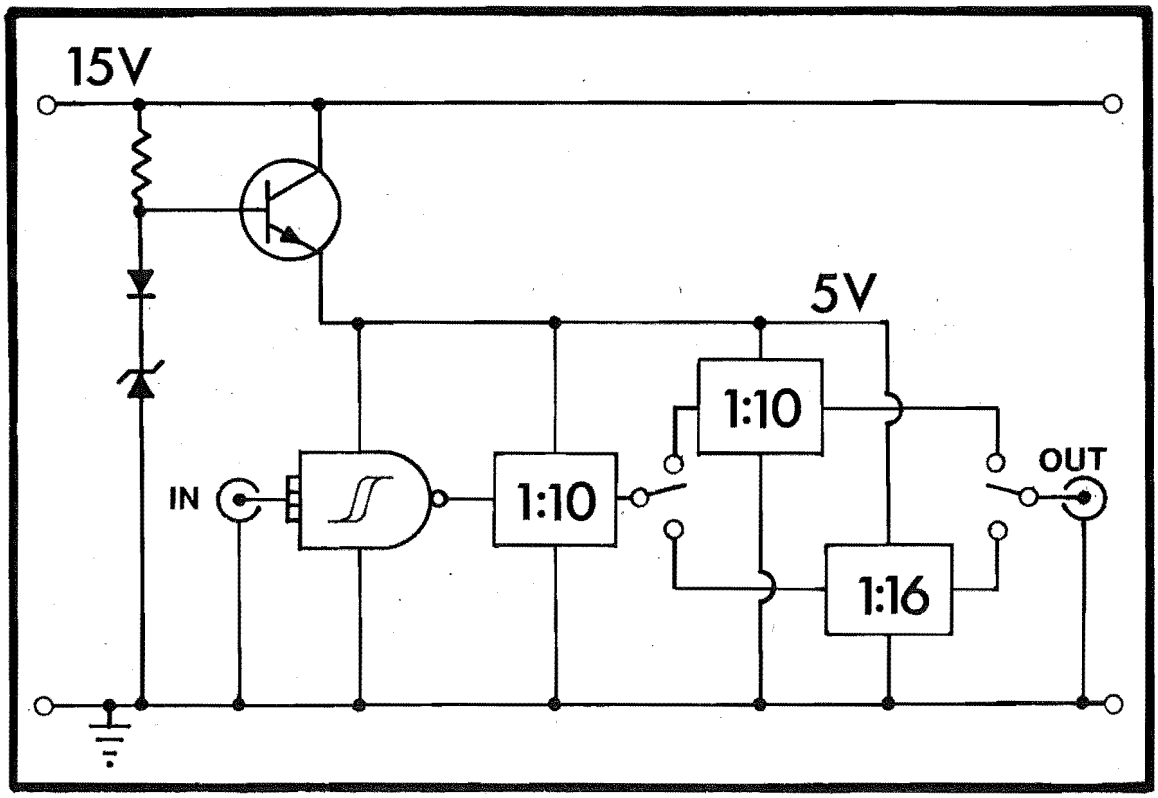

Fig. II-19. FREQUENCY DIVIDER CIRCUIT.

Zener diode = 4.7 V Resistor = 470 Ω

Transistor = 2N3053 Schmitt trigger = 7413

1:16 divider = 7493 1:10 divider = 7490

Max. input voltage = 5 V
Output = symmetric square wave 5 V pk-pk.

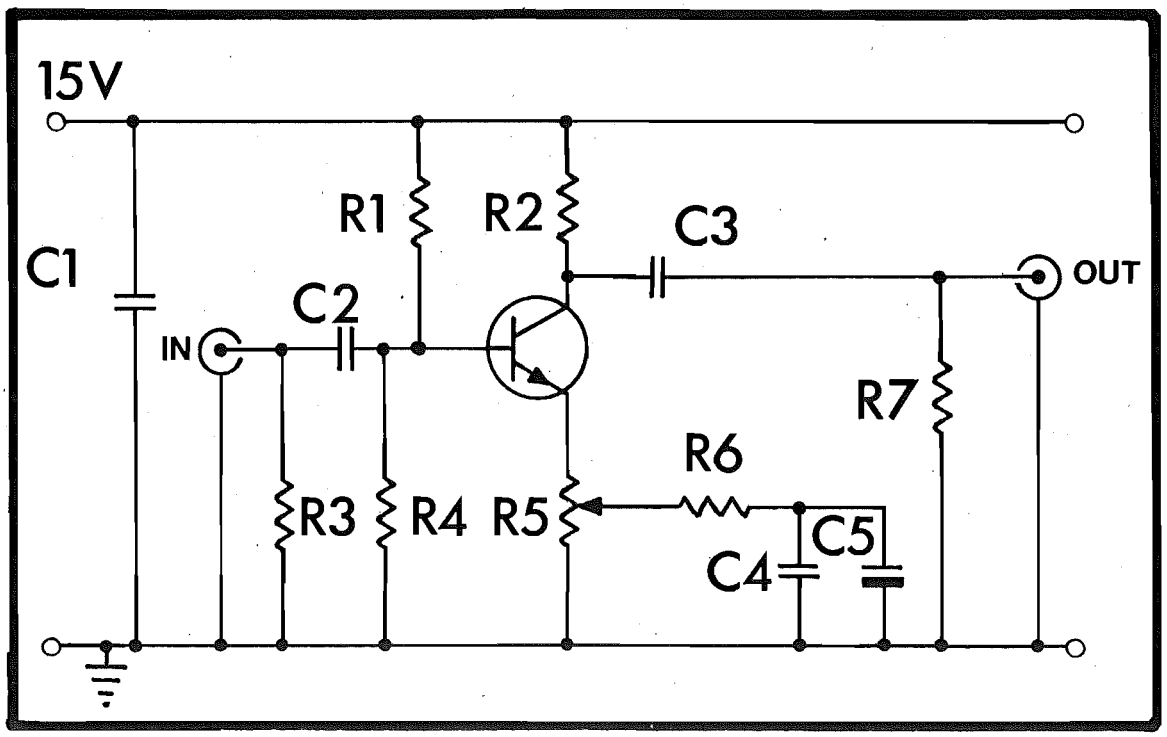

Fig. II-20. CIRCUIT OF THE AMPLIFIER TRIGGERING THE LASER.

R1 = 15 kΩ	R2 = 1 kΩ
R3 = 56 Ω	R4 = 4.7 kΩ
R5 = 470 Ω	R6 = 47 Ω
R7 = 100 kΩ	C1 = C4 = 0.1 μF
C2 = 0.47 μF	C3 = 0.47 kpF
C5 = 10 μF	Transistor = BC 293B

Input impedance = 50 Ω
Voltage gain = 5 - 20.

frequency was only 500 Hz. The frequency divider provided division by 100 or 160, and in both cases its output was a symmetric square wave.

The delayed trigger output from the boxcar was fed to an amplifier (Fig. II-20) whose output was taken to the laser control console. Initially, a monostable multivibrator was used to provide the voltage required to trigger the laser circuitry, but because switching transients from the laser's coolant compressor made the multivibrator misfire, it was replaced by the amplifier which was unaffected by these transients.

The averaged signal available at the boxcar's "Inverted Output" jack and the time base voltage, also available at the rear of the instrument, were taken to the microcomputer by way of the A/D interface. The data were accumulated in the processor and eventually stored on disk for future Fourier analysis. The routine for the Fourier analysis and that for the data collection from the boxcar were written by Professor Phillips.

(b) TRS-80 Software

(i) Fourier Analysis Routine. The Fourier analysis program provided a visual display of the collected waveforms and carried out the calculation of the waveforms' phase shifts.

The modulated exciting light, and the fluorescence and luminescence resulting from the periodic excitation, can be described by a Fourier series of the form:

$$f(\omega t) = \frac{b_0}{2} + \sum_{n=1}^{n=\infty} [a_n \sin(n\omega t) + b_n \cos(n\omega t)] \quad . \qquad (2.3)$$

Alternatively, rather than a series of sines and cosines, $f(\omega t)$ can be expressed solely in terms of cosines or sines if a phase angle is introduced into the the expression[88]. Thus,

$$f(\omega t) = \frac{b_0}{2} + \sum_{n=1}^{n=\infty} A_n \, \mathrm{Sin}(n\omega t + \phi_n) \tag{2.4}$$

where

$$A_n^2 = a_n^2 + b_n^2 \tag{2.5}$$

and

$$\phi_n = \tan^{-1}\left(\frac{b_n}{a_n}\right) \tag{2.6}$$

If the exciting modulation is considered to be a symmetric square wave that "switches on" at $\omega t = -\frac{\pi}{2}$ and "switches off" at $\omega t = \frac{\pi}{2}$, $f(\omega t)$ is expressed as a series of sine terms so that b_n equals zero, and consequently, so does ϕ_n. Hence, ϕ_1 for any observed emission will be the lag of that emission's fundamental frequency with respect to the exciting light.

The numerical integration subroutine calculated A_1 and ϕ_1 through the expressions,

$$a_1 = \frac{1}{\pi} \sum_{j=1}^{m} I_j \sin(\theta_j)\Delta\theta_j \tag{2.7}$$

and

$$b_1 = \frac{1}{\pi} \sum_{j=1}^{m} I_j \cos(\theta_j)\Delta\theta_j \quad , \tag{2.8}$$

where m is the number of data points between the points corresponding to 0° and 360°, I_j is the signal intensity at the jth point, θ_j is the angle to which the jth point corresponds and $\Delta\theta_j$ is the angle increment between the jth and (j-1)th points.[88]

Having read the data file to be analysed from the disk, the routine presented the waveform, or a fraction of it, on the visual display unit at a resolution selected by the experimenter. This display of the collected waveforms served two purposes: it allowed the data file to be checked to ascertain whether errors had occurred during the transfer of data to, or from, the disk, and it enabled the data points corresponding to 0° and 360° to be determined. These two points were taken as the points in the 326.1 nm fluorescence waveform, that reflected two successive "switch ons" of the lamp, that is, the points at two successive intensity minima. Once these points had been determined by eye, they were returned to the program to obtain ϕ_1 and A_1 for all three species.

Although phase calculations using the integration boundaries determined by this method were made, an improved method of boundary determination was used for the final calculation (section III-2(c)).

(ii) A/D Interface Routine. The A/D interface routine's task was to control the sampling of data from the boxcar and to write the collected data to a disk files.

Two A/D input ports of the interface unit received separately from the boxcar the averaged signal intensity (0-10 V) and the time base ramp (0 - 10 V). Along with the run's title and the number of data points collected during the run, the data points were written to the disk files as a voltage pair, one voltage being the intensity datum and the other the time base ramp voltage at which the point was collected.

The first version of this routine provided a choice of the means by which the rate of data collection was controlled; data transfers (from the boxcar to the microprocessor) could be activated at constant time intervals or at constant voltage intervals along the time base ramp. Both intervals were variable, and the ultimate rate of data collection in both cases was limited by the speed of execution of the BASIC subroutine. At constant time intervals the fastest execution would allow the collection of about 100 points/minute while at a voltage interval of 0.02 V (maximum rate for this subroutine) about 260 points/minute could be collected.

When the subroutine that transferred data at constant time intervals was in use, the boxcar's scan had to be started manually after the data transfer was started. This resulted in a variation between runs of the point in the datafile that corresponded to the beginning of the scan. Although there was no variation in which point of the datafile was the first of the scan when the data were collected at voltage intervals, there was some variation in the first point's time-base voltage, as this value was set manually.

The determination of the 0° and 360° points in the first trial experiments to obtain the phase delays between the three species, was by a modified version of the method outlined in section III-2(b)(i). Rather than all the analyses using the 0° and 360° points found from the 326.1 nm fluorescence, the two points were found independently for each waveform. Using this procedure, the variation in the scan start presented no problem as the relative positions

of the minima in the data file, or along the time base, were immaterial. However, when these phase calculations yielded nonsensical values for the lags between the three species, it became apparent that the 0° and 360° points had to be taken at the same instant along the time base for all waveforms irrespective of whether these points corresponded to intensity minima for all species. To ensure this, the jth data point had to be the same interval along the time base in all data files.

Furthermore, in these test runs long scan times were used to accommodate the large time constants necessary to obtain a reasonable signal to noise ratio.‡ This was found to be unsatisfactory for two reasons. First, despite all the precautions taken to keep the instrumentation as cool as possible, the laser's protection relays and its triggering circuitry sometimes malfunctioned in the warm room. These malfunctions, which either shut down the whole laser unit or just stopped it firing, became more frequent with an increased room temperature or a decreased air circulation within the room; shorter scan times reduced the likelihood of such a malfunction occurring during the data collection. Secondly, slow drifts in the laser's intensity during the long scans sometimes resulted in the collected 508.5 nm waveform being slightly distorted.

The modified A/D interface routine used for the final data collection provided the two options for the data transfer control, allowed any number of fast scans to be averaged, and incorporated a means of ensuring that the jth points in all

‡ The relationship between the boxcar parameters is given in the following section.

data files were synchronous. The averaging subroutine made the provision for a single scan to be rejected, if it was thought likely to be distorted, before it was added to the accumulated data that were to be subsequently averaged. Stream-lining of the subroutine that transferred data at time intervals, enabled it to execute as quickly as the subroutine operating at voltage intervals. Synchronization between the data files was achieved by triggering, and halting, the transfer of data at two preselected threshold voltages along the time base. The variation in the time-base voltage of equivalent points from different scans was at most 0.002 V in a total range of 9-10 V.

(c) Experimental Procedure. Before a set of runs was conducted, the oven, the vacuum line and the ammonia were prepared in the manner already described in section III-1(b). Aliquots of gas were admitted in the manner described in section III-1(b), but because data for the three species at one ammonia pressure took 2½ to 3 hours to collect, usually only one aliquot of gas was admitted to the cell between pump-outs. In this way the possibility of impurity levels within the cell rising to a level that would adversely affect the measurements was reduced. Between each set of runs the cell was pumped on for at least 45 minutes, usually longer. At low pressures this pump-out time was especially necessary if reasonable reproducibility was to be attained. Further comment is made on this matter in section II-4 of the next chapter.

Preparation for the boxcar measurements also required the time consuming adjustment of the laser's wavelength tuning.

An approximate wavelength setting for the dye laser was found by passing the beam through the monochromator (no photomultiplier mounted), set at 467.8 nm, and adjusting the laser's output wavelength until the maximum beam intensity was passed. The monochromator was then removed, and the beam's wavelength was very slowly scanned either side of this setting until the fluorescence signal was observed. Once the first faint fluorescence was detected, the boxcar's timing settings were optimized, and the very fine adjustment of the laser's output wavelength was made to maximize the fluorescence signal.

A full set of runs at one ammonia pressure required the storage of five waveforms. However, all five waveforms were not always recorded, as at the pressure extremes the intensity of either the 508.5 nm fluorescence or the 430 nm luminescence was too low for reliable measurements to be made, and the waveform for that particular emission was omitted.

The first signal to be scanned in each data set was the 326.1 nm fluorescence; this was followed by the fluorescence at 508.5 nm. As the CS 3-70 filter used to observe the 508.5 nm fluorescence passed a portion of the long wavelength wing of the exciplex band, a background run was then recorded. The background waveform was collected under the same conditions as the 508.5 nm fluorescence signal but without the laser excitation. Initially, background data was collected at all pressures, but it was found that at pressures below about 8 Torr the background contribution to the LIF data was insignificant, so that background runs

in this pressure region were discontinued. The fourth and fifth waveforms stored were the 430 nm luminescence and a repeat of the $^3P_1$ fluorescence respectively. The two $^3P_1$ phase values were averaged to provide the reference phase for the other two species.

Tests were conducted to ascertain whether the light passing through the CS 3-74 and CS 3-70 filters was solely from the $CdNH_3^*$ exciplex and $^3P_1$ state respectively. With the cell empty no modulated signal was observed through the CS 3-74 filter, implying that scattered lamp light was not passing to the photomultiplier; nor was there any signal when cadmium was admitted to the illuminated cell, implying that cadmium atomic lines were not being passed by the filter.

Other than the low background exciplex luminescence noted above, no signal was observed through the CS 3-70 filter unless the vapour/gas mixture was being probed by the laser. The disappearance of the signal with the removal of the 326.1 nm exciting radiation, and the fact that the signal was modulated, ruled out the possibility of it being scattered laser light. The emission's extreme sensitivity to the laser's output wavelength strongly suggested that the observed signal originated from the laser's probing of an atomic line, and the laser photon's wavelength, together with the wavelength region of the observed signal, confirmed that the $Cd(^3P_0)$ species was the atomic level being probed.

Before each set of runs was started, the boxcar's aperture time was optimized by adjusting the setting to give the maximum signal from the 508.5 nm fluorescence.

A delay of about 1 μs existed between the trigger signal being applied to the laser control console and the laser firing. As the laser was triggered by the boxcar's delayed trigger signal, which was synchronous with the instrument's gate opening, the laser pulse occurred after the photomultiplier's signal had been sampled, and therefore the 508.5 nm signal should have been unobservable without modifications to the boxcar's timing circuitry. However, for reasons that are still unclear, by carefully setting the aperture time, the LIF could be observed. Because of the LIF signal being very sensitive to the aperture time, unlike the 326.1 nm fluorescence and 430 nm luminescence signals, the aperture time was set by the maximization of the 508.5 nm fluorescence signal.

Because the laser's output intensity was abnormally high when first switched on, the laser was usually run with its output blocked while the 326.1 nm waveform was collected, to give the beam intensity time to settle to a constant level.

When the lamp, and if necessary the laser, were operating, the requisite filter was in position and the A/D interface routine was loaded into the microcomputer, the collection of data could proceed. The boxcar's parameters were set to the values given below, the interface routine's execution was begun (data transfers were set to occur at constant time intervals) and the boxcar's gate was scanned across the time base.

The time base used in all but a few scans was 50 μs, as this setting allowed just over a full modulation cycle

to be scanned at the experimental frequency of 30 kHz. The threshold voltages controlling the beginning and end of data transfer were set at 5.5% and 98% of the time base. The first percentage was chosen because the delayed trigger, when operated in the "scan" mode, would not start to scan at less than 5% of the time base; the second was selected because the ramp voltage at 100% of the time base was slightly more than the 10 V the A/D converter would accept.

The first scan collected after the interface routine had been loaded into the microcomputer was always discarded because the number of points collected during this run was invariably significantly smaller than the number normally collected. The number of scans averaged for a data file usually ranged from six to eighteen depending on the waveform's signal to noise ratio. At ammonia pressures below 5 Torr, where the 326.1 nm fluorescence and 508.5 nm fluorescence signals were near their maxima , the averaging of only three scans per datafile was adequate.

The requirement of a short scan time (2 minutes was chosen to enable a reasonable number of points to be obtained) and the dictation of the aperture time by the laser's triggering characteristics, limited the choice of the remaining boxcar parameters through expressions (2.9) and (2.10).

$$\text{Minimum Scan Rate} = \frac{\text{TB x OTC}}{\text{AT x 12}} \text{ (minutes)} \qquad (2.9)$$

(OTC = Observed Time Constant)

$$\text{OTC} = \frac{1}{f}\left(\left(\frac{TC_{HR}}{AT}\right)^2 + \left(\frac{TC_{NR}}{ST}\right)^2\right)^{\frac{1}{2}} \qquad (2.10)$$

At an operating frequency (f) of 188 Hz, a stretch time (ST) of 30 μs, a high resolution mode time constant (TC_{HR}) of 30 ns, a time base (TB) of 50 μs and an aperture time (AT) of 0.36 μs, a normal resolution mode time constant (TC_{NR}) of 1 ms was required. The fraction of the time base scanned, and the rate at which it was scanned, allowed 532 $\pm$ 1 data points to be collected per run. The variation in the number of points per scan, during the collection of one data set (all five waveforms) was normally one, occasionally two.

For reasons given in section II-4 of the next chapter, a few scans were carried out at the following settings: AT = 50 ns and 100 ns, TB = 100 μs, TC_{HR} = 30 ns, TC_{NR} = 1 ms and 0.3 ms, scan time = 5 min. With the thresholds for data transfer set at 38% and 85% of the time base, 671 data points could be collected during a scan.

Superimposed on the variation of 0.002 V in a data point's time base voltage was a jitter in the delay between the pilot trigger to the boxcar and the gate opening of at most 0.08% of the time base (manufacture's figure). The value for jitter expected in the laser's output is unknown, but is probably little more than the smallest aperture time used (50 ns).

Once the data had been collected and stored on disk using the A/D interface routine, the waveforms' phase shifts were determined by the Fourier analysis program. Two methods were used to determine the points in a data file fed to the routine as the 0° and 360° points. The first was described in section III-2b(i), but this method was replaced for the

final data analysis, because, even in waveforms with a good signal to noise ratio, it was often difficult to accurately determine the 0° and 360° points by eye. To obtain the most reliable final phase shifts, the square wave from the Schmitt trigger was scanned to accurately determine the number of data points in the modulation period. With 532 points collected per scan, 416 points corresponded to a full modulation cycle, and with 671 points per scan a modulation cycle corresponded to 513 points. The Fourier analysis was performed between the same two points for all three species. Although the 0° and 360° points chosen for all data sets were selected to lie near the usual minima of the 326.1 nm fluorescence waveform, the relative shifts between the species were unaffected by the choice of where the modulation period was defined along the waveform.

(3) Measurement of the Exciplex Luminescence Intensity as a Function of the Ammonia Pressure

(a) Light Detection and Instrumentation. Measurements of the band emission intensity as a function of the ammonia pressure were made using the same light detection system used for the boxcar measurements, except in this case the signal from the photomultiplier's preamplifier was taken to the lock-in amplifier (fitted with a type D preamplifier - 100 MΩ input impedance).

(b) Experimental Procedure. The cell was baked and pumped on in the manner described in section III-1(b), and the

cell temperature and cadmium pressure were brought to the same levels used for the boxcar measurements. The cell pressure was then increased in steps, as already detailed in section III-1(b), and when after each increment the intensity measurement was made, the lock-in amplifier's phase setting was adjusted to ensure the intensity reading was that of the in-phase component. The photomultiplier's gain was kept constant for a set of readings. After each set the cell was pumped on for at least 45 minutes before the next run was started.

This procedure was carried out at frequencies of 30 kHz, 1 kHz and 70 Hz.

(4) Band Contour Measurements

(a) Instrumentation and Experimental Procedure. The luminescence band contour measurements were made using the monochromator fitted with the 0.25 mm slit pair (1 nm bandwidth). The incident microwave lamp output, modulated at 1 kHz, was filtered by the CS 7-54 glass filter before entering the cell. The photomultiplier's preamplifier was the same as that used for the boxcar measurements, as were the cadmium pressure and cell temperature. A YOKOGAMA 3046 chart recorder, whose input was damped by a 250 μF capacitor across its input terminals, received the lock-in amplifier's averaged signal.

Gas was admitted to the cell in the usual way, and with the lamp operating, the monochromator's wavelength setting was scanned from 310 nm to 250 nm.

(b) Monochromator/Photomultiplier Sensitivity. The monochromator/photomultiplier combination was positioned to receive the unfocused emission from an incandescent tungsten strip lamp. The slit width of the monochromator was 0.25 mm and the output of the photomultiplier was taken directly to a KEITHLEY 417 high speed picoammeter.

The intensity of the emission from the tungsten strip, at a temperature determined with a CAMBRIDGE optical pyrometer, was measured at intervals from 300 nm to 600 nm. The lamp's strip filament was run at a temperature of 2030 K.

The relative sensitivity of the monochromator/photomultiplier combination as a function of wavelength can be determined by comparison of the measured intensities with those calculated from Wien's law. Providing $\lambda T < 2 \times 10^{-3}$ mK the law is valid, and at a given absolute temperature T may be expressed as,[89]

$$I_{(\lambda)} = 2E_{(\lambda)}Ac_1\lambda^{-5} \exp(-c_2/\lambda T)d\lambda \qquad (2.11)$$

$I_{(\lambda)}$ is the intensity in watts per unit solid angle normal to the incandescent surface, $E_{(\lambda)}$ is the emissivity of tungsten at the wavelength λ, A is the surface area of the incandescent body and $c_1 (= 0.588 \times 10^{-16}$ $Wm^2)$ and $c_2 (= 1.438 \times 10^{-2}$ mK) are the first and second radiation constants.

Equation (2.11) can be expressed in photons.s^{-1}.$ster^{-1}$ rather than watts.$ster^{-1}$ through the division of (2.11) by hc/λ ($\hbar$ and c have their usual meanings). Thus,

$$N_{(\lambda)} = \frac{I(\lambda)}{hc/\lambda} \text{ photons.s}^{-1}\text{.ster}^{-1} \qquad (2.12)$$

As the observation geometry remained unchanged for measurements at all wavelengths, and because the monochromator's dispersion is approximately constant from 300 nm to 900 nm,‡ the same fraction of the total number of photons emitted per second reached the photomultiplier at each wavelength. A relative intensity, $N'_{(\lambda)}$, could therefore be calculated from emissivity data[90] and the wavelength. The relative sensitivity, $S_{(\lambda)}$, was then found by the division of the photomultiplier's current by $N'_{(\lambda)}$. A plot of $\log(S_{(\lambda)})$ as a function of wavelength is given in Fig. II-13.

(5) Measurement of the Exciplex Intensity/326.1 nm Intensity Ratio as a Function of the Ammonia Pressure

(a) Light Detection and Instrumentation. To obtain a good signal to noise ratio at low cadmium pressures during these measurements, the filter system used for the boxcar measurements was employed. The signal from the dry-ice-cooled, d.c.-coupled photomultiplier was taken directly to the KEITHLEY picoammeter, and the microwave lamp was operated unmodulated.

(b) Experimental Procedure. After the cell was baked and pumped out in the usual way, the cell temperature was brought to, and maintained at 550 K. At this cell temperature

---

‡ The monochromator's dispersion is approximately 4.0 nm/mm from 300 nm to 900 nm.

the metal's reservoir temperature would not drop below about 476 K [Cd] = 3.1 x 10^{-4} Torr; this marked the lowest cadmium pressure at which measurements were made.

Once the required amount of ammonia had been admitted to the cell, the lamp was energized and intensity measurements were made of the emission intensities at 326.1 nm and 430 nm. Although the room was darkened and the photomultiplier dry-ice-cooled, a background component was present in all signals and this was subtracted from the signal to obtain the final reading. All intensity measurements were made at the same photomultiplier voltage except for one set of 326.1 nm measurements which were made at a slightly higher voltage; these were later corrected to give equivalent readings at the common gain.

After the readings at a particular cadmium pressure had been made the lamp was turned off to avoid erroneous results being obtained because of the possible photosensitised decomposition of the ammonia.[73] The power setting for the cadmium reservoir was then increased, and the reservoir was given 25 - 40 minutes to reach its new temperature and for the cadmium pressure in the cell to equilibrate.

The metal vapour's pressure was calculated from the empirical equation of Aldred et al.,[91]

$$\log_{10}[P_{Cd}(\text{torr})] = 9.404 - 6146/T \qquad (2.13)$$

where T is the absolute temperature.

CHAPTER III

RESULTS AND DISCUSSION

I INTRODUCTION TO THE PHASE-SHIFT TECHNIQUE

Excited states, be they atomic or molecular, exist for a finite time which, in the case of exponential decay, can be expressed as a mean lifetime τ. Similarly, processes involving both excited and ground states occur at a finite rate. One of the consequences of these processes occuring at a limited rate is that although an excitation source of periodically varying intensity will cause the concentration of an excited species produced by the irradiation to oscillate at the source frequency, the phase of the oscillation will normally show a lag with respect to the phase of the initiating source. The extent of this lag is dependent upon both the frequency of modulation and the rates at which processes occur in the system.

The phase-shift technique has been employed many times to measure the lifetimes of short-lived fluorescent species (see, for example, references 92-94). In simple cases where an exponential fluorescence decay is expected, the expression

$$\tan \beta = \frac{2\pi f}{k} \qquad (3.1)$$

where f is the frequency of modulation, relates the observed phase shift β, to k, the first-order or pseudo first-order rate constant for the removal of the species.

The section that follows shows the limitations of equation (3.1), demonstrates the dependence of phase relationships on the nature of the decay of the species for the two simplest cases that may be encountered, and briefly notes some studies concerned with more complex systems to which the technique has been applied. (A number of studies have been reviewed in more detail by Phillips.[87]) Most of this section is gleaned from the reviews of Birks and Munro[95], and Phillips.[87] Section I-2 describes the experimental pitfalls generally attendant upon the technique.

(1) Phase-shift Theory

If the decay of a fluorescing species, after an excitation pulse that can be described by a δ-function of unit intensity, is g(t), and if the exciting light function is given by p(t), then the observed response function f(t) of the system (i.e., the fluorescence intensity) is defined by the convolution

$$f(t) = \int_{-\infty}^{t} p(t')\, g(t-t')dt' \quad , \tag{3.2}$$

assuming the fluorescence intensity is proportional to the concentration of the emitting species.[95] In the case of the light source being amplitude modulated at angular frequency, ω, p(t) can be written as a Fourier series. Thus,

$$p(t) = c[1 + \sum_{j} m_j \exp(i\omega_j t)] \quad . \tag{3.3}$$

Usually, the detecting device is designed to exclude all

frequencies except the fundamental, so for simplicity, equation (3.3) may be written as

$$p(t) = c(1 + me^{i\omega t}) \tag{3.4}$$

where m is the degree, or amplitude, of modulation, the phase is defined as zero, and c is a constant.

If an excited species possesses an exponential fluorescence decay, that is,

$$g(t) = ae^{-kt}$$

where a is a constant, and the excitation function is given by equation (3.4), then substitution of g(t) and p(t) into equation (3.2) yields

$$f(t) = \frac{ca}{k}\left[1 + m\left(\frac{k}{k+i\omega}\right) e^{i\omega t}\right] \quad . \tag{3.5}$$

Equation (3.5) implies that the fluorescence observed from such a system is exactly in step with the modulated radiation entering the fluorescing medium. In reality a phase lag is observed. This lag can be taken into account by considering p(t) as being phase-shifted and rewriting equation (3.4) as,[96]

$$p(t) = c[1 + me^{i(\omega t + \beta)}] \quad . \tag{3.6}$$

Accordingly, equation (3.5) is modified to give

$$f(t) = \frac{ca}{k}[1 + m\left(\frac{k}{k+i\omega}\right) e^{i(\omega t + \beta)}] \tag{3.7}$$

By now defining M as the fraction of m found in the fluorescent signal, equation (3.7) gives

$$M = \frac{k}{k+i\omega} e^{i\beta} \quad ,$$

from which can be derived the relationships sought, namely,

$$M = \cos \beta = k/(k^2 + \omega^2)^{\frac{1}{2}}$$

and

$$\tan \beta = \omega/k \quad . \qquad [3.1]$$

Therefore, for fluorescence having a purely exponential decay the first-order (or pseudo first-order) rate constant for the removal of the fluorescing species (which may be simply the reciprocal of its radiative lifetime) can be determined by measuring either the phase shift of the fluorescence or its degree of modulation. Scheme III-1 is presented as containing an example of an exponentially decaying species S*.

Scheme III-1

$$\begin{aligned} S + h\nu &\rightarrow S^* \\ S^* &\rightarrow S + h\nu \\ Q + S^* &\rightarrow \text{Products} \\ Q + S^* &\rightarrow S^{**} + Q \\ S^{**} &\rightarrow S + h\nu' \\ Q + S^{**} &\rightarrow \text{Products} \end{aligned} \qquad (3.8)$$

[S* and S** are different excited states of S.]

However, if the species of interest is S**, it is found that the nature of its decay becomes more complex and

correspondingly so does the expression for its phase shift. Integration of the differential equation governing the time response of S**, after excitation by a δ-function pulse, yields the expression[95]

$$[S^{**}] = K(e^{-k_a t} - e^{-k_b t}) \quad ,$$

where K is a constant (at constant [Q]) and k_a and k_b are the rate constants for the removal of S* and S** respectively. When g(t) is of this form equation (3.2) gives

$$f(t) = K'\left(\frac{k_b - k_a}{k_a k_b}\right)\left(1 + \frac{m\, k_a k_b\, e^{i(\omega t + \gamma)}}{(k_a + i\omega)(k_b + i\omega)}\right)$$

Again, by defining a degree of modulation

$$M' = \frac{k_a k_b\, e^{i\gamma}}{(k_a + i\omega)(k_b + i\omega)}$$

an expression for tan γ can be derived.

$$\tan \gamma = \frac{\omega(k_a + k_b)}{k_a k_b - \omega^2} \quad , \qquad (3.9)$$

from which it is found that

$$\gamma = \beta_a + \beta_b \qquad (3.10)$$

where β_a and k_a are related by equation (3.1), as are β_b and k_b.

If the reverse of process (3.8)

$$Q + S^{**} \rightarrow S^{*} + Q \qquad (3.11)$$

is now included in Scheme III-1 the response of S** is given by

$$[S^{**}] = L(e^{-m_a t} - e^{-m_b t})$$

where L is a constant (at constant [Q]).‡ The inclusion of the reversible step results in the decay constants m_a and m_b no longer having the simple significance of being the rate constants for the removal of the two species; they are the roots of a quadratic equation whose coefficients involve k_a, k_b and the pseudo first-order rate constants of (3.11) and (3.8). The expression for tan γ is also increased in complexity. Now

$$\tan \gamma = \frac{\omega(k_a + k_b)}{k_a k_b - k_8 k_{11}[Q]^2 - \omega^2} \quad . \tag{3.12}$$

The extra term in the denominator of (3.12), absent in (3.9), means that when a reverse process is introduced into a kinetic scheme like Scheme III-1 the simple relationship between the total shift and β_a and β_b (equation 3.10) holds no longer.

From the preceding discussion it becomes clear that equation (3.1) is to be used with caution, as $\omega/\tan \beta$ may not be equal simply to k. This is not to say that useful phase measurements are limited only to situations where equation (3.1) is applicable. While the measurement of only the total phase lag of one species in a system may often be of little value in determining process rates, some feature of the system (the lack of quenching of $HgNH_3^*$ by

---

‡ The expression for S* also changes form but this will not be considered here.

ammonia in the Hg/NH_3 system for example[82]) or the measurement of the shift of more than one species, can make this information accessible. From equation (3.10) it is evident that if the shifts of S* and S** (i.e., β_a and γ) are measured, the subtraction of one from the other will allow the evaluation of k_a and k_b. It may also happen that under certain experimental conditions, high or low reactant concentrations or modulation frequency, for example, that terms in either the numerator or denominator become negligible and the expression for tan γ simplified.

Although Metcalf[97] derived phase equations for a generalized scheme involving two excited species only, phase equations can be derived for a scheme including more excited states if required. Metcalf's work was extended by Schlag et al..[98] The set of differential equations describing the system was encapsulated in matrix form, and the excitation function was expressed as the sum of two complex exponential terms. No limit was placed on the number of species that could be included in the mechanism which, like Metcalf's, made no assumption as to the form of the fluorescence decay. Schlag et al. showed that the phase equations are not only valid for sine wave excitation but also for an excitation function given by a series of sine terms of different frequencies. This is perhaps to be expected, as Foster in his review[99] states that Duschinsky in a much earlier paper (1933) had shown that equation (3.1) remains valid whatever the shape of the exciting waveform.

The phase-shift technique, in various forms, has been applied to the measurement of processes in systems of greater

complexity than those considered above. In systems in which a sufficiently high concentration of an intermediate species is produced, reactions second-order in that species may occur to an extent that necessitates their inclusion in the system's rate equations. (The terminating step in radical chain reactions is a good example of this type of behaviour.) Second-order rate equations may take the forms:

$$\frac{dc}{dt} = k - k'c^2 \qquad (3.13)$$

or

$$\frac{dc}{dt} = k - k'c - k''c^2 \qquad (3.14)$$

where c is the species concentration. Deriving their equations in different ways, Paukert and Johnston[88], and Hunziker[100] obtained rate constants from phase-shift measurements of systems represented by equations (3.13) and (3.14) respectively.

In atomic fluorescence studies of resonance transitions the bothersome phenomenon of radiation trapping‡ may be encountered. At large optical depths (high degree of trapping), the decay of the imprisoned radiation occurs in an exponential manner where the decay constant equals g/τ (τ is the natural radiative lifetime and g is a constant, at constant pressure, but decreases with increasing optical density). In these systems the substitution of the measured phase shift into equation (3.1) yields the trapping time ($= \tau/g$). However, at low optical density Blickensderfer

---

‡ The multiple reabsorption and re-emission of fluorescence photons.

et al.[101] have shown that for three types of cell geometry the fluorescence decay is given by a series of exponential terms. Umemoto et al.[8] derived an equation which, after trial and error determination of the necessary parameters, gave fits to their data from such a system.

Electron impact can be used to populate excited states for study that are inaccessible by optical excitation. However, unlike optical excitation, by which it is possible to populate only the state of interest, electron impact often produces higher states that decay into the state under consideration, distorting its lifetime. Lawrence and Savage[102], in experiments to determine the lifetimes of some states of boron, nitrogen and carbon, derived equations that allowed the true lifetimes to be extracted from phase shifts measured under cascading conditions.

These are examples of the more complex systems that have been studied. It should be noted that in these cases it is necessary for simplifying assumptions to be made to obtain analytical solutions, or for numerical methods to be employed.

The main drawback of the phase-shift technique, in relation to direct decay measurements, is that the phase value obtained carries no indication of the form of the species' decay. To some extent this hinders mechanistic interpretation, and for radiative lifetime determinations from a phase measurement at a single frequency, it creates the possibility of errors in the evaluated lifetimes, unless the species is known to decay exponentially. Although the phase-shift method suffers from this disadvantage, it must

be remembered that in situations where the lifetime of a state is so short that the exciting pulse width employed may make lifetime determinations difficult because of the need for deconvolution of the data, the phase-shift technique can be used without this complication. Furthermore, there are cases in which the phase-shift method readily provides rate information, in the form of rates of removal, that is not easily obtained from other techniques. The complimentary use of pulsed and phase-shift techniques is demonstrated by the work of Phillips and co-workers on the Hg/N_2 system.[84,103,104]

(2) Experimental Considerations

In the design of his apparatus, the experimenter must be aware of features of its design that may lead to systematic errors in his phase measurements. Most of the factors discussed below give rise to delay errors that are of nanosecond magnitude and therefore are mainly of concern to those wishing to make measurements of lifetimes of this magnitude. It is usual for two phase measurements to be made when phase lags are being determined, one for the shift of the sample, and the other to serve as a zero or reference shift. The latter can be found by measuring the shift of either a sample of known lifetime or the shift of the scattered exciting radiation. Either way, as will be seen, systematic errors resulting from variations in the transit time through the photo-detection system and electronics are reduced if both the zero and sample phase measurements are made under closely similar conditions.

(a) Scattered Exciting Light. It often happens that the fluorescence band to be observed and the exciting light are in close spectral proximity and that because low fluorescence intensity may prohibit the use of a monochromator, or because a suitable sharp-cut filter is unavailable, scattered exciting light cannot be fully excluded from the detection system. As the exciting light corresponds to zero phase, any of this radiation entering the detection system causes a reduction in the measured phase shift when it is averaged with the fluorescence signal, resulting in a reduced apparent lifetime. Brewer et al.[92] noted that if the total modulated signal S, the amplitude of the scattered signal N, and the measured phase shift ϕ_m are known, the true lifetime τ can be obtained from a measurement distorted by scattered light, through the expression

$$\tau = \tau_m \, S \, \text{Cos} \, \phi_m / (S \, \text{Cos} \, \phi_m - N) \quad .$$

[τ_m = lifetime calculated from the distorted measurement.] It is preferable to reduce any scattered light to a minimum under the limitations of the experimental system.

(b) Operating Conditions of the Photomultiplier. Errors in lifetime determination may also result from effects inherent in the detection system. Müller et al.[93] made an extensive study of the way in which the transit time of the signal through the photomultiplier varies with the photomultiplier's operating conditions. It was found that the transit time for a pulse through the photomultiplier was reduced by increasing the voltage either across the full dynode chain or

between the photocathode and the first dynode. The transit time is less strongly dependent on the applied voltage in tubes having a focused dynode structure.

The wavelength of the incident radiation was also found to affect the transit time, the change of transit time with wavelength being greatest at low cathode - first dynode voltages. This wavelength dependence introduces errors which may be of the order of nanoseconds (depending on the type of photomultiplier in use) if there is a large spectral separation between the exciting light and the fluorescence maximum.

Two other factors also affect the transit time. There is a variation of the delay with the photocurrent, and a lessening of the delay with a decreasing illumination area of the photocathode. Venetta[94] also noted this increasing delay with increasing incident intensity, attributing it to non-linear components in the photomultiplier and amplifier circuits.

To minimize the errors brought about by all these factors, the following steps were taken. The reference and sample photomultipliers (which were of the same type) were operated from a common, very stable, high voltage supply. A fixed diaphragm was attached to each photocathode to give a constant, reduced, illumination area, and a neutral density filter was placed in front of the reference photomultiplier to reduce its photocurrent to a level similar to that of the sample photomultiplier. Lastly, to minimize the wavelength dependence of the measurement, white light was scattered from the cell through the same filter used to isolate the fluorescence to give the zero phase measurement.

(c) Observation Geometry. A numerical study by Phillips[105], of radiation trapping at large optical depths, showed that the phase shift observed varies with the viewing position; the variation may be tens of nanoseconds at 3MHz, lessening with modulation frequency. He concluded that this variation can be reduced if a monochromator is used, by aligning its slits at right angles to the exciting beam.

II RESULTS AND DISCUSSION

(1) Exciplex Band Profile

Although band contours and the band maximum of the $CdNH_3^*$ emission have been published previously[71,73,75], either they were recorded at a temperature and cadmium pressure lower than those used in this work or they were uncorrected for the photomultiplier sensitivity. The absence of a full, corrected band contour for the conditions of this work led to the collection of the data for Fig. III-1, which shows the shape and spectral extent (monochromator/photomultiplier sensitivity corrected) of the exciplex luminescence at 550 K with an ammonia pressure of 80.4 Torr.

Sato and his co-workers[73] stated that the band maximum does not shift, nor does the band profile change, with increasing ammonia pressure, so the band shape and position of Fig. III-1 can be taken as representative of the band over a wide range of pressures. The luminescence intensity peaks at about 430 nm and the band shows the slight asymmetry present in the uncorrected data of Morten et al.[71]. At the resolution of these measurements (1 nm) there is, as may be expected from

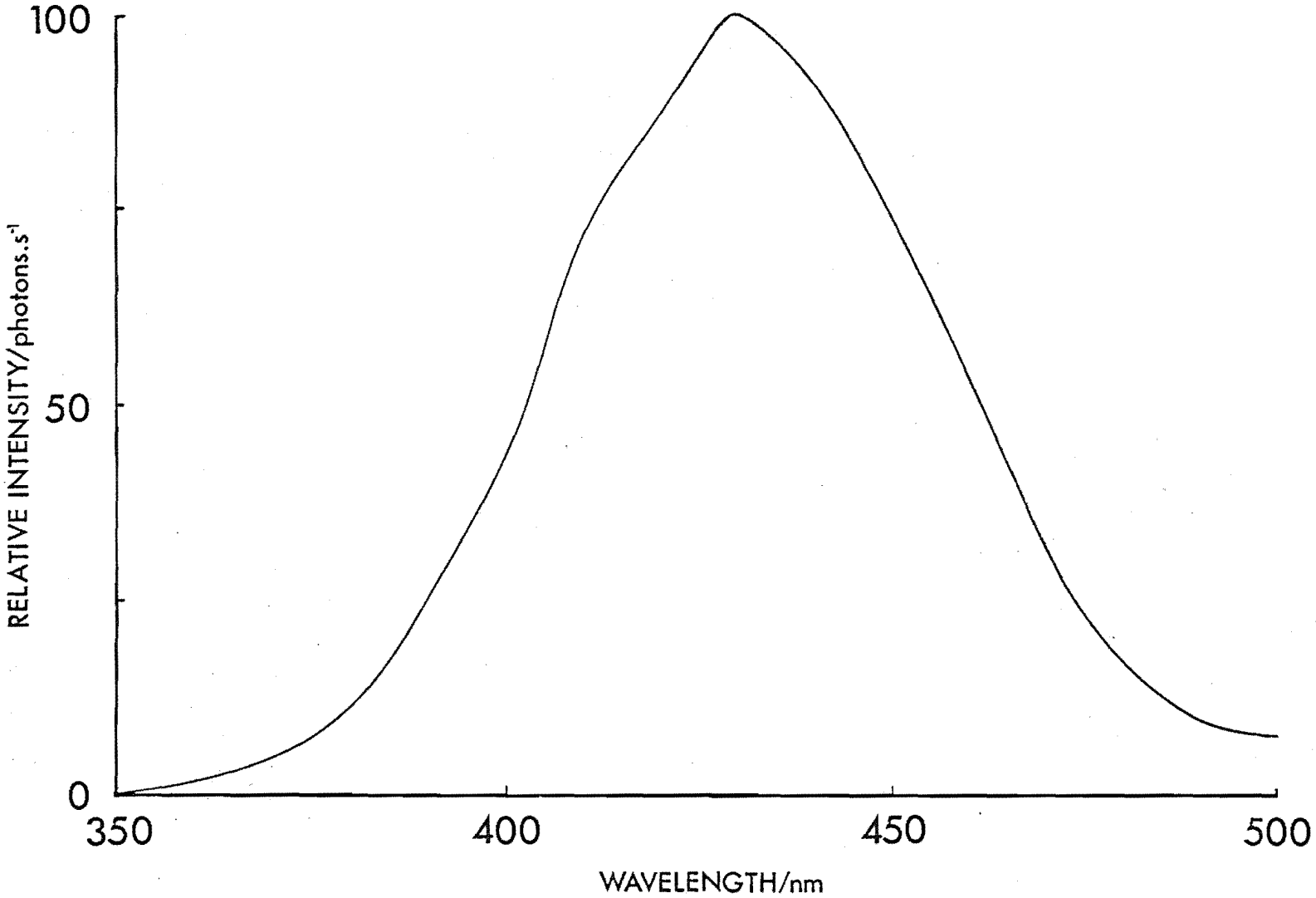

Fig. III-1. THE 430 NM EXCIPLEX BAND PROFILE

Temperature = 550 K; ammonia pressure = 80.4 Torr; cadmium pressure = 12 mTorr.

a bound - unbound transition, no indication of structure in the band.

Work on the Hg/N_2 system[84] showed that the production of significant amounts of the Hg_2^* excimer is feasible at mercury pressures of about 2×10^{-3} Torr, when nitrogen is in admixture with the metal vapour. The data of Fig. III-1 exclude the possibility of the observed emission band being the 470 nm Cd_2^* band.

(2) The Intensity of the 430 nm Band as a Function of the Ammonia Pressure

The representative data from these measurements are plotted in Fig. III-2. Although the data of different runs at the same frequency were found to vary beyond the estimated limits of uncertainty in the intensity measurements, the qualitative form of the plots showed, unmistakably, a monotonous increase in intensity with increasing ammonia pressure. With increasing frequency the intensity at a given pressure decreases. This is to be expected, as the average concentration of the exciplex produced by the modulated excitation decreases with the decreasing modulation period. A slight curvature present in the lower frequency plots is not so apparent with increasing frequency. The equivalent data of Sato's group (Figs. I-5(c) and (e)), obtained at 100 Hz, show a much greater levelling-off than do the present results. The reduced curvature in the plots of this work is consistent with an increase in the amount of light being absorbed as the ammonia pressure is increased. As a constant pressure was not maintained by the addition of excess buffer gas in this

Fig. III-2. REPRESENTATIVE PLOTS OF THE 430 NM BAND INTENSITY AS A FUNCTION OF THE AMMONIA PRESSURE.

Cadmium pressure = 12 mTorr. Open circles = 70 Hz data; filled circles = 1 kHz data; half-filled circles = 30 kHz data. The 30 kHz data are displaced upwards by one unit for clarity.

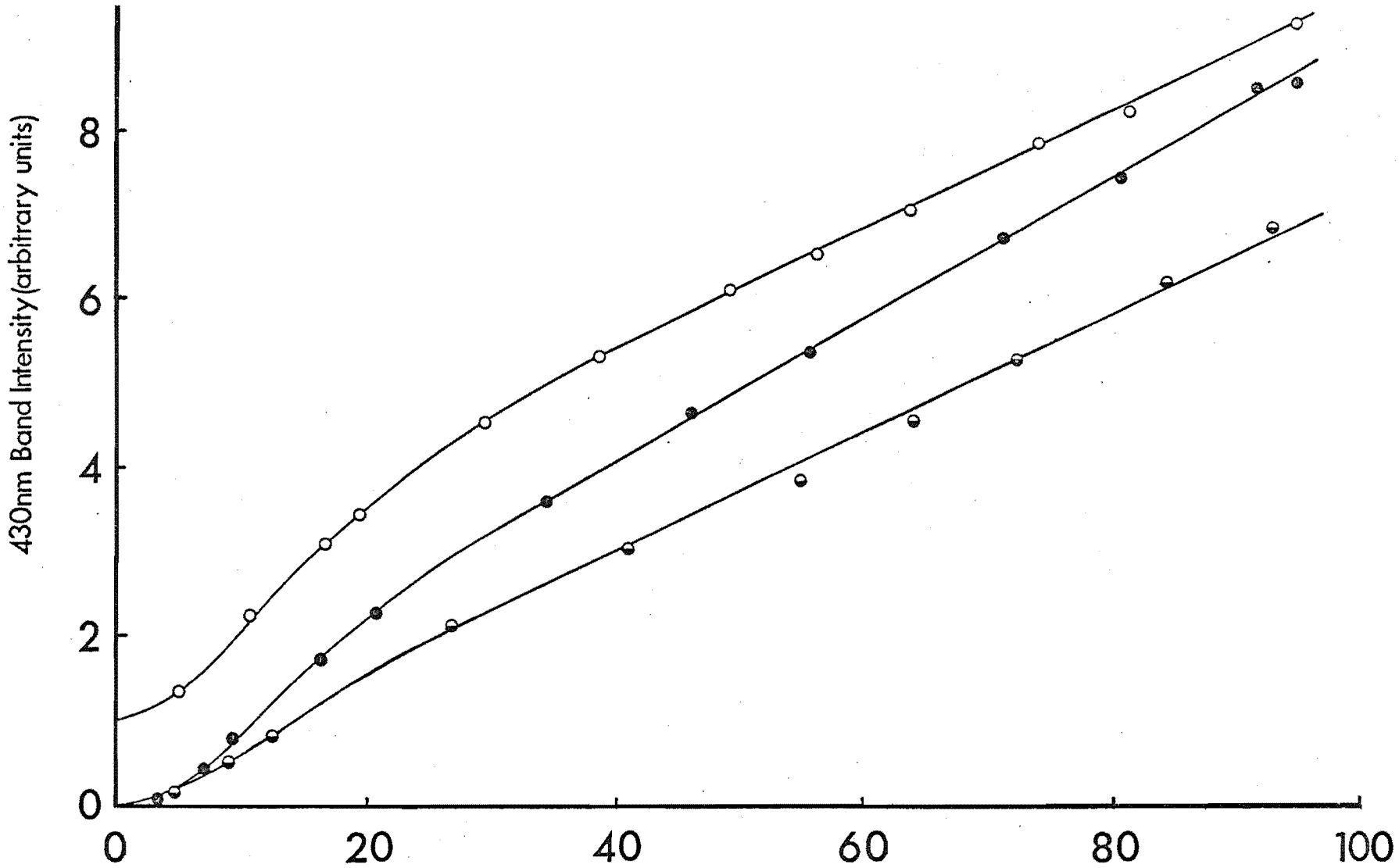

(Caption on facing page.)

work, pressure broadening of the absorption line could explain this observation if the lamp's exciting line-width is greater than that of the absorbing line. Although the output from the electrodeless lamp can be expected to be relatively narrow, the long path length through the cell's upper arm is probably responsible for the broadening and reversal of the lamp's line, so creating the conditions that lead to increased absorption with pressure broadening.

(3) Lock-in Amplifier Phase Measurements

The phase measurements made at 20,30,40,50 and 60 kHz are presented as the phase difference between the 326.1 nm fluorescence and the 430 nm luminescence in Fig. III-3(a)+(b) and in Table III-1. (Estimated uncertainties in all observables are tabulated in Appendix C.) All measurements were made at an over-all cell temperature of 550 $\pm$ 4 K and a metal reservoir temperature 17 $\pm$ 1 K lower (Cadmium pressure = 7.5×10^{-3} Torr), except for a few of the low and high pressure 30 kHz measurements which were made at a cadmium pressure of 1.2×10^{-2} Torr (543 K). Despite the difference in the metal pressure, these latter results are in excellent agreement with the data obtained at the lower cadmium pressure.

The phase shifts from these measurements are in reasonable agreement with those found by Morten et al.[71], but the agreement with the phase differences of Umemoto et al.[77] is somewhat poorer; at a given ammonia pressure the phase shifts of the Japanese are larger than the values of this work. The finding from the present study, that differing cadmium pressures have no effect on the measured shifts,

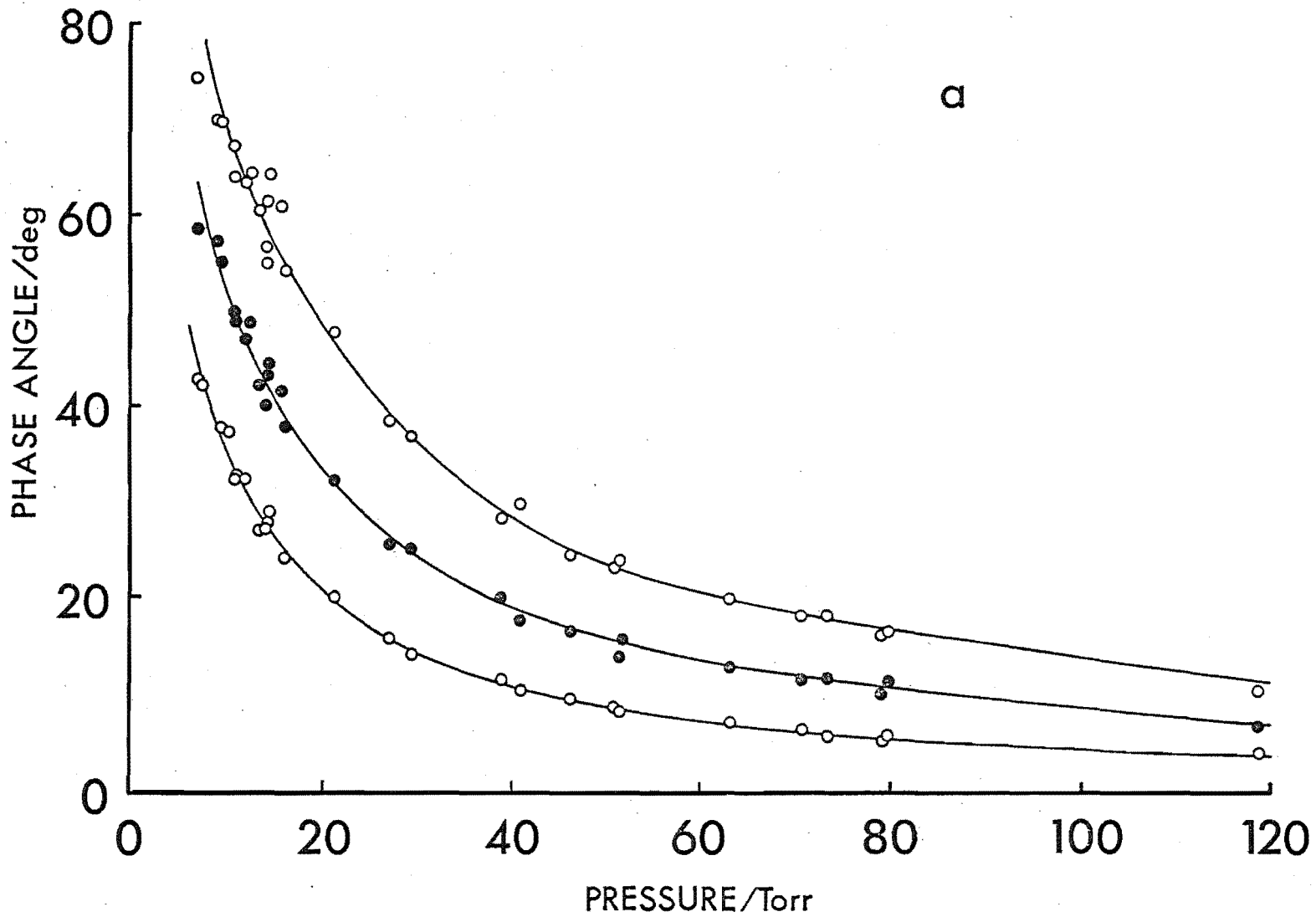

Fig. III-3. THE $CdNH_3^*$ - $Cd(^3P_1)$ PHASE DIFFERENCE AS A FUNCTION OF THE AMMONIA PRESSURE.

Temperature = 550 K; cadmium pressure = 7.5 mTorr.
Reading from top to bottom, the curves represent 60, 40, and 20 kHz data.

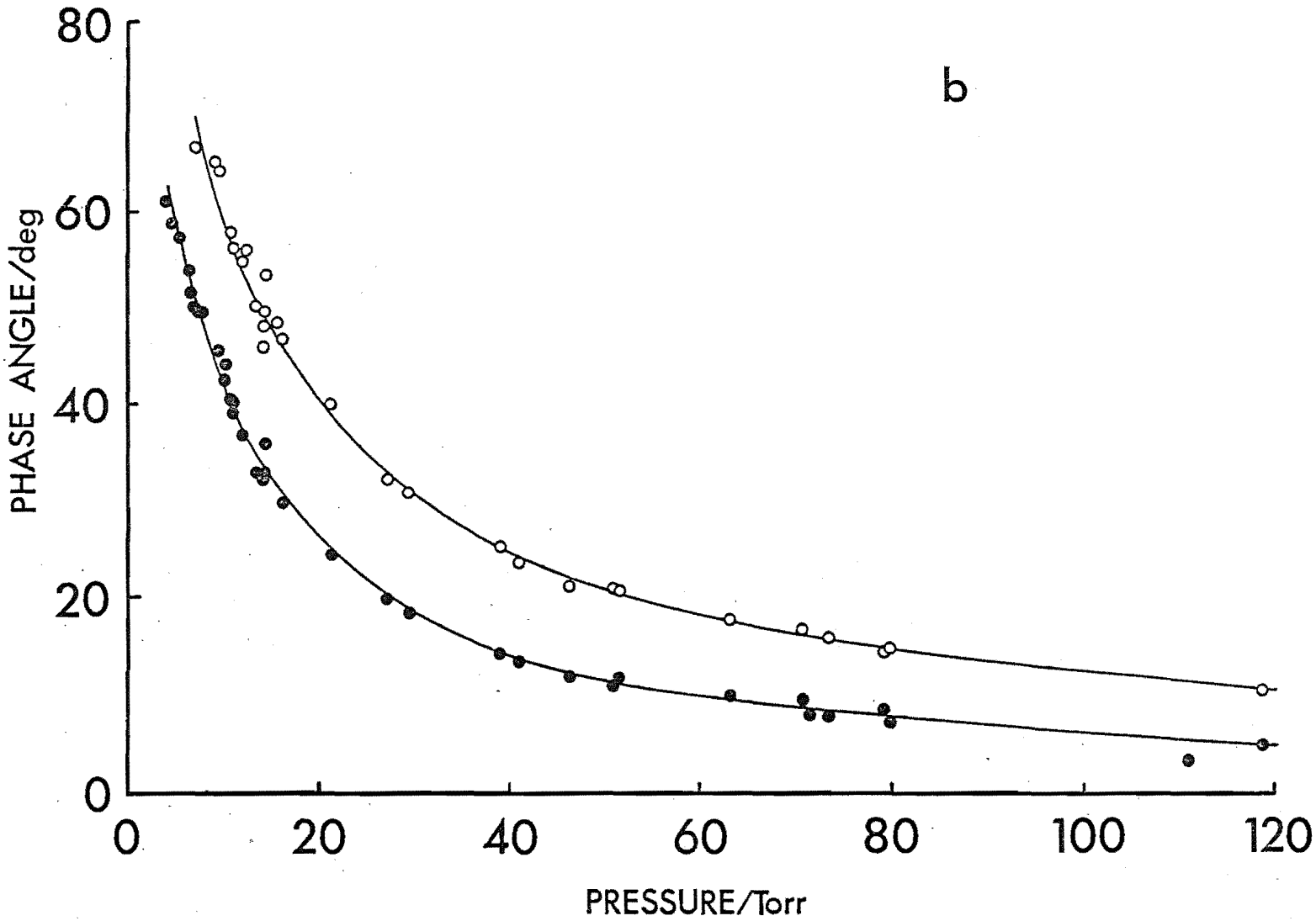

Fig. III-3. THE $CdNH_3^*$ - $Cd(^3P_1)$ PHASE DIFFERENCE AS A FUNCTION OF THE AMMONIA PRESSURE.

Temperature = 550 K; cadmium pressure = 7.5 mTorr.
The upper curve is 50 kHz data; the lower is 30 kHz data.

Table III-1. Phase Data from the Lock-In Amplifier Measurements. Under each frequency, Column A contains the phase shift $CdNH_3^*$ - $^3P_1$ (degrees), Colum B contains $2\pi f/\tan\phi/10^5 s^{-1}$ Column C contains $2\pi f/\tan\phi'/10^5 s^{-1}$.

Ammonia Pressure / Torr	20 kHz			40 kHz			50 kHz			60 kHz		
	A	B	C	A	B	C	A	B	C	A	B	C
6.8	42.9			58.6			66.9			74.1		
7.3	42.2											
8.8				57.2			65.4			69.9		
9.4	37.7			55.0			64.3			69.6		
10.1	37.3											
10.6	32.1			49.8			57.9			67.1		
10.8	32.9			48.8			56.3			63.9		
11.8	32.3			47.0			54.9			63.3		
12.4				48.7			56.0			64.3		
13.3	26.8			42.1			50.2			60.3		
14.0	27.6			40.1			45.9			54.8		
14.0	27.0			40.0			48.0			56.5		
14.1	27.7			43.3			49.6			61.3		
14.3	28.9			44.5			53.5			64.1		
15.5				41.6	2.83	3.41	48.5	2.78	3.49	60.7	2.12	2.85
16.0	24.0	2.82	3.21	37.7	3.25	3.95	46.7	2.96	3.72	54.1	2.73	3.60
21.2	20.0	3.45	4.01	32.0	4.02	4.98	40.0	3.74	4.75	47.6	3.44	4.52
27.0	15.7	4.47	5.40	25.5	5.27	6.79	32.4	4.95	6.47	38.5	4.74	6.35
29.3	14.1	5.00	6.18	25.0	5.39	6.98	30.9	5.25	6.93	36.9	5.02	6.77
38.8	11.5	6.18	8.02	20.0	6.91	9.51	25.4	6.62	9.18	28.2	7.03	10.1
40.9	10.3	6.91	9.29	17.6	7.92	11.4	23.6	7.19	10.2	29.7	6.61	9.38
46.2	9.5	7.51	10.4	16.5	8.5	12.6	21.2	8.10	12.0	24.3	8.35	12.7
50.7	8.6	8.31	12.0	15.6	9.00	13.7	21.1	8.14	12.1	23.0	8.88	13.9
51.5	8.2	8.72	12.8	13.9	10.2	16.4	20.6	8.36	12.5	23.9	8.51	13.1
63.2	7.1	10.1	16.0	12.8	11.1	18.8	17.6	9.90	16.0	19.1	10.4	17.6
70.8	6.3	11.4	19.4	11.5	12.4	22.8	16.6	10.5	17.6	18.0	11.6	21.0
73.5	5.6	12.8	24.0	11.6	12.2	22.4	15.7	11.2	19.4	18.0	11.6	21.0
79.1	5.2			10.0			14.3			16.1		
79.7	5.7			11.3			14.8			16.6		
118.7	4.0			6.9			10.4			10.5		
153.0	3.1			5.2			8.0			8.9		
172.5	3.0			5.2			7.7			7.8		

Table III-1 (Cont)

Ammonia Pressure / Torr	30 kHz A	B	C	Ammonia Pressure / Torr	30 kHz A	B	C
‡ 3.9	61.0			27.0	19.8	5.24	6.62
‡ 4.4	58.8			29.3	18.3	5.70	7.34
‡ 5.1	57.3			38.8	14.2	7.45	10.4
‡ 6.3	53.9			40.9	13.3	7.97	11.4
‡ 6.6	51.5			46.2	11.8	9.02	13.6
6.8	50.1			50.7	10.7	9.98	15.8
7.3	49.7			51.5	11.7	9.10	13.8
‡ 7.6	49.5			63.2	9.8	10.9	18.2
9.4	45.6			70.8	9.4	11.4	19.6
‡ 10.0	42.5			‡ 71.5	7.7		
10.1	44.1			73.5	7.6	14.1	29.1
10.6	40.5			79.1	8.4		
10.8	39.2			79.7	7.1		
‡ 10.9	40.3			‡ 110.8	3.1		
11.8	36.9			118.7	4.8		
13.3	33.0			‡ 137.6	4.2		
14.0	32.2			‡ 143.8	6.3		
14.0	32.4			‡ 151.5	2.8		
14.1	33.0			153.0	6.6		
14.3	36.0			‡ 171.2	2.6		
16.0	29.9	3.28	3.86	172.5	4.5		
21.2	24.5	4.14	5.01	‡ 176.6	5.1		

‡ Data obtained using the filter system at the same cadmium pressure used for the boxcar runs.

suggests that it is the temperature difference between the two studies, rather than the differing metal concentrations, that may go some way to accounting for the disagreement. The better degree of agreement with the results of Morten et al., obtained at 556 K, supports this explanation. The implication of this temperature dependence is the presence of a process contributing to the phase lag that has a significant activation energy.

Data, which are not shown in Fig. III-3, were collected to about 170 Torr of ammonia. At this pressure the phase difference between the exciplex and $Cd(^3P_1)$ had not reached zero. Phillips and his co-workers, in their studies of Hg/gas mixtures and the Cd/NH_3 system, took the residual phase shift at high added gas pressures to be a measure of the lifetime of the exciplex. Luther et al.[106] showed, however, by the comparison of their direct measurement of the $Hg(^3P_0)$ level in the Hg/CH_3OH and Hg/H_2O systems with the measurements of Freeman et al.[107], that this indirect method of lifetime evaluation may be in considerable error (two orders of magnitude) if the true limiting high-pressure shift is not reached. Therefore, the possibility that the phase difference may eventually go to zero, or a value too small to measure at the frequencies used in these experiments, must not be overlooked.

The possibility of the depletion of the phase shift to zero at very high ammonia pressures presents another mode of interpretation which was used by Freeman and Phillips[108] in explanation of their phase measurements of the Xe*/CO system. In that work, the total observed phase shift was

the sum of two components, the second of which was dependent upon the lifetime of CO* and the rate of removal of CO* by CO. The decrease in this phase component with increasing pressure arose from the latter process, therefore the zero-pressure phase shift was a measure of CO*'s lifetime.

If the lifetime of $CdNH_3^*$ is represented by the limiting high-pressure phase difference then the following inferences can be drawn from the data of Fig.III-3. The decreasing phase shift between the $^3P_1$ fluorescence and the exciplex emission with increasing ammonia pressure shows that the major process of exciplex formation is not directly from the $^3P_1$ level. Were this the case, a constant shift equal to the limiting lag would be expected at all pressures because phase measurements made with respect to the 326.1 nm fluorescence do not include any contribution from reactions removing the $^3P_1$ state. The two previous phase-shift studies[71,77] identify the intermediate species as $Cd(^3P_0)$ atoms in one case and as an unstabilised $CdNH_3^\dagger$ complex, in equilibrium with the $^3P_1$ and $^3P_0$ levels, in the other. The phase data between the $^3P_1$ level and the exciplex, alone, are insufficient to allow a distinction between these two schemes.

The phase differences measured with the lock-in amplifier at pressures greater than 15 Torr are plotted in Figs. III-4 and III-5, together with some of the boxcar measurements. The significance of these plots and the rate constants evaluated from them are discussed in section II-6.

Fig. III-4. PLOTS OF $2\pi F/TAN\phi$ AS A FUNCTION OF THE AMMONIA PRESSURE.

ϕ is the $CdNH_3^*$ - $Cd(^3P_1)$ phase difference (see section II-6).

◑ = 20 kHz data; o = 30 kHz data; ◒ = 40 kHz data; ● = 50 kHz data; ◐ = 60 kHz data; ◒ = boxcar data.

(The small size of the points is for clarity and doesnot reflect the accuracy of the data.)

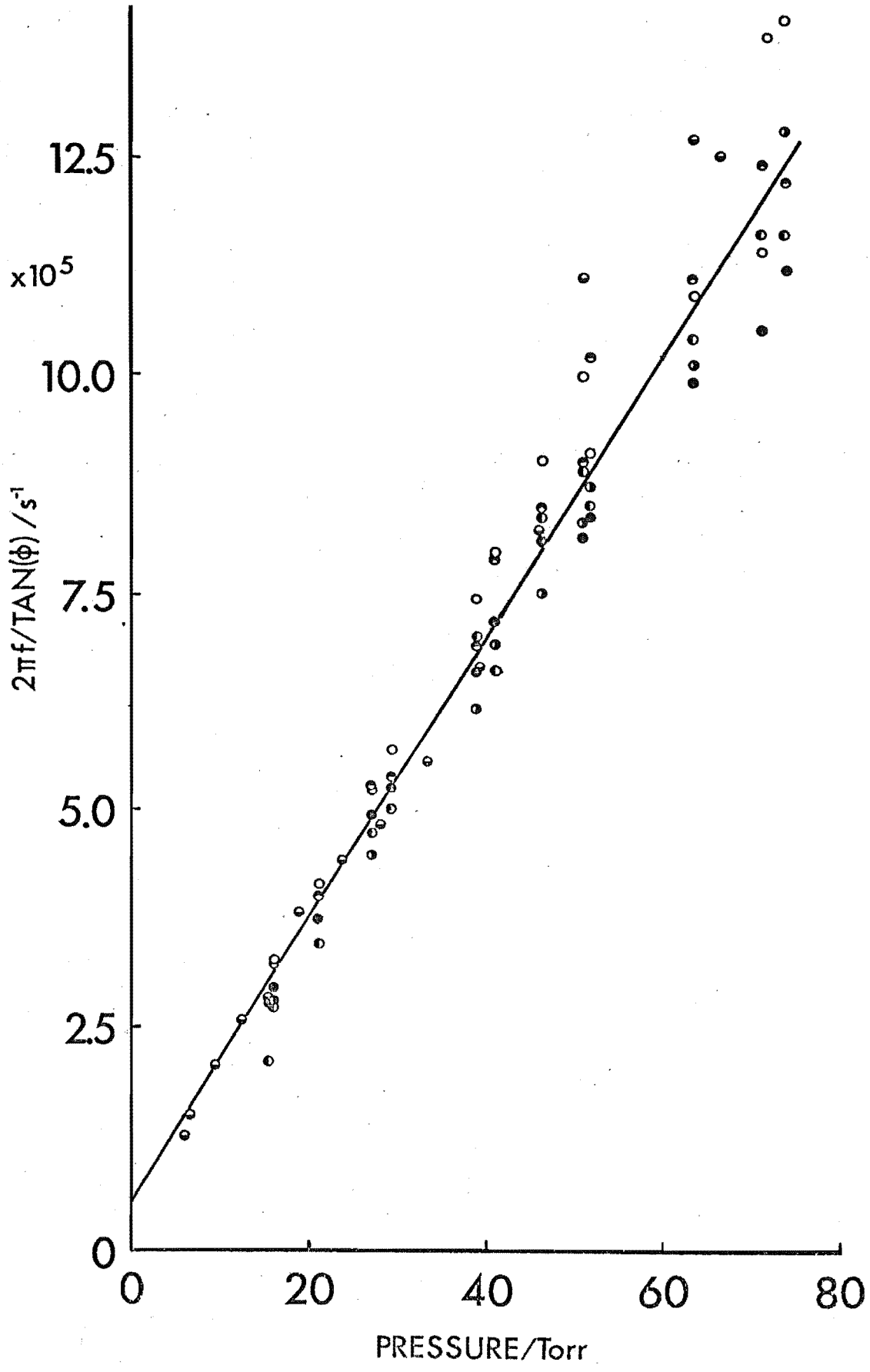

(Caption on facing page.)

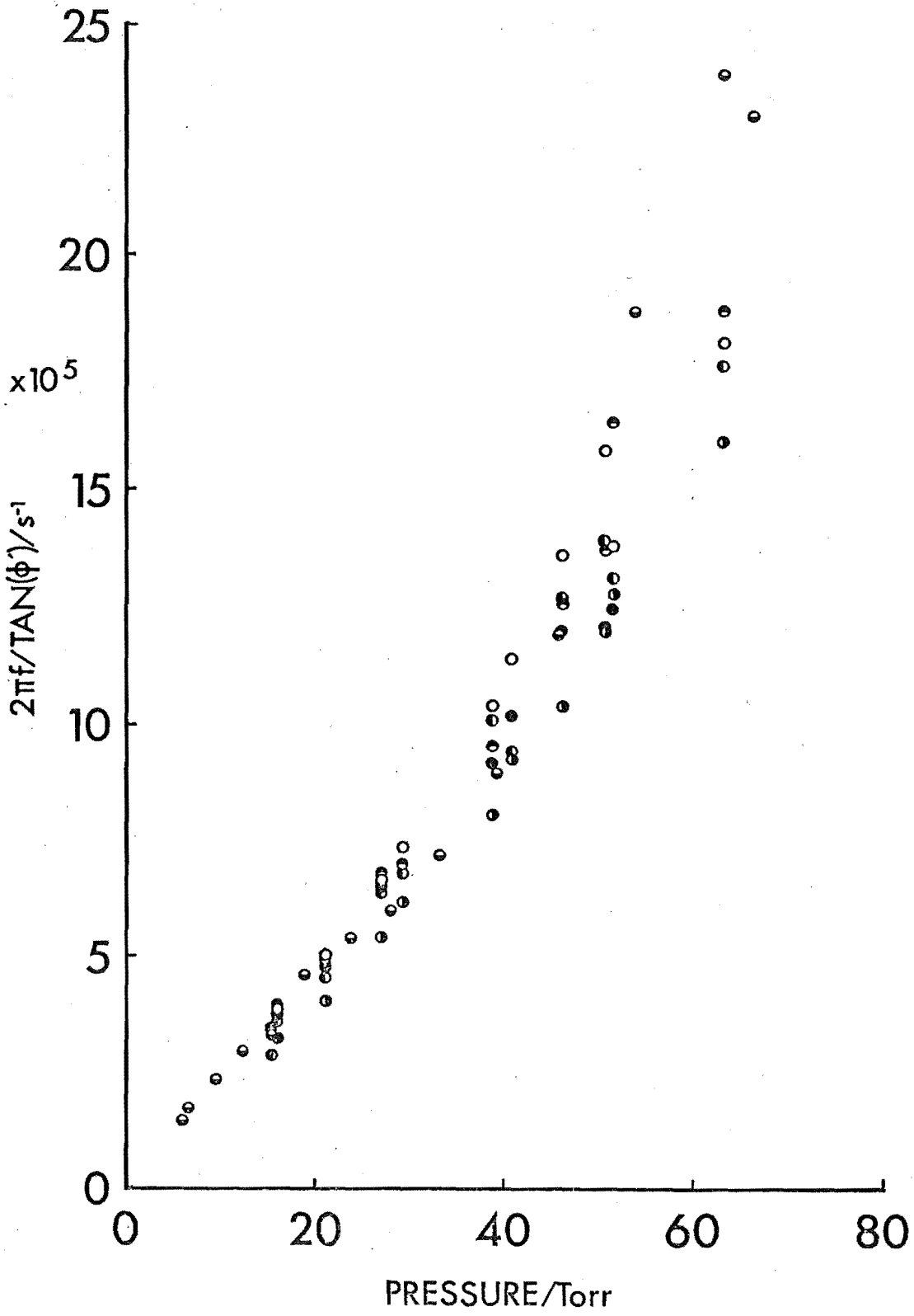

Fig. III-5. PLOTS OF $2\pi F/\tan\phi'$ AS A FUNCTION OF THE AMMONIA PRESSURE.

$\phi' = \phi - \phi_\infty$, where ϕ_∞ is the phase shift recorded at 170 Torr. Different frequencies are denoted in the same fashion as in Fig. III-4.

(4) Boxcar Phase Measurements

Examples of the modulated emission signals obtained using the technique described in Section III-2 of the preceding chapter are shown in Fig. III-6. These waveforms were recorded at a low ammonia pressure (≈ 5 Torr); the large phase lag of the 430 nm emission and the smaller lag of the 508.5 nm fluorescence behind the 326.1 nm fluorescence are clearly shown.

The phase shifts calculated directly from the waveforms showed the phase difference between the $^3P_1$ level and the exciplex emission to be in excellent agreement with the 30 kHz data obtained from the lock-in amplifier measurements. However, while the phase of the $^3P_0$ level was found to lag that of the $^3P_1$ level at low ammonia pressures, at pressures above about 3 Torr the Cd($^3P_0$) phase led that of Cd($^3P_1$). The explanation for this behaviour appears to lie in the laser's triggering delay described in section III-2(c) of Chapter II. The relative shifts of the Cd($^3P_1$) and exciplex populations are in agreement with the lock-in amplifier results because in these cases, each time the boxcar's input was gated open the signal sampled was representative of the fluorescence at the same time interval through the modulation cycle for both the 326.1 nm and 430 nm emissions; apparently this is not the case with the LIF signal. The signal representative of the $^3P_0$ level seems to be advanced from its true phase for a reason that remains unidentified, but which appears to involve the delay in the laser triggering circuitry. As the phase of the Cd($^3P_0$) population led that of the Cd($^3P_1$) population by an approximately constant value

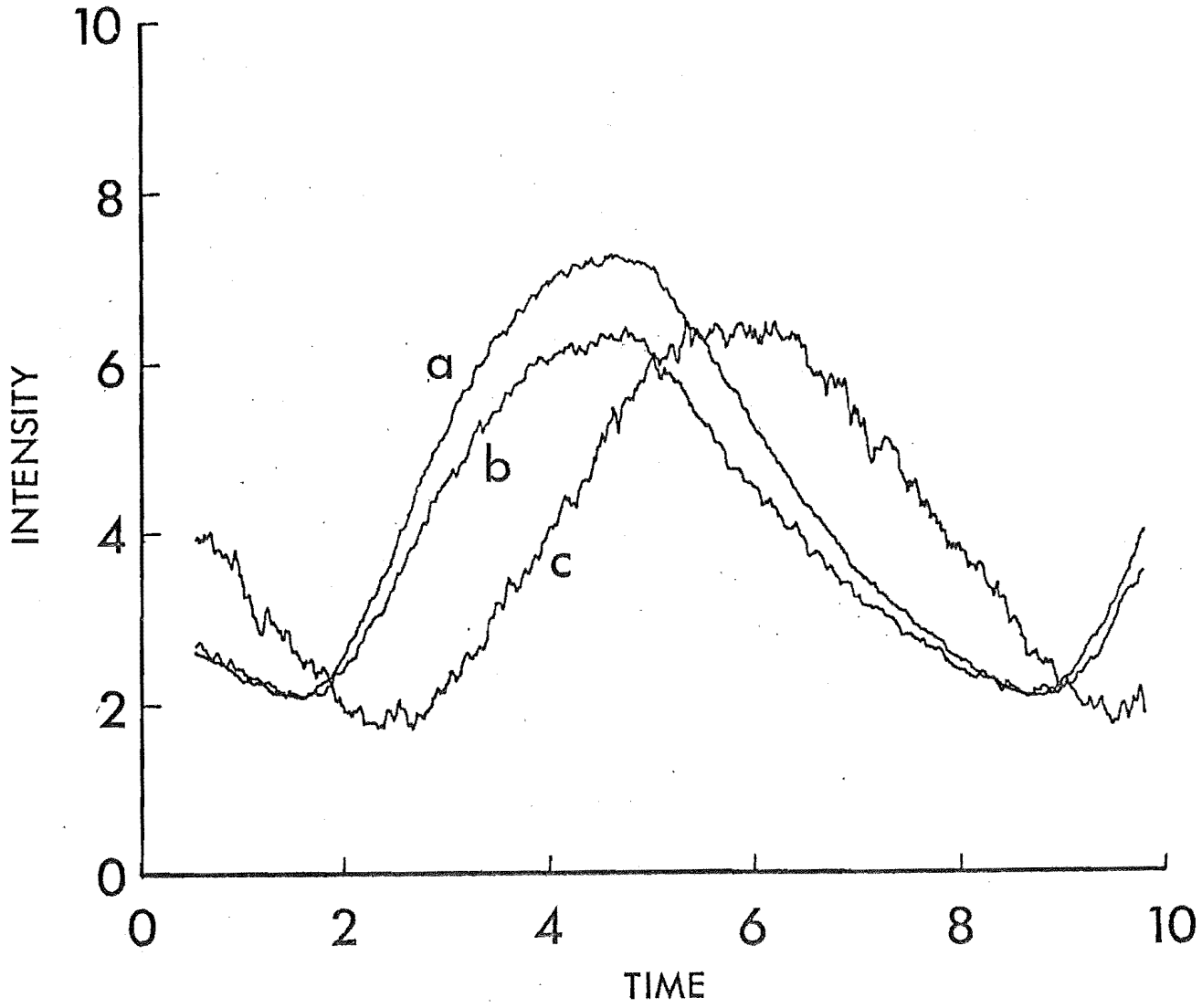

Fig. III-6. TYPICAL WAVEFORMS PLOTTED FROM COMPUTER DISK FILES OBTAINED FROM THE BOXCAR INTEGRATOR.

Curve a is $Cd(^3P_1)$ fluorescence excited by the cadmium lamp; curve b is 508.5 nm fluorescence ($Cd(^3P_0)$) excited by the dye laser and curve c is exciplex emission excited by the cadmium lamp. Modulation frequency = 30.0 kHz; ammonia pressure = 5.9 Torr; cadmium pressure = 12 mTorr; boxcar aperture time = 0.385 s; scan time = 2 minutes. Ten scans were averaged for curves a and c; 15 scans were averaged for curve b.

of 10.3° at ammonia pressures greater than about 12 Torr, this shift was taken as being equal to the $Cd(^3P_1)$ phase angle so that all raw $Cd(^3P_0)$ phase lags were correspondingly corrected by the addition of 10.3°. The attributing of this phase displacement to the firing delays of the laser and the assumption that the $Cd(^3P_1)$ and $Cd(^3P_0)$ shifts are identical from the point at which the $Cd(^3P_0)$ shift becomes constant are supported by three factors: (a) at 30 kHz a shift of 10.3° is equivalent to a delay of 0.95 μs which is approximately the delay expected in the laser trigger circuitry; (b) it is known from previous studies (see Introduction and Review) that a large number of gases, including ammonia,[18] establish a rapid equilibrium between $Cd(^3P_1)$ and $Cd(^3P_0)$; (c) it appears that it is impossible to devise a mechanism that predicts the change from $Cd(^3P_0)$ lagging $Cd(^3P_1)$ to its leading $Cd(^3P_1)$.

To ensure that the settings of time constant and aperture time of the boxcar were not distorting the waveforms and hence the phase shifts, some runs were conducted with first the time constant then the aperture time altered. When the aperture time was decreased it was also found necessary to increase the time base in order that a maximum signal might be obtained. This dependence of the aperture time setting on the time base presumably has its roots in the phenomenon that allows the LIF signal to be retrieved despite the triggering delay. As the measured phase shifts were invariant with the change in any of the experimental settings, all data were obtained using the first settings given in Section III-2(c) of the previous chapter.

As the corrected $Cd(^3P_0)$ phase shifts give the plot in Fig. III-7 (and Table III-2), the mechanism suggested

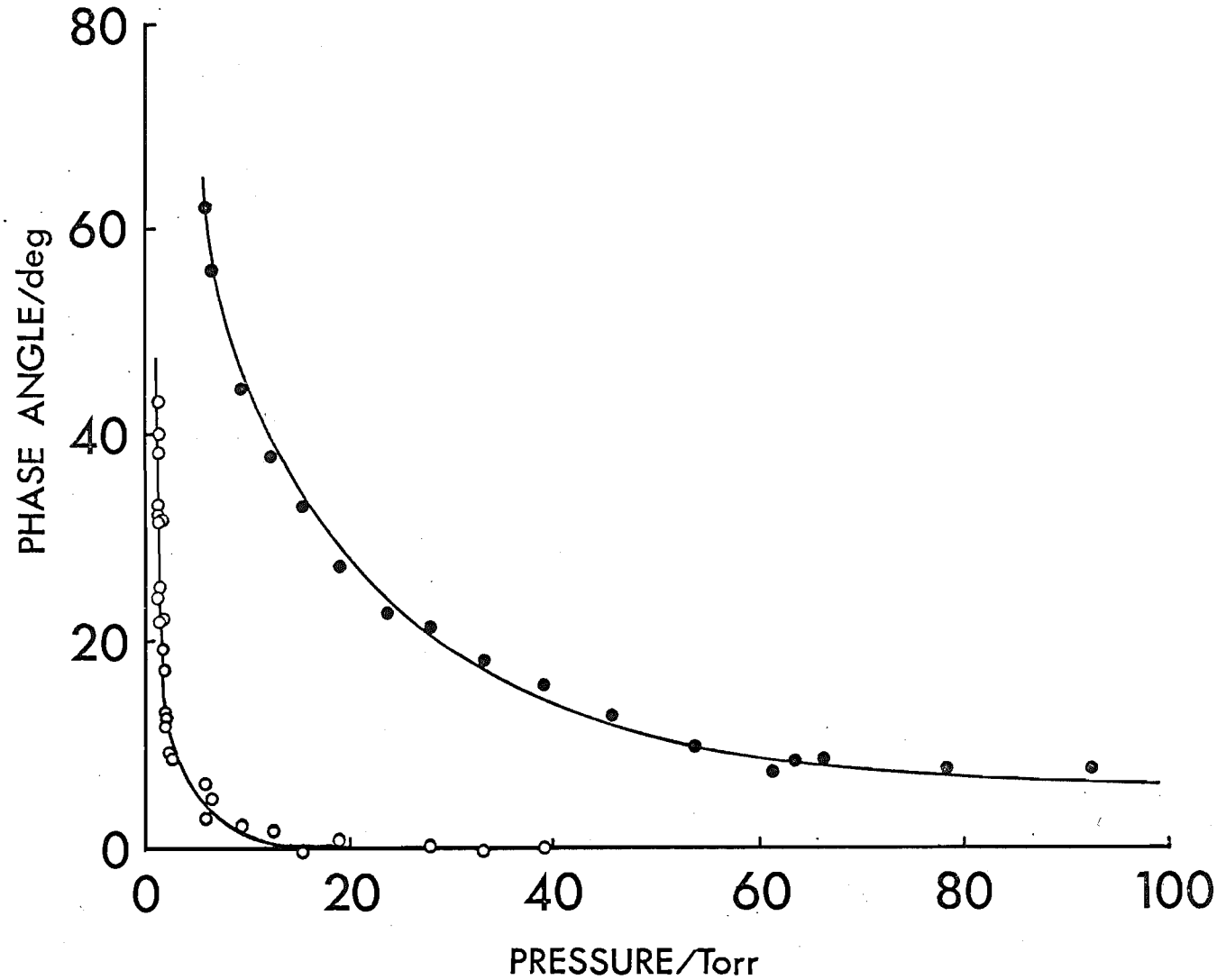

Fig. III-7. PHASE SHIFTS CALCULATED BY THE FOURIER ANALYSIS OF THE MODULATED WAVEFORMS AS A FUNCTION OF THE AMMONIA PRESSURE.

Temperature = 550 K; cadmium pressure = 12 mTorr; modulation frquency = 30.0 kHz. ● = $CdNH_3$* - Cd($^3P_1$) phase difference; o = Cd($^3P_0$) - Cd($^3P_1$) phase difference.

Table III-2. Phase Data from the Fourier Analysis of Fluorescence Waveforms.

Ammonia Pressure (Torr)	Phase Differences (degrees) $CdNH_3^*-{}^3P_1$	$^3P_0-{}^3P_1$	$CdNH_3^*-{}^3P_0$	$\frac{2\pi f}{\tan\theta}/10^5 s^{-1}$	$\frac{2\pi f}{\tan\phi}/10^5 s^{-1}$	$\frac{2\pi f}{\tan\phi'}/10^5 s^{-1}$
‡1.06		32.4		2.97		
‡1.18		19.1		5.45		
‡1.20		21.4		4.80		
1.23		43.3		2.00		
‡1.26		12.4		8.56		
1.26		38.4		2.38		
‡1.28		16.7		6.27		
1.33		33.1		2.89		
1.34		40.2		2.23		
1.35		24.2		4.20		
1.36		32.3		2.98		
1.38		31.5		3.08		
1.43		22.0		4.67		
1.43		25.4		3.96		
1.50		32.6		2.95		
1.52		19.4		5.36		
1.58		22.1		4.65		
1.69		17.1		6.12		
1.71		10.9		9.80		
1.80		13.1		8.12		
1.89		12.6		8.43		
2.36		9.1		11.7		
2.50		8.5		12.6		
5.77		2.9		37.9		
5.91	62.2	6.3	55.9	17.2	1.27	1.47
6.49	56.1	4.7	51.4	23.0	1.50	1.73
9.43	44.3	2.1	42.3	52.7	2.07	2.38
12.2	38.0	1.7	36.2	62.4	2.57	2.98
15.4	33.1	-0.4	33.5		2.84	3.31
19.0	27.1	0.9	26.2		3.83	4.60
23.8	23.1		23.1		4.41	5.40
28.0	21.5	-0.1	21.4		4.82	5.99

‡Data from low pressure runs with short pump-out times (see text).

Table III-2 Cont.

Ammonia Pressure (Torr)	Phase Differences (Degrees)			$\frac{2\pi f}{\tan\theta}/10^5 s^{-1}$	$\frac{2\pi f}{\tan\phi}/10^5 s^{-1}$	$\frac{2\pi f}{\tan\phi'}/10^5 s^{-1}$
	$CdNH_3^* - {}^3P_1$	${}^3P_0 - {}^3P_1$	$CdNH_3^{*'} - {}^3P_0$			
33.2	18.1	0.6	18.6		5.59	7.17
39.3	15.8	-0.1	15.8		6.67	8.96
45.9	12.9		12.9		8.22	11.9
53.8	9.6		9.6		11.1	18.8
61.2	7.3		7.3		14.8	32.0
63.3	8.4		8.4		12.7	23.9
66.2	8.6		8.6		12.5	23.0

by Morten et al.[71] must be abandoned. Their mechanism predicts that the shift between $Cd(^3P_0)$ and $CdNH_3^*$ is constant; evidently this is not so. Rather, the data imply the presence of a species intermediate between triplet cadmium and the exciplex, or, if the high pressure shift is zero, possibly an ammonia dependent process that returns the exciplex to its precursors. (Any process by which ammonia removes $CdNH_3^*$ would fit the phase data, but the lack of any indication of quenching of the exciplex by ammonia rules out any significant contribution from a collision resulting in quenched products.) The identical shifts of the $^3P_1$ and $^3P_0$ levels do not allow the adjudgement of either one as the sole precursor of the exciplex.

Phase data from the boxcar measurements are plotted in Figs. III-4, III-5 and III-8. Again the significance of these plots is discussed in section II-6. However, at this stage comment on the divergence from linearity at low pressures in Fig. III-8 is necessary. The increasing importance of diffusion to the walls at low pressures in a plot of this sort requires an increasingly positive deviation from the line with decreasing pressure, rather than the negative deviation of Fig. III-8. The observed deviation implies that the phase difference at a particular pressure is larger than the higher pressure data of the plot predict. This is probably attributable to the indirect method of pressure determination used in this study. Reasonable reproducibility for the phase shifts of the $^3P_0$ level at low pressures could only be obtained if a sufficiently long pump-out time was allowed between runs; short pump-out

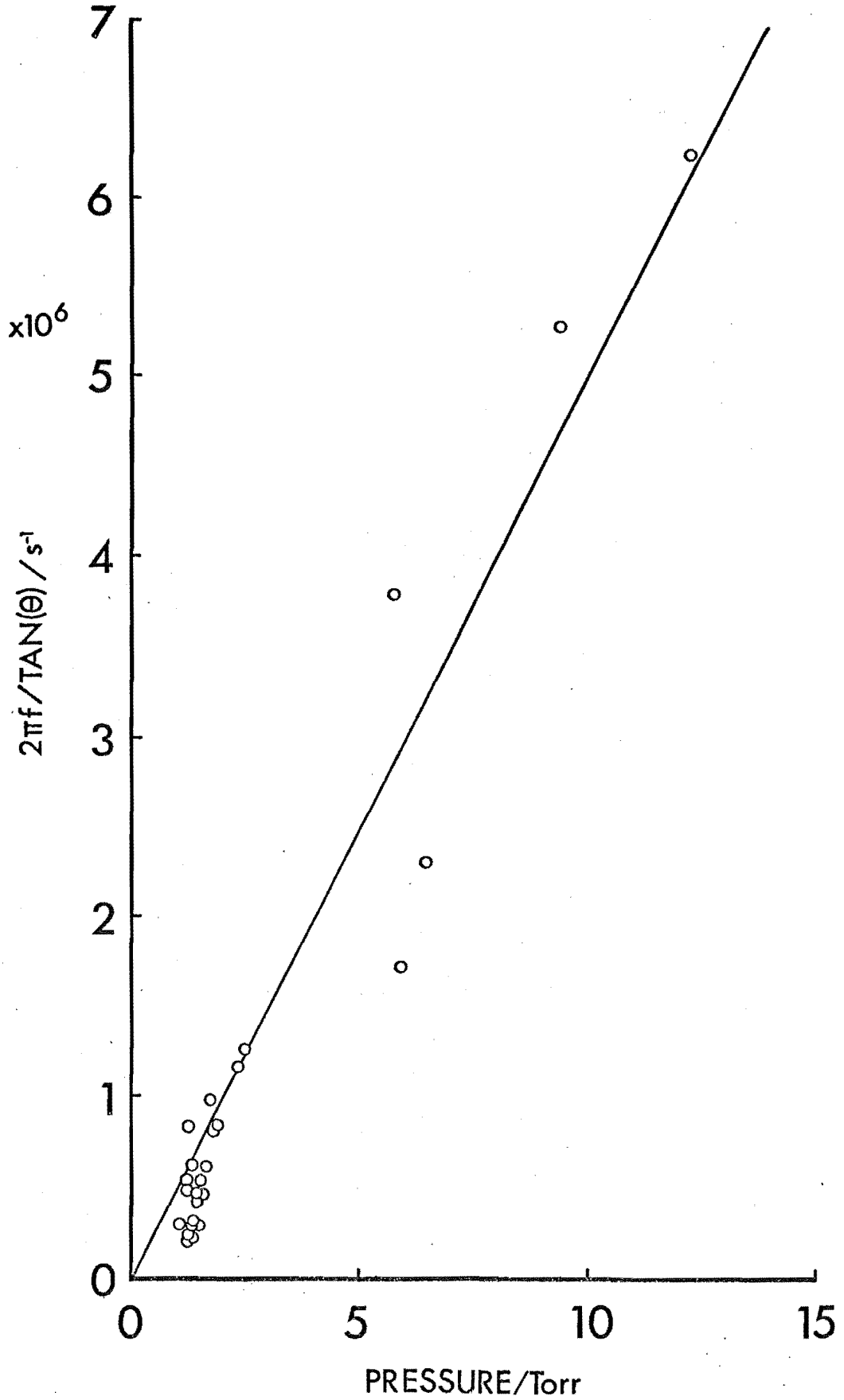

Fig. III-8. PLOT OF $2\pi F/\tan\theta$ AS A FUNCTION OF THE AMMONIA PRESSURE.

All data are from the boxcar measurements.
is the phase shift between $Cd(^3P_0)$ and $Cd(^3P_1)$.

times gave significantly smaller shifts. The points falling on, or close to, the straight line at the lowest pressures are those obtained with little pump-out time between runs; most of those falling below the line were obtained after a thorough pump-out.

The very strong dependence of the phase difference on the ammonia pressure in this region would lead to a considerable increase in the measured shift if, because of ammonia being adsorbed onto surfaces within the cell, the actual cell pressure was slightly less than that calculated. This is consistent with the dependence of the measurements on the pump-out time. At the cell temperatures used, the amount of ammonia adsorbed is expected to be very small but perhaps sufficient to cause this deviation. The effect is not noticeable elsewhere because of the weaker pressure dependence of the phase difference.

(5) The Ratio of the Exciplex Intensity to the 326.1 nm Fluorescence Intensity as a Function of the Cadmium Pressure

The $I_{430}/I_{326.1}$ measurements were made in an attempt to identify a long-lived excimer state as the intermediate whose possible existence could be read from the phase measurements. Fig. III-9 (the data are also listed in Table III-3) shows that although at a high fixed ammonia pressure the ratio is constant with increasing cadmium pressure, at much lower pressures there is a dependence that scales linearly with the cadmium pressure. The behaviour

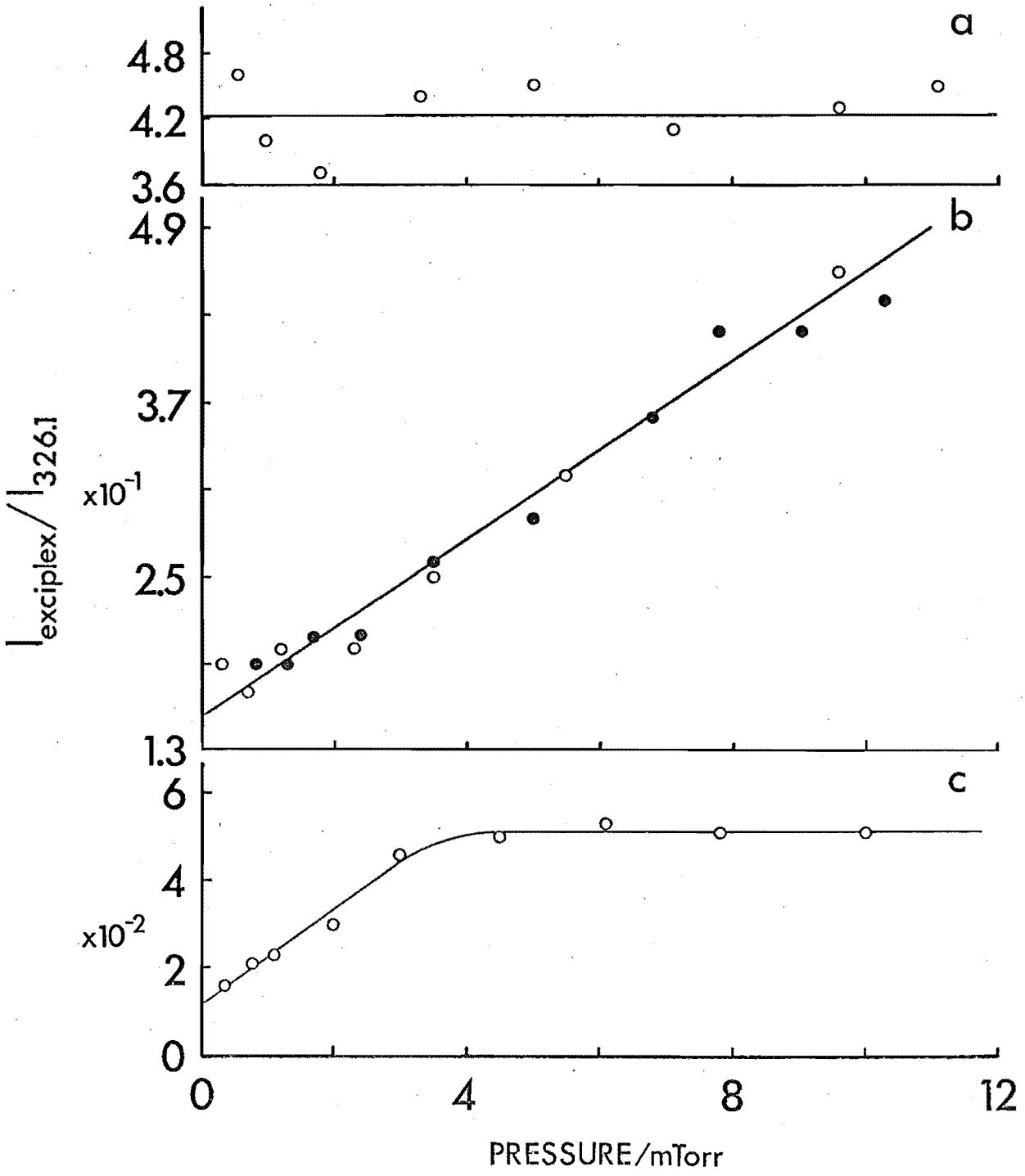

Fig. III-9. $I_{430}/I_{326.1}$ AS A FUNCTION OF THE CADMIUM PRESSURE IN DIFFERING AMMONIA PRESSURE REGIONS.

Temperature = 550 K. Curve a, ammonia pressure = 67.0 Torr; curve b, ammonia pressure = 7.3 Torr (open circles) and 7.8 Torr (filled circles); curve c, ammonia pressure = 2.7 Torr.

Table III-3. $I_{430}/I_{326.1}$ Ratios as a Function of the Cadmium Pressure

$[NH_3]$ = 67.0 Torr		$[NH_3]$ = 7.3 Torr		$[NH_3]$ = 7.8 Torr		$[NH_3]$ = 2.7 Torr	
Cadmium Pressure/mTorr	$\frac{I_{430}}{I_{326.1}}$	Cadmium Pressure/mTorr	$\frac{I_{430}}{I_{326.1}}/10^{-1}$	Cadmium Pressure/mTorr	$\frac{I_{430}}{I_{326.1}}/10^{-1}$	Cadmium Pressure/mTorr	$\frac{I_{430}}{I_{326.1}}/10^{-2}$
0.54	4.6	0.31	1.9	0.82	1.9	0.34	1.6
0.92	4.0	0.69	1.7	1.3	1.9	0.77	2.1
1.8	3.7	1.2	2.0	1.7	2.1	1.1	2.3
3.3	4.4	2.3	2.0	2.4	2.1	2.0	3.0
5.0	4.5	3.5	2.5	3.5	2.6	3.0	4.6
7.1	4.1	5.5	3.2	5.0	2.9	4.5	5.0
9.6	4.3	9.6	4.6	6.8	3.6	6.1	5.3
11.1	4.5			7.8	4.2	7.8	5.1
				9.1	4.2	10.0	5.1
				10.3	4.4		

of the ratio in the different ammonia pressure regions strongly supports the presence of two parallel processes leading to the exciplex, one dependent on ammonia and the other incorporating a step involving a ground-state cadmium atom. At high ammonia pressures the first of these pathways is dominant.

(6) Discussion and Rate Constant Evaluation

In understanding the reasons for the final interpretation placed upon the results of the present work, it is instructive to examine the possible mechanistic schemes that may be called upon to fit the experimental results both from this and previous work, to see why they fail or succeed.

Recapitulating, the experimental criteria to be met by the correct mechanism are:

(i) The establishment of a rapid equilibrium between $Cd(^3P_1)$ and $Cd(^3P_0)$ at pressures above about 12 Torr (this and previous work).

(ii) The presence of some process in the system, other than absorption of the exciting quanta, that is dependent on the ground-state cadmium atom concentration (this work).

(iii) The high quantum efficiency of 0.67 of the $CdNH_3^*$ luminescence.[75]

(iv) Stern-Volmer plots for the quenching of 326.1 nm fluorescence requiring a combined quenching constant for $Cd(^3P_1)$ and $Cd(^3P_0)$ by ammonia to be of the order of 10^{-12} cm^3 $molecule^{-1}$ s^{-1}.[18]

(v) The form of the ammonia dependence of the exciplex emission intensity implying little or no quenching of the exciplex by ammonia.[74]

Consideration is first given to Scheme III-2 where processes (3.19) and (3.20) may be partly or wholly termolecular or bimolecular respectively. M is any collision partner, and Cd_2^* is the emitter of the 470 nm excimer band.

Scheme III-2

$$Cd + h\nu \rightarrow Cd_1 \quad (3.15)$$

$$Cd_1 \rightarrow Cd + h\nu \quad (3.16)$$

$$A + Cd_1 \rightarrow Cd_0 + A \quad (3.17)$$

$$A + Cd_0 \rightarrow Cd_1 + A \quad (3.18)$$

$$A + Cd_0 \xrightarrow{(m)} CdA^* \quad (3.19)$$

$$CdA^* \xrightarrow{(m)} Cd_0 + A \quad (3.20)$$

$$CdA^* \rightarrow Cd + A + h\nu' \quad (3.21)$$

$$A + Cd + Cd_0 \rightarrow Cd_2^* + A \quad (3.22)$$

$$A + Cd_2^* \rightarrow Cd_0 + Cd + A \quad (3.23)$$

$$Cd_2^* \rightarrow Cd + Cd + h\nu'' \quad (3.24)$$

$$A + Cd_2^* \rightarrow CdA^* + Cd \quad (3.25)$$

$$Cd + CdA^* \rightarrow Cd_2^* + A \quad (3.26)$$

To enable this scheme to predict the data of Fig. III-9, at the cadmium pressures used in this work, it must be assumed that reaction (3.19) is a very slow two-bodied reaction if reaction (3.22) is to have a rate constant typical of a termolecular process (at most 10^{-30} cm^6 $molecule^{-2}$ s^{-1}). However, as the only means of removal of triplet cadmium is through complex formation, this value of k_{19} is inconsistent with the Stern-Volmer quenching results; the removal of excited cadmium atoms by complex formation cannot compete with losess by the radiative pathway. Increasing k_{19} requires k_{22} to become several orders of magnitude greater than is feasible for a termolecular process, and the inclusion of a fast quenching reaction is not in accord with the exciplex's quantum efficiency.

The possibility that a reaction similar to (3.22), but producing a stabilised excimer by a bimolecular reaction, is also out of the question, as a diatomic molecule has insufficient degrees of freedom to dissipate the 100 kJ $mole^{-1}$ (approximately) of the excimer's binding energy. The possibility of an unstabilised excimer being sufficiently long-lived to compete with exciplex formation by ammonia is discussed later.

Still considering the data of Fig. III-9, mechanisms such as those of Schemes III-3 and III-4, in which the cadmium atom enters the reaction system by collision with any species other than a triplet cadmium atom cannot predict the cadmium pressure dependence.

Scheme III-3

$$Cd + h\nu \rightarrow Cd_1 \qquad [3.15]$$

$$Cd_1 \rightarrow Cd + h\nu \qquad [3.16]$$

$$A + Cd_1 \rightarrow Cd_0 + A \qquad [3.17]$$

$$A + Cd_0 \rightarrow Cd_1 + A \qquad [3.18]$$

$$A + Cd^* \rightarrow CdA^\dagger \qquad (3.27)$$

$$A + CdA^\dagger \rightarrow CdA^* + A \qquad (3.28)$$

$$Cd + CdA^\dagger \rightarrow Cd_2^* + A \qquad (3.29)$$

$$A + Cd_2^* \rightarrow CdA^* + Cd \qquad [3.25]$$

$$CdA^* \rightarrow Cd + A + h\nu' \qquad [3.21]$$

$$I_{430}/I_{326.1} = \frac{k_{27}[A]}{k_{16}} \text{ or } \frac{k_{27}k_{17}[A]}{k_{16}k_{18}}$$

depending on whether Cd* is Cd_1 or Cd_0 respectively.

Scheme III-4

$$Cd + h\nu \rightarrow Cd_1 \qquad [3.15]$$

$$Cd_1 \rightarrow Cd + h\nu \qquad [3.16]$$

$$A + Cd_1 \rightarrow Cd_0 + A \qquad [3.17]$$

$$A + Cd_0 \rightarrow Cd_1 + A \qquad [3.18]$$

$$A + Cd^* \rightarrow CdA^* \qquad (3.30)$$

$$Cd + CdA^* \rightarrow Cd_2^* + A \qquad [3.26]$$

$$A + Cd_2^* \rightarrow CdA^* + Cd \qquad [3.25]$$

$$CdA^* \rightarrow Cd + A + h\nu' \qquad [3.21]$$

$$I_{430}/I_{326.1} = \frac{k_{30}[A]}{k_{16}} \text{ or } \frac{k_{30}k_{17}[A]}{k_{16}k_{18}} \quad .$$

Moreover, unless k_{21} is very small, Scheme III-4 also fails to explain the phase measurements of Fig. III-3, because the removal of $CdNH_3^*$ by cadmium to produce the excimer is unlikely to be able to compete with exciplex losses through (3.21) at the cadmium pressures used, so giving an approximately constant phase difference with increasing ammonia pressure.

Even the proposal that stimulated emission is responsible for the 430 nm band (see Scheme III-5), which is consistent with the observed dependence of the exciplex emission on the ammonia pressure, does not account for the cadmium dependence of $I_{430}/I_{326.1}$.

Scheme III-5

$$Cd + h\nu \rightarrow Cd_1 \quad [3.15]$$

$$Cd_1 \rightarrow Cd + h\nu \quad [3.16]$$

$$A + Cd_1 \rightarrow Cd_0 + A \quad [3.17]$$

$$A + Cd_0 \rightarrow Cd_1 + A \quad [3.18]$$

$$A + Cd^* \rightarrow CdA^* \quad [3.30]$$

$$A + CdA^* \rightarrow Cd + A + A + h\nu' \quad (3.31)$$

$$Cd + CdA^* \rightarrow Cd + Cd + A + h\nu' \quad (3.32)$$

$$Cd + CdA^* \rightarrow Cd_2^* + A \quad [3.26]$$

$$A + Cd_2^* \rightarrow CdA^* + Cd \quad [3.25]$$

It is clear from the foregoing discussion that at moderate and high ammonia pressures a species other than Cd_2^* must be looked to if an intermediate species is to be held responsible for the shift between excited cadmium and the exciplex. Some form of Cd/NH_3 complex is the only remaining candidate for this rôle. An unstabilised complex, $CdNH_3^\dagger$ is used to model the results of the present study.

The proposed mechanism for the Cd/NH_3 system, Scheme III-6, is basically the same as that proposed by the Japanese group[77], but as will be seen later, the rate constants obtained from the phase data cannot be compared with those of Umemoto et al. because of a difference in interpretation proposed in this work.

Scheme III-6

$$Cd + h\nu \rightarrow Cd_1 \quad [3.15]$$

$$Cd_1 \rightarrow Cd + h\nu \quad [3.16]$$

$$A + Cd_1 \rightarrow CdA^{\dagger} \quad (3.33)$$

$$CdA^{\dagger} \rightarrow Cd_1 + A \quad (3.34)$$

$$CdA^{\dagger} \rightarrow Cd_0 + A \quad (3.35)$$

$$CdA^{\dagger} \rightarrow \text{quenched products} \quad (3.36)$$

$$CdA^{\dagger} \rightarrow Cd + A + h\nu''' \quad (3.37)$$

$$A + Cd_0 \rightarrow CdA^{\dagger} \quad (3.38)$$

$$A + CdA^{\dagger} \rightarrow CdA^{*} + A \quad [3.28]$$

$$A + CdA^{*} \rightarrow CdA^{\dagger} + A \quad (3.39)$$

$$CdA^{*} \rightarrow Cd + A + h\nu' \quad [3.21]$$

No process whereby an excited species diffuses to the cell walls to be quenched is included in Scheme III-6 as on the reaction time scale of the modulation frequencies used in this work their contribution to the observed system kinetics is insignificant. This is verified experimentally by the lack of curvature attributable to wall reactions in Figs. III-4 and III-8. The finding, by Sato's group, that only one emitting species is present in the system (see Chapter I section II-3) implies that emission process (3.37) is negligible. The same result also makes it unnecessary to include, by analogy with the mercury system[72], the possibility of more than one ammonia molecule binding to an excited cadmium atom to form an emitting complex.

The magnitude of the phase differences in Fig. III-7 indicate that processes causing equilibration between $Cd(^3P_1)$ and $Cd(^3P_0)$ are at least an order of magnitude faster than those leading to the final exciplex emission. To simplify

the expression for tan θ [θ is the phase difference between $Cd(^3P_1)$ and $Cd(^3P_0)$] then, processes (3.28), (3.39) and (3.21) are initially omitted from the analysis, thus allowing rate constant evaluation. At angular frequency ω, the phase analysis of Scheme III-6 yields (see Appendix B)

$$\frac{\tan \theta}{\omega} = (k_{38}[A] + k_r)/(k_{38}[A](k_r - k_{35}) - \omega^2), \qquad (3.40)$$

where $k_r = (k_{34} + k_{35} + k_{36} + k_{37})$. The ammonia pressure range over which equation (3.40) is of interest is approximately from 2-12 Torr (3×10^{16} - 2×10^{17} molecules cm^{-3}). Processes (3.34) and (3.35), being unimolecular dissociations, are expected to possess rate constants in the range 10^9 s^{-1} to 10^{13} s^{-1}, and k_{38}, a bimolecular constant, can be reasonably assumed to be of the order of 10^{-10} cm^3 $molecule^{-1}$ s^{-1}, or less. From these estimations, $k_{38}[A]$, over the stated pressure range, is negligible in comparison with k_r as is ω^2 in comparison with $(k_r - k_{35})$. Additionally, if k_{36} is very much smaller than $(k_{34} + k_{35})$ (which is justified shortly) equation (3.40) reduces to

$$\frac{\tan \theta}{\omega} = \frac{1}{k_{38}[A]}\left(1 + \frac{k_{35}}{k_{34}}\right) \quad . \qquad (3.41)$$

With $CdNH_3^{\dagger}$ regarded as a collision complex (represented diagramatically in Fig. III-10), that is, reactions (3.33) and (3.38) produce the same species, the branching ratio of k_{35}/k_{34} is determined statistically by the ratio of the degeneracy factors of the triplet levels. (This assumes that the statistical ratio (1:3) is not upset by the energy

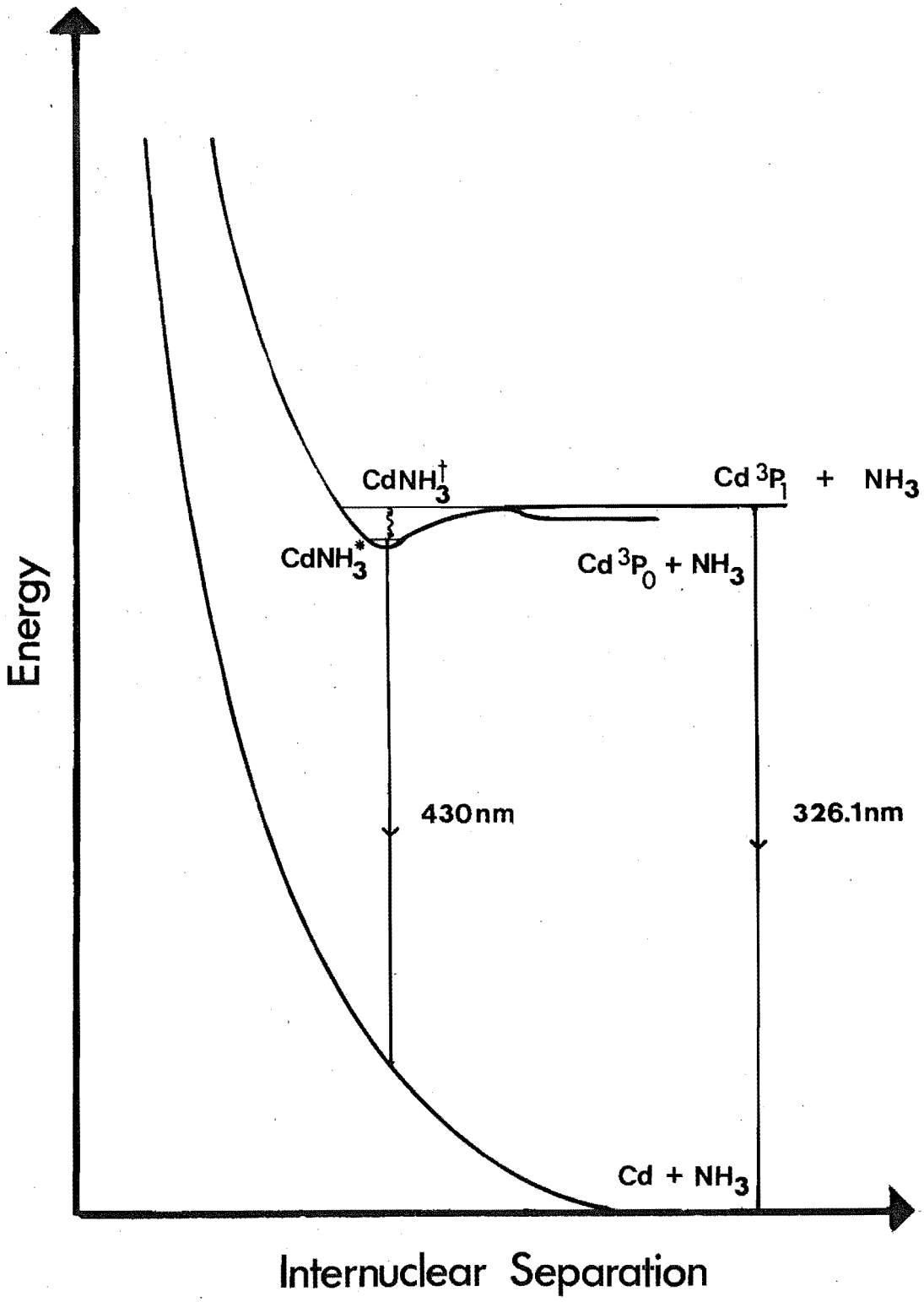

Fig.III-10. QUALITATIVE POTENTIAL CURVES FOR THE Cd^*/NH_3 SYSTEM, PROPOSED FROM THE FINDINGS OF THE PRESENT WORK.

$CdNH_3^\dagger$ is proposed to be of the same energy as the $^3P_1$ level so that the production of $CdNH_3^\dagger$ from $Cd(^3P_0)$ atoms has an activation energy equal to the energy spacing of the two atomic levels.

The wavy line denotes the collisional stabilization of $CdNH_3^\dagger$ to $CdNH_3^*$, and the reverse process.

separation of the $^3P_1$ and $^3P_0$ levels.) Thus,

$$\frac{\tan \theta}{\omega} = 1.33/k_{38}[A] \quad . \tag{3.42}$$

From the slope of Fig. III-8 it is found that $k_{38} = 2.1 \times 10^{-11}$ cm^3 molecule^{-1} s^{-1} at 550 K and hence $k_{33} = 8.7 \times 10^{-11}$ cm^3 molecule^{-1} s^{-1}, both having an uncertainty of about $\pm$ 20%.

The analysis that follows justifies the omission of k_{36} from the above derivation. The rate of photon emission as 326.1 nm fluorescence in the absence of ammonia must, under steady-state conditions, equal the total rate at which energy quanta are lost from the system with ammonia present (when the rate of energy absorption is the same in each case). So neglecting process (3.37) and letting $[Cd_1]_0$ represent the concentration of $Cd(^3P_1)$ in the absence of ammonia, equation (3.43) is obtained.

$$k_{16}[Cd_1]_0 = k_{16}[Cd_1] + k_{36}[CdA^\dagger] + k_{21}[CdA^*] \tag{3.43}$$

As the quantum efficiency determined by Yamamoto and Sato[75] is 0.67 (average over the range 5-50 Torr), the radiative process (3.21) and the non-radiative process (3.36) must occur in the ratio 2:1, i.e.,

$$0.67\ k_{36}[CdA^\dagger] = 0.33\ k_{21}[CdA^*] \quad . \tag{3.44}$$

Equation (3.43) can be rearranged to

$$k_{21}[CdA^*] = 0.67\ k_{16}([Cd_1]_0 - [Cd_1]) \quad , \tag{3.45}$$

and a steady-state analysis for $[CdA^\dagger]$ gives

$$[CdA^{\dagger}] = \frac{[A](k_{33}[Cd_1] + k_{38}[Cd_0] + k_{39}[CdA^*])}{k_r + k_{28}[A]} \qquad (3.46)$$

Rearrangement of equation (3.43) and the subsequent substitution of equations (3.44), (3.45) and (3.46) into it yields:

$$k_{16}(I_0/I - 1) = \frac{k_{36}[A](k_{33}+k_{38}K+0.67k_{39}k_{16}(k_0/I - 1)/k_{21})}{0.22(k_r+k_{28}[A])}, \qquad (3.47)$$

where $I_0/I = [Cd_1]_0/[Cd_1]$ and K is less than or equal to the equilibrium constant for the conversion of $Cd(^3P_1)$ to $Cd(^3P_0)$. From a Stern-Volmer analysis a quenching constant k_q can be defined.

$$k_q = (I_0/I - 1)k_{16}/[A] \qquad (3.48)$$

Finally, substituting (3.48) into (3.47), equation (3.49) is reached.

$$k_q = \frac{k_{36}(k_{33}+k_{38}K+0.67k_{39}k_q[A]/k_{21})}{0.33(k_r+k_{28}[A])} \qquad (3.49)$$

From their Stern-Volmer plot Sato and co-workers quoted a half-quenching pressure of 12.6 Torr because of the slight curvature they found. Taking k_{16} as 4.3×10^5 s^{-1} [109], this pressure corresponds to a k_q value of about 2×10^{-12} cm^3 $molecule^{-1}$ s^{-1} at 493 K. Breckenridge et al.[18] from their plot, which showed no curvature, reported a k_q of 1.2×10^{-12} cm^3 $molecule^{-1}$ s^{-1} at 553 K. Taking the latter value for k_q estimating $k_{39} \approx 10^{-12}$ cm^3 $molecule^{-1}$ s^{-1} and $k_{21} \approx 10^5$ s^{-1}, and noting that k_r is much greater than $k_{28}[A]$, the ratio

$$k_{36}/k_r \approx 3 \times 10^{-3}$$

is obtained, vindicating the neglect of k_{36} in the earlier expressions.

The derivation of an expression for tan ϕ (ϕ is the phase shift between $Cd(^3P_0)$ and $CdNH_3^*$) can be approached in different ways, each of which leads to the same result. The full expression for this phase shift is (see Appendix B)

$$\frac{\tan \phi}{\omega} = \frac{k_{38}[A] - (k_{39}[A] + k_{21})}{k_{38}[A](k_{39}[A]+k_{21}) + \omega^2} \quad . \tag{3.50}$$

As processes responsible for the equilibrium between $Cd(^3P_0)$ and $Cd(^3P_1)$ are an order of magnitude faster than reactions (3.28),(3.39) and (3.21), an approximation that neglects $(k_{39}[A] + k_{21})$ in the numerator and ω^2 in the denominator gives,

$$\frac{\tan \phi}{\omega} = \frac{1}{k_{39}[A] + k_{21}} \tag{3.51}$$

The linearity of Fig. III-4 and its non-zero intercept support the assumptions about relative magnitudes made in the derivation of (3.51). The least-squares fit of the data gives a value of 9.1×10^{-13} cm^3 molecule^{-1} s^{-1} for k_{39} with an estimated uncertainty of $\pm$ 15% and a value of 6×10^4 s^{-1} for k_{21}, with an uncertainty of at least $\pm$ 50%. A firm upper limit of 1×10^5 s^{-1} will be taken for k_{21}. It should be noted that the reverse assumption that $(k_{39}[A] + k_{21})$ is very much greater than k_{38} not only predicts a straight line that passes through the origin but also a negative phase shift, which is not observed.

Fig. III-5 is plotted in a form similar to Fig III-4, but here $\phi' = \phi - \phi_\infty$ (ϕ_∞ is the phase shift at 170 Torr from the lock-in amplifier results). The failure of the data treated in this way to give a linear fit indicates that it is very likely the limiting shift at high pressures is very small or zero. It also supports the equation of the constant $Cd(^3P_0)$ phase shift with that of $Cd(^3P_1)$.

Equation (3.51) can also be reached by a consideration of the character of $CdNH_3^\dagger$. If this species is a relatively short-lived collision complex whose production from, and dissociation to, $Cd(^3P_1)$ and $Cd(^3P_0)$ are fast, the phase difference between $CdNH_3^\dagger$ and $Cd(^3P_1)$ or $Cd(^3P_0)$ will be insignificant. Therefore the difference between $Cd(^3P_0)$ and and $CdNH_3^*$ is equivalent to the difference between $CdNH_3^\dagger$ and $CdNH_3^*$ so that equation (3.51) is reached directly (see Appendix B).

The difference in interpretation of the results, while modelling them on basically the same mechanism, between the present work and the Japanese study must now be examined. While the interpretation given here requires rapid equilibration between $Cd(^3P_1)$, $Cd(^3P_0)$ and $CdNH_3^\dagger$ so that the observed shift between $Cd(^3P_0)$ (or $Cd(^3P_1)$ at the higher pressures) must depend upon processes removing $CdNH_3^*$, the Japanese hold that the phase lag between $CdNH_3^\dagger$ and $CdNH_3^*$ is negligible, i.e., $k_{39}[A] + k_{21}$ is large. This implies a slow, ammonia dependent process, or processes, participating in Scheme III-6 before $CdNH_3^*$ is produced. The set of rate constants determined numerically by the Japanese to fit their data (listed in section II-3 of Chapter I) are self-consistent,

but as Umemoto et al. point out they are not necessarily unique as only two shifts were measurable in their work. The inability of the group to obtain analytical results from their measurements stems from only being able to work with the phase difference between $Cd(^3P_1)$ and $CdNH_3^*$. The complexity of the resulting phase equation can be seen in their paper.[77] In the present work, the additional information about the phase shift of $Cd(^3P_0)$ has allowed a simplification of the expression for the shift between the 326.1 nm fluorescence and the 430 nm emission at the appropriate pressures. The derivation of equation (3.50), which is the result of this simplification, makes no assumption about the magnitudes of the rate constants, however, the acceptance by the Japanese that $k_{39}[A] + k_{21}$ is very much greater than $k_{38}[A]$ does not fit the experimental data, as has been pointed out above.

An upper limit of 22 kJ $mole^{-1}$ for the binding energy of $CdNH_3^*$ (i.e., the activation energy of reaction (3.39)) is obtained if a reasonable pre-exponential factor of 1×10^{-10} cm^3 $molecule^{-1}$ s^{-1} for reaction (3.39) together with the value for k_{39} are inserted into the Arrhenius equation. This value is supported by the use of the Japanese group's data plotted in Fig. I-5(k). (This plot is the same as Fig. III-4 of this work but with the inverse of the variables plotted.) From the rate (equivalent to k_{39}) extracted from Fig I-5(k), that from the present work, and the two experimental temperatures, an activation energy of 24 kJ $mole^{-1}$ is found for process (3.39). A value of about 5×10^4 s^{-1} for k_{21} can also be reclaimed from their data.

The validity of ignoring processes (3.28, (3.39) and (3.21) in deriving equation (3.40) can be assessed if the full expression for tan θ is derived (see Appendix B).

$$\frac{\tan\theta}{\omega} = \frac{\{(k_{39}[A]+k_{21})[(k_{38}[A]+k_r+k_{28}[A])(k_{39}[A]+k_{21})-k_{28}k_{39}[A]^2] + k_{38}k_{28}k_{39}[A]^3+\omega^2(k_{38}[A]+k_r+k_{28}[A])\}}{\left\{\begin{array}{l}\omega^2[k_{38}[A](k_r-k_{35}+k_{28}[A])-\omega^2-k_{28}k_{39}[A]^2] \\ +\ (k_{39}[A]+k_{21})\{[k_{38}[A](k_r-k_{35}+k_{28}[A])-\omega^2](k_{39}[A]+k_{21}) \\ \qquad - k_{38}k_{28}k_{39}[A]^3\}\end{array}\right\}} \qquad (3.52)$$

With $k_r > 3 \times 10^9$ s^{-1}, $k_9 = 1 \times 10^{-10}$ cm^3 molecule^{-1} s^{-1} and $\omega^2 = 4 \times 10^{10}$ s^{-1} together with the rate constants above, it is seen that equation (3.40) is accurate to within about 10% up to an ammonia concentration of 2×10^{17} molecule cm^{-3}. A departure of this magnitude from the line of Fig. III-8 would be hard to detect; nevertheless, it appears that a value of k_r smaller than 10^9 s^{-1} can definitely be ruled out.

At the beginning of this discussion it was shown how termolecular reactions producing Cd_2^* cannot compete with complex formation by ammonia at the cadmium pressures employed in this work. To account for the results of Fig. III.9 it therefore becomes necessary to consider the involvement of a short-lived collision complex $Cd_2^\dagger$, analogous to $CdNH_3^\dagger$.

Scheme III-7.

$$Cd + Cd_1 \rightarrow Cd_2^{\dagger} \quad (3.53)$$

$$Cd_2^{\dagger} \rightarrow Cd_1 + Cd \quad (3.54)$$

$$Cd_2^{\dagger} \rightarrow Cd_0 + Cd \quad (3.55)$$

$$Cd + Cd_0 \rightarrow Cd_2^{\dagger} \quad (3.56)$$

$$A + Cd_2^{\dagger} \rightarrow Cd^{*} + A \quad (3.57)$$

$$A + Cd_2^{\dagger} \rightarrow CdA^{*} + Cd \quad (3.58)$$

$$A + Cd_2^{*} \rightarrow CdA^{*} + Cd \quad (3.59)$$

$$Cd + CdA^{*} \rightarrow Cd_2^{*} + A \quad [3.26]$$

Consideration of the emission wavelength of Cd_2^* and $CdNH_3^*$ points to the emitting excimer state being more strongly bound than $CdNH_3^*$, thereby making process (3.59) endothermic. The emission of the 470 nm band from Cd_2^* is not included in Scheme III-7 because the data of Drullinger and Stock[58] indicate that even at temperatures as high as 850 K the decay rate of the band is only about 1.4×10^3 s^{-1}. As the decay rate shows a rapid decrease with decreasing temperature and pressure, at 550 K emission from the excimer is unlikely to be able to compete with the other processes in the scheme.

McGeoch's interpretation of these results was described in the Introduction (section II-2). The presence of a long-lived emitting excimer whose removal kinetics are controlled by the rate of thermal excitation to its dissociation limit provides another explanation for the decay characteristics of the 470 nm band. Whichever interpretation is correct, at low ammonia pressures an increasing cadmium concentration will eventually lead to an increase in the population of the lower-lying Cd_2^* states at the expense of $CdNH_3^*$. This seems

to be the reason for the levelling-off of the ratio in Fig. III-9(c).

Neglecting reaction (3.26) because of the low cadmium concentration and noting that $k_{39}[A][CdA^*] \ll (k_{33}[Cd_1] + k_{38}[Cd_0])[A]$, a steady-state treatment at the intermediate ammonia pressure yields:

$$\frac{I_{430}}{I_{326.1}} = \frac{k_{21}[A]}{k_{16}} \times \frac{\frac{k_{28}(k_{33}+k_{38}K)[A]}{(k_r+k_{28}[A])} + \frac{(k_{57}+k_{58})(k_{53}+k_{56}K)[Cd]}{(k_r' + (k_{57}+k_{58})[A])}}{k_{39}[A]+k_{21}} \tag{3.60}$$

where $k_r' = k_{54} + k_{55}$. Some notion of the relative magnitudes of k_r and k_r', and therefore the dissociative lifetimes of $CdNH_3^\dagger$ and $Cd_2^\dagger$ can be gained from an evaluation of the intercept/slope ratio from Fig. III-9(b) and the sloping portion of Fig. III-9(c). From the first of these the ratio is 5×10^{-3} Torr; from the latter 1×10^{-3} Torr is obtained. With $k_r >> k_{28}[A]$ and $k_r' >> (k_{57} + k_{58})[A]$ the ratio gives

$$\frac{k_{28}(k_{33}+k_{38}K)_r'}{(k_{57}+k_{58})(k_{53}+k_{56}K)k_r} \approx 5 \times 10^{-4}$$

The interconversion cross sections of Sato et al.[6,7] and Penkin and Redko[3] suggest that $(k_{33}+k_{38}K)$ is of the same order of magnitude as $(k_{53}+k_{56}K)$, so with the assumption that k_{28} and $(k_{57}+k_{58})$ do not differ by more than an order of magnitude, k_r' is necessarily two or three orders of magnitude smaller than k_r. This implies that k_r must be

near the higher end of the 10^9-$10^{13}s^{-1}$ range already assumed.

The additional vibrational degrees of freedom available to $CdNH_3^\dagger$ aid in prolonging its lifetime, however, the observed ratio of k_r'/k_r requires the presence of a mechanism capable of compensating $Cd_2^\dagger$ for its lack of vibrational modes. From the potential curves of Bender et al.,[62] which show a large number of electronic states of $Cd_2^\dagger$ near the dissociation limit, there arises the possibility that by curve crossing of the colliding atoms onto the potential surface of a bound state correlating with a higher energy asymptote the complex's lifetime is increased. Furthermore, some contribution to the length of the complex's lifetime may come from the colliding atoms being trapped behind a centrifugal barrier.

CHAPTER IV

SUMMARY AND CONCLUSIONS

The differing mechanistic proposals put forward by the two groups of workers who have studied exciplex formation in irradiated Cd/NH_3 mixtures led to this further investigation of the system. Both groups were hampered in the interpretation of their phase-shift results by having only the $Cd(^3P_1)$ - $CdNH_3^*$ phase difference from which to draw their conclusions. As LIF techniques allow the $Cd(^3P_0)$ level to be monitored and because its rôle was one of the points of disagreement between Sato and his co-workers, and Morten et al., the study described here was undertaken to provide kinetic information about the metastable species.

To do this, the $Cd(^3P_0)$ level was probed by a laser tuned to the $^3P_0 \rightarrow {}^3S_1$ transition and the resulting fluorescence at 508.5 nm was observed. Experimental complications did not allow decay measurements of $Cd(^3P_0)$ to be made; instead, through the collection, storage and subsequent Fourier analysis of the modulated LIF intensity data by a microcomputer, the phase measurements for this species were made. The elimination of timing delays (which approach the time resolution of the experimental modulation frequency) in the laser circuitry or a means of correcting the data for them were found to be crucial in the correct phase determination.

The form of the dependence of the $Cd(^3P_0)$ - $CdNH_3^*$ phase difference as a function of ammonia pressure indicates

that the scheme of Morten et al. must be abandoned and suggests the possible presence of an intermediate species between the triplet cadmium levels and the emitting complex. Steady-illumination measurements of $I_{430}/I_{326.1}$ (exciplex intensity/326.1 nm fluorescence intensity) as a function of cadmium pressure indicate that at certain ammonia pressures a process involving cadmium plays a kinetically significant part in the system. This is taken to indicate the formation of cadmium excimers. However, an examination of the possible kinetic schemes reveals that at the cadmium pressures used in this work, the importance of the production of the emitting exciplex from the cadmium excimer is restricted to the low ammonia pressure region. Accordingly, a mechanism virtually the same as that proposed by Sato and his co-workers was adopted to explain the phase data (see Scheme III-6).[77]

From the additional information about the phase relationships between $Cd(^3P_0)$ and the other excited species in the system, available from the present work, it seems necessary to look upon $CdNH_3^\dagger$ as a short-lived collision complex. This leads to an interpretation of the data at variance with that presented by the Japanese. From the phase data, the following rate constants were found:

$$CdNH_3^* + NH_3 \rightarrow CdNH_3^\dagger + NH_3$$

$$k = 9.1 \times 10^{-13} \text{ cm}^3 \text{ molecule}^{-1} \text{ s}^{-1} \quad (\pm 15\%)$$

$$CdNH_3^* \rightarrow Cd + NH_3 + h\nu$$

$$k \approx 6 \times 10^4 \text{ s}^{-1} \quad (\pm 50\%)$$

$$Cd(^3P_0) + NH_3 \rightarrow CdNH_3^\dagger$$

$$k = 2.1 \times 10^{-11} \text{ cm}^3 \text{ molecule}^{-1} \text{ s}^{-1} \quad (\pm 20\%)$$

$$Cd(^3P_1) + NH_3 \rightarrow CdNH_3^\dagger$$

$$k = 8.7 \times 10^{-11} \text{ cm}^3 \text{ molecule}^{-1} \text{ s}^{-1}. \quad (\pm 20\%)$$

The steady-illumination data imply that at low ammonia pressures metastable Cd_2^* formed through the collision complex $Cd_2^\dagger$ provides an additional energy reservoir in the system and that the dissociative lifetime of $Cd_2^\dagger$ must be two or three orders of magnitude greater than that of $CdNH_3^\dagger$. This requires the lifetime of $CdNH_3^\dagger$ to be in the range 10^{-11} -10^{-13} s.

The LIF technique devised for the present work provides another way (other than phase-sensitive absorption spectroscopy[106]) by which the phase shifts of non-radiating species may be determined. While it is probably a more sensitive technique than the absorption method, its application is limited to systems in which the species of interest can be promoted to an upper state whose lifetime is sufficiently short that it does not interfere with the phase of the state of interest. For cases in which the LIF is very weak, it is advantageous for the induced fluorescence and the pump photon to be of different wavelengths.

The insignificance of the radiative decay of $CdNH_3^\dagger$, because of the species' short dissociative lifetime, and the importance of the reaction,

$$CdNH_3^* + NH_3 \rightarrow CdNH_3^\dagger + NH_3$$

in interpreting the phase data of the Cd/NH_3 system indicate further differences in the photochemical mechanisms of Group IIb metal systems. In comparison, an emitting unstabilized complex formed by the bimolecular reaction between $Hg(^3P_0)$ and ammonia is found in the Hg/NH_3 system[81] but no exciplex luminescence has been observed at all from the Zn/NH_3 system.[110]

The $HgNH_3^*$ excimer has been examined as a possible laser system[17]. The results of the present work indicate that gain is unlikely to be observed from Cd/NH_3 mixtures for two reasons. First, increasing ammonia pressures will aid the return of the exciplex to its precursors rather than allowing radiative decay, so increasing the energy loss from the system through 326.1 nm fluorescence. Secondly, the presence of metastable cadmium excimer reservoirs will reduce the likelihood of obtaining gain, unless the equilibrium between $CdNH_3^*$ and Cd_2^* is strongly in the exciplex's favour. Phase-shift measurements similar to those made in this work but over a range of higher cadmium pressures (at fixed ammonia pressure) should allow the determination of the rate at which $CdNH_3^*$ is removed by cadmium.

Although only the $Cd(^3P_0)$ level was probed in this study, the use of the LIF technique to monitor the involvement of the $Cd(^3P_2)$ level could also be the basis of further work.

APPENDICES

I APPENDIX A

Calibrated Volumes

The compartments are defined by the valves (see Fig.II-8) by which they are bounded.

Known volume (V_4) = 11.995 $\pm$ 0.001 ml

Calibrated volume (V_3-V_4-V_5) = 37.33 $\pm$ 0.06 ml

Adaptor line (V_5-leak valve) = 7.13 $\pm$ 0.15 ml

Stainless Steel cell = 360.0 $\pm$ 2.5 ml

II APPENDIX B

The Derivation Phase and Steady-State Equations

The following differential equations can be set down from Scheme III-6

$$\frac{d[Cd_1]}{dt} = I + k_{34}[CdA^{\dagger}] - [Cd_1](k_{16} + k_{33}[A]) \qquad (A.1)$$

$$\frac{d[Cd_0]}{dt} = k_{35}[CdA^{\dagger}] - [Cd_0]k_{38}[A] \qquad (A.2)$$

$$\frac{d[CdA^{\dagger}]}{dt} = k_{33}[A][Cd_1] + k_{38}[A][Cd_0] + k_{39}[A][CdA^*] - [CdA^{\dagger}](k_{34} + k_{35} + k_{36} + k_{37} + k_{28}[A]) \qquad (A.3)$$

$$\frac{d[CdA^*]}{dt} = k_{28}[A][CdA^{\dagger}] - [CdA^*](k_{39}[A] + k_{21}) \qquad (A.4)$$

Writing $u = [Cd_1]$, $x = [Cd_0]$, $y = [CdA\dagger]$ and $z = [CdA^*]$ together with

$a = k_{34}$ $\quad\quad$ $g = k_{39}[A]$

$b = k_{16}+k_{33}[A]$ $\quad\quad$ $k_r = k_{34}+k_{35}+k_{36}+k_{37}$

$c = k_{35}$ $\quad\quad$ $m = k_{28}[A]$

$d = k_{38}[A]$ $\quad\quad$ $p = k_{39}[A]+k_{21}$

$f = k_{33}[A]$

Equations (A.1) to (A.4) may therefore be written as:

$$\dot{u} = I + ay - ub \tag{A.5}$$

$$\dot{x} = cy - dx \tag{A.6}$$

$$\dot{y} = fu + dx + gz - y(k_r + m) \tag{A.7}$$

$$\dot{z} = my - zp \tag{A.8}$$

(1) Phase-Shift equations.

Under conditions of modulated excitation the concentrations can be written as: $u = u_0 e^{i\omega t}$; $x = x_0 e^{i(\omega t-\theta)}$; $y = y_0 e^{i(\omega t-\psi)}$; $z = z_0 e^{i(\omega t-\chi)}$. These expressions ignore a d.c. term which is of no consequence in the phase determination and are referenced to the 326.1 nm fluorescence. The negative phase angle implies that all species lag the $Cd(^3P_1)$ concentration.

Substituting these identities into (A.5) to (A.8) and separating the time dependent and independent parts, the following are obtained:

$$u_0(i\omega+b) = I + ay_0 e^{-i\psi} \tag{A.9}$$

$$x_0 e^{-i\theta}(i\omega+d) = cy_0 e^{-i\psi} \tag{A.10}$$

$$y_0 e^{-i\psi}(i\omega+k_r+m) = fu_0+dx_0 e^{-i\theta}+gz_0 e^{-i\psi} \tag{A.11}$$

$$z_0 e^{-i\chi}(i\omega+p) = my_0 e^{-i\psi} \quad . \tag{A.12}$$

Substitution and rearrangement of these equations then gives,

$$(i\omega+p) = \frac{my_0 e^{i(\chi-\psi)}}{z_0} \quad , \tag{A.13}$$

$$\frac{pd+\omega^2+i\omega(d-p)}{d^2+\omega^2} = \frac{mx_0 e^{i(\chi-\theta)}}{cz_0} \quad , \tag{A.14}$$

and

$$\frac{[d(k_r+m)-\omega^2+i\omega(d+k_r+m)][p^2+\omega^2]-gm[pd+\omega^2-i\omega(p-d)]-dc(p^2+\omega^2)}{p^2+\omega^2} = \frac{fcu_0 e^{i\theta}}{x_0} \tag{A.15}$$

Separating the real and imaginary parts, (A.13) gives an expression for the shift between $CdNH_3^{\dagger}$ and $CdNH_3^{*}$:

$$\tan(\chi-\psi) = \frac{\omega}{k_{39}[A]+k_{21}} \tag{3.51}$$

(A.14) gives an expression for the shift between $Cd(^3P_0)$ and $CdNH_3^{*}$:

$$\tan(\chi-\theta) = \frac{\omega[k_{38}[A] - (k_{39}[A]+k_{21})]}{k_{38}[A](k_{39}[A]+k_{21}) + \omega^2} \tag{3.50}$$

(A.15) yields the full expression for the shift between $Cd(^3P_1)$ and $Cd(^3P_0)$:

$$\frac{\tan\theta}{\omega} = \frac{\begin{array}{l}\{(k_{39}[A]+k_{21})[(k_{38}[A]+k_r+k_{28}[A])(k_{39}[A]+k_{21})-k_{28}k_{39}[A]^2] \\ +k_{38}k_{28}k_{39}[A]^3+\omega^2(k_{38}[A]+k_r+k_{28}[A])\}\end{array}}{\left(\begin{array}{l}\omega^2[k_{38}[A](k_r-k_{35}+k_{28}[A])-\omega^2-k_{28}k_{39}[A]^2] \\ +(k_{39}[A]+k_{21})\{[k_{38}[A](k_r-k_{35}+k_{28}[A])-\omega^2](k_{39}[A]+k_{21}) \\ \qquad -k_{38}k_{28}k_{39}[A]^3\}\end{array}\right)}$$

This equation reduces to equation (3.40) if processes (3.28), (3.29) and (3.21) are neglected, that is, under conditions of low ammonia pressure.

(2) Steady-State Equations for $I_{430}/I_{326.1}$

Under steady-state conditions the emission intensity at 430 nm is given by:

$$I_{430} = k_{21}[CdA^*] \tag{A.16}$$

Schemes III-6 and III-7 provide two sources of $CdNH_3^*$. If process (3.26) is neglected, and steady-state conditions are assumed, equation (A.17) is obtained.

$$[CdA^*] = \frac{k_{28}[A][CdA^\dagger]+k_{58}[A][Cd_2^\dagger]+k_{59}[A][Cd_2^*]}{k_{39}[A] + k_{21}} \tag{A.17}$$

Steady-state expressions for $CdNH_3^\dagger$, Cd_2^* and $Cd_2^\dagger$ are derived from Schemes III-6 and III-7 respectively.

$$[CdA^\dagger] = \frac{k_{33}[A][Cd_1] + k_{28}[A][Cd_0] + k_{39}[A][CdA^*]}{k_r + k_{28}[A]} \tag{A.18}$$

$$[Cd_2^*] = \frac{k_{57}[A][Cd_2^\dagger]}{k_{59}[A]} \tag{A.19}$$

$$[Cd_2^\dagger] = \frac{k_{53}[Cd][Cd_1]+k_{56}[Cd][Cd_0]}{k_r' + (k_{57}+k_{58})[A]} \tag{A.20}$$

Noting that $k_{39}[A][CdA^*] << k_{33}[A][Cd_1] + k_{38}[A][Cd_0]$, letting $K[Cd_1] = [Cd_0]$ and substituting (A.19), (A.18) and (A.20) into (A.17), it is found that

$$[CdA^*] = \frac{[Cd_1][A] \times \left[\frac{k_{28}(k_{33}+k_{38}K)[A]}{(k_r+k_{28}[A])} + \frac{(k_{57}+k_{58})(k_{53}+k_{56}K)[Cd]}{(k_r'+(k_{57}+k_{58})[A])} \right]}{k_{39}[A] + k_{21}} \qquad (A.21)$$

Equation (A.21) leads to:

$$\frac{I_{430}}{I_{326.1}} = \frac{\frac{k_{21}[A]}{k_{16}} \times \left[\frac{k_{28}(k_{33}+k_{38}K)[A]}{(k_r+k_{28}[A])} + \frac{(k_{57}+k_{58})(k_{53}+k_{56}K)[Cd]}{(k_r'+(k_{57}+k_{58})[A])} \right]}{k_{39}[A] + k_{21}}$$

III APPENDIX C

Estimated Uncertainties

Frequency = $\pm$ 0.02 kHz

Calibrated glass line temperature = $\pm$ 0.4 K

Cell temperature (over-all) = $\pm$ 5 K (uncertainty in centre of cross probably $\pm$ 2 K)

Cadmium pressure = $\pm$ 5% (average)

Ammonia pressure = $\pm$ 2% (average)

Phase shifts (with respect to lamp, i.e. the uncertainty is doubled on determining the phase differences) = $\pm$ 1° (typically)

$I_{430}/I_{326.1}$ = 5-20% (depending on the ammonia and cadmium pressures).

IV APPENDIX D

The TRS-80 Software Listings

(1) Input routine for the boxcar integrator.

```
5 GOTO 100
10 OUT M0,M2:MA=INP(M1):MB=INP(M2):MX=MA+M3*MB/M3:RETURN
40 NP=NP+1:GOSUB 10:MX=MX:T(NP)=MX/RA:MZ=M4:GOSUB 10:VA(NP)=MX/RA:IF NP=2000 OR
MX>MU THEN RETURN
50 FOR N=1 TO ND:NEXT:PRINT@1000," ";NP;" ";MZ=M3:GOTO 40
70 NP=NP+1:GOSUB 10:MX=MX:MZ=M4:GOSUB 10:VA(NP)=MX/RA:T(NP)=MX/RA:MZ=M3:IF NP=20
00 OR MX>MU THEN RETURN
80 GOSUB 10:IF (MX-MX)<MB GOTO 80
90 PRINT@1000," ";NP;" ";:GOTO 70
100 CLS:PRINTCHR$(23):PRINT:PRINT"   INPUT ROUTINE FOR":PRINT:PRINT"  BOXCAR IN
TEGRATOR"
200 CLEAR 500:DEFINT M,N:DEFSTR S:DIM Y(2000),X(2000),VA(2000),T(2000):S1=STRING
$(66,"*"):S2=STRING$(60,"-"):S8=STRING$(10," "):NC=0:MM=128:M1=127:M2=126:M3=16:
M4=4:Y.5:MA=17
300 CLS:PRINT"ENTER TITLE OF THIS RUN (FOR LINEPRINTER RECORD)":PRINT:LINE INPUT
 S1:PRINT:PRINT"BOXCAR SHOULD HAVE TIME AXIS ON A/D CHANNEL 1":PRINT"INTENSITY D
ATA SHOULD BE ON A/D CHANNEL 2":PRINT"ENTER FILENAME FOR DISK FILE (INCLUDE /DAT
:1 IN NAME)":PRINT
400 LINE INPUT SF:PRINT:PRINT"CAN HAVE DATA READ IN AT REGULAR INTERVALS OR IN R
ESPONSE TO":PRINT"CHANGING INPUT SIGNALS":INPUT"DATA INPUT AT REGULAR INTERVALS
(Y/N)";SY:IF SY="Y"GOSUB 1000
450 IF SY="N" GOSUB 2000
500 OPEN"O",1,SF:PRINT"FILE ";SF;" OPENED FOR DATA INPUT":PRINT#1,ST
600 PRINT"RESUME SCAN COVERS RANGE 0 - 10V APPROXIMATELY ON CHANNEL #1":INPUT"EN
TER VALUE OF CHANNEL 1 INPUT TO BEGIN SCAN";T1:INPUT"ENTER VALUE OF CHANNEL 1 IN
PUT TO TERMINATE SCAN";T2:MZ=M3:NP=0:MT=T1+RA:MU=T2+RA
650 FOR N=1 TO 50:SA=INKEY$:NEXT:SA="":PRINT"PRESS ANY KEY TO BEGIN"
700 SA=INKEY$:IF SA="" GOTO 700
750 PRINT@1000,SA;
800 OUT M0,M2:MA=INP(M1):MB=INP(M2):MX=MA+M3*MB/M3:IF MX<MT GOTO 800
900 IF SY="Y" GOSUB 40
920 IF SY<>"Y" GOSUB 70
950 GOTO3000
1000 INPUT"ENTER NUMBER OF FOR/NEXT DELAY STEPS REQUIRED BETWEEN INPUTS";ND:ND=N
D+1:RETURN
2000 PRINT"A/D CHANNEL NUMBER 1 WILL BE MONITORED FOR CHANGE":INPUT"MINIMUM VOLT
AGE CHANGE TO TRIGGER INPUT";VM:ND=VM*400.5:PRINT"CORRESPONDING NUMBER OF DATA B
ITS = ";ND:PRINT:RETURN
3000 PRINT:LPRINT CHR$(7):PRINT S1:PRINT:PRINT"THIS SCAN RUNS FROM ";T(1);" TO "
;T(NP);" V":INPUT"INCLUDE THIS SCAN IN AVERAGE (Y/N)";SA:IF SA="Y" GOTO 6000
3650 PRINT NC;" SCANS ACCUMULATED IN X,Y ARRAYS":INPUT"ADD ANOTHER SCAN BEFORE S
TORING ON DISK (Y/N)";SA:IF SA<>"Y"GOTO 3200
3100 NP=0:MZ=M3:SA="":PRINT"PRESS ANY KEY TO RESTART":GOTO 700
3200 INPUT"STORE THIS DATA ON DISK (Y/N)";SA:IF SA="Y" GOSUB4000
3300 INPUT"WANT LINEPRINTER OUTPUT (Y/N)";SA:IF SA="Y" GOSUB 3500
3400 INPUT"DO ANOTHER RUN (Y/N)";SA:IF SA="Y" THEN GOTO4500
3420 END
```

Input routine for the boxcar integrator (cont.).

```
3500 LPRINT S0;S2:LPRINT:LPRINT S0;ST:LPRINT:LPRINT S0;S2:LPRINT S0;"NUMBER OF S
CANS AVERAGED = ";NC;"   POINTS PER SCAN = ";NP:LPRINT S0;"RANGE OF SCAN = ";T1;
" - ";T2;" VOLTS ON X AXIS":LPRINT S0;"DATA STORED ON DISK FILE:  ";SF
3600 IF SY="Y" LPRINT S0;"POINTS TAKEN AT FIXED TIME INTERVALS (";ND;" DELAY STE
PS)"
3700 IF SY="N" LPRINT S0;"DATA TRANSFER CAUSED BY ";ND;" BITS CHANGE IN T INPUT"
3800 LPRINT S0;S1:RETURN
4000 FOR N=1 TO NP:Y(N)=Y(N)/NC:X(N)=X(N)/NC:NEXT N:PRINT#1,NP; :FOR N=1 TO NP:PR
INT#1,X(N);Y(N); :NEXT N:CLOSE 1:PRINT"FILE ";SF;" NOW CLOSED":PRINT S1:RETURN
4500 CLOSE 1:FOR N=1 TO NP:X(N)=0:Y(N)=0:NEXT N:NC=0:NP=0:GOTO 300.
5000 FORN=1 TONP:PRINTT(N); :NEXT
6000 NC=NC+1:FOR N=1 TO NP:X(N)=X(N)+T(N):Y(N)=Y(N)+VA(N):NEXT:GOTO 3650
```

(2) Fourier analysis program.

```
100 CLS:PRINT CHR$(23):PRINT:PRINT"     FOURIER ANNALYSIS":PRINT:PRINT:PRINT"
   PROGRAM":PRINT:PRINT:PRINT"     FOR A/D INTERFACE":PRINT:PRINT"       DATA F
ILES":FOR N=1 TO 1000:NEXT
200 CLEAR 500:DEFSTR S:DEFINT N,N:P2=6.283185:ST=STRING$(60,"*")
300 DIM VA(2),SF(5),X(20000),Y(20000):CLS
400 SK="N":PRINT"CAN HAVE UP TO 20000 POINTS PER CHANNEL IN SOURCE DATA FILE":PRI
NT:LINE INPUT"ENTER DESCRIPTION OF THIS RUN  ";SF(1):PRINT"GIVE NAME OF SOURCE F
ILE FOR DATA"; :INPUT SF(2)
420 INPUT"WANT TO SUBTRACT A BACKGROUND FILE (Y/N)";SB:IF SB="N" GOTO 500
440 INPUT"GIVE NAME OF BACKGROUND FILE";SF(4)
460 OPEN"I",2,SF(4)
500 OPEN "I",1,SF(2):INPUT#1,SF(3),NP:PRINT"DATA FILE IS LABELLED: ";SF(3):PRINT
"NUMBER OF DATA CHANNELS IS ASSUMED TO BE 2":PRINT"NUMBER OF POINTS PER CHANNEL
IS";NP
520 IF SB="N" GOTO 600
540 INPUT#2,SF(5),NO:PRINT"BACKGROUND FILE IS LABELLED: ";SF(5):PRINT"NUMBER OF
BACKGROUND POINTS IS";NO
600 INPUT"FOR DATA FILE, CHANNEL NUMBER FOR X VARIABLE";MX:INPUT"CHANNEL NUMBER
FOR Y VARIABLE";MY
680 FOR N=1 TO NP:INPUT#1,VA(1),VA(2):X(N)=VA(MX):Y(N)=VA(MY):NEXT N:NC=NP:CLOSE
 1:PRINT"DATA FILE CLOSED"
900 IF SB="N"GOTO 1000
920 INPUT"FOR BACKGROUND FILE, CHANNEL NUMBER FOR X VARIABLE IS";MX:INPUT"CHANNE
L NUMBER FOR Y VARIABLE IS";MY
940 FOR N=1 TO NO:INPUT#2,VA(1),VA(2):Y(N)=Y(N)-VA(MY):NEXT N:CLOSE 2:PRINT"BACK
GROUND FILE CLOSED"
1000 PRINT:N1=NC:N0=1:INPUT"NEED TO CHECK POINTS ARE IN ORDER OF INCREASING X (Y
/N)";SY:IF SY ="Y" GOSUB 2000
```

```
1050 INPUT"NEED TO CHECK FOR POINTS WITH SAME X VALUE (Y/N)";SY:IF SY="Y"GOSUB 2
300
1100 PRINT ST:PRINT:PRINT"REFER ALL WAVEFORMS TO TURN-ON OF LAMP AS TIME ZERO":P
RINT:PRINT ST:PRINT:INPUT"PLOT NEEDED TO DETERMINE START AND FINISH OF WAVEFORM(
Y/N)";SY:IF SY="Y" INPUT"MINIMUM AND MAXIMUM VALUES OF Y VARIABLE FOR PLOT";Y0,Y
1:GOSUB 3000
1150 INPUT"POINT NUMBERS CORRESPONDING TO 0 AND 360 DEGREES ARE";N0,N1
1200 CLS:T=X(N1)-X(N0):AS=0:BS=0:PRINT"FOURIER ANALYSIS FOR DATA BETWEEN POINT";
N0;"AND POINT";N1:FOR N=N0+1 TO N1-1:H=(X(N)-X(N-1))/T:D=X(N)-X(N0):TH=P2*D/T:AS
=AS+Y(N)*H*SIN(TH):BS=BS+Y(N)*H*COS(TH):NEXT N:BS=BS+Y(N0)*(X(N0+1)-X(N0))/T+Y(N
1)*(X(N1)-X(N1-1))/T
1400 PRINT ST:PRINT:DL=ATN(BS/AS)*360/P2:PRINT"PHASE-SHIFT DELTA OF FUNDAMENTAL
= ";DL;" DEGREES":CN=SQR(AS*AS+BS*BS):PRINT:PRINT"COEFFICIENT OF SIN(OMEGA*T-DEL
TA) IS";CN:PRINT:PRINT ST:PRINT:INPUT"WANT LINEPRINTER OUTPUT (Y/N)";SY:IF SY="Y
"GOSUB 4000
1450 INPUT"TRY ANALYSIS AGAIN WITH SAME DATA (Y/N)";SR:IF SR="Y" GOTO 1100
1500 INPUT"REPEAT WITH DIFFERENT DATA (Y/N)";SY:IF SY="Y"GOTO 400 ELSE END
2000 FOR N=2 TO NC
2100 IF X(N)<X(N-1) GOTO 2500
2200 NEXT:RETURN
2500 FOR N=1 TO NC-1:IF X(N)=X(N+1) GOTO 2800
2400 NEXT:PRINT"NUMBER OF DIFFERENT X VALUES IS";NC:RETURN
2500 M=N-1
2600 M=M-1:IF X(N)<X(M) AND M>1 GOTO 2600
2700 XR=X(N):YR=Y(N):FOR MM=M TO N+1 STEP -1:X(MM)=X(MM-1):Y(MM)=Y(MM-1:NEXT
MM:X(N)=XR:Y(N)=YR:GOTO 2200
2800 N=N+1
2900 N=N+1:IF X(N)=X(M) AND NC=NC GOTO 2900
2920 YR=0:FOR MM=N TO M-1:YR=YR+Y(MM):NEXT MM:Y(N)=YR/(M-N):IF N<>NC GOTO 2960
2940 FOR MM=N TO NC:M1=N+1+MM-M:X(M1)=X(MM):Y(M1)=Y(MM):NEXT
2960 NC=NC-N+N+1:GOTO 2400
3000 RY=Y1-Y0:RX=X(N1)-X(N0):CLS:MX=0:FOR MY=0 TO 47:SET(MX,MY):NEXT:MY=47:FOR M
X=0 TO 127:SET(MX,MY):NEXT:PRINT@12,"POINTS";N0;"-";N1;:FOR N=N0 TO N1:MX=(X(N)-
X(N0))*126/RX+1:MY=47-(Y(N)-Y0)*47/RY:IF MY<0 OR MY>47 MY=47
3050 IF MX<0 OR MX>126 MX=0
3060 SET(MX,MY):NEXT:PRINT@896,"PRESS ANY KEY TO CONTINUE";
3100 SY=INKEY$:IF SY="" GOTO 3100
3400 PRINT:PRINT"X VALUES RUN FROM";X(N0);"TO";X(N1);:INPUT"CHANGE RANGE OF POINT
S ON X-AXIS (Y/N)";SY:IF SY="Y"INPUT"NEW LOWER AND UPPER POINT NUMBERS FOR DISPL
AY";N0,N1
3500 PRINT"Y AXIS RANGE IS";Y0;"TO";Y1:INPUT"ALTER RANGE OF VALUES ON Y-AXIS (Y/
N)";SZ:IF SZ="Y" INPUT"NEW LOWER AND UPPER LIMITS ON Y-AXIS";Y0,Y1
3600 IF SY="Y" OR SZ="Y" GOTO 3000 ELSE RETURN
4000 SF=STRING$(79,"*"):IF SR="N"LPRINT SF:LPRINT:LPRINT"                    ";SF(1):LPRINT:LPR
INT SF:LPRINT"  SOURCE FILE USED:  ";SF(2):LPRINT"   NAME OF SOURCE DATA ";SF(3):
LPRINT"  SOURCE FILE HAS 2 CHANNELS,  X-AXIS IS CHANNEL ";N0;",  Y-AXIS IS CHANNEL
 ";N1:GOTO 4100
4050 LPRINT CHR$(15);"REPEAT FOURIER ANALYSIS WITH SAME DATA";CHR$(14)
4100 LPRINT"  NUMBER OF POINTS =";NC:LPRINT"   FOURIER ANALYSIS USED POINTS ";N0
;" TO ";N1:LPRINT"   RANGE OF X:";X(N0);" TO ";X(N1):LPRINT:LPRINT"   AMPLITUDE
 OF FUNDAMENTAL = ";CN:LPRINT"   PHASE SHIFT = ";DL;" DEGREES":LPRINT:LPRINT STRI
NG$(79,"-"):RETURN
```

REFERENCES

(1) P. Bender, Phys. Rev., 36, 1535,(1930).

(2) H.C. Lipson and A.C.G. Mitchell, Phys. Rev., 48, 625, (1935).

(3) N.P. Penkin and T.P. Redko, Optika Spektrosk., 22, 699, (1967).

(4) P.J. Young, G. Greig and O.P. Strausz, J. Am. chem. Soc., 92, 413 (1970).

(5) S. Yamamoto, M. Takaoka, S. Tsunashima and S. Sato, Bull. chem. Soc. Japan, 48, 130, (1975)

(6) H. Umemoto, S. Tsunashima and S. Sato, Chem. Phys. 43, 93, (1979).

(7) H. Umemoto, S. Tsunashima and S. Sato, Chem. Phys. 47, 257, (1980).

(8) H. Umemoto, S. Tsunashima and S. Sato, Chem. Phys. 47, 263, (1980).

(9) W.H. Breckenridge and T.W. Broadbent, Chem. Phys. Letters, 29, 421, (1974).

(10) E.W.R. Steacie and D.J. LeRoy, J. chem. Phys., 10, 22, (1942).

(11) D.J. LeRoy and E.W.R. Steacie, J. chem. Phys., 12, 117, (1944).

(12) E. Whalley, Can. J. Chem., 35, 565, (1957).

(13) W.H. Breckenridge and A.B. Callear, Chem. Phys. Letters, 5, 17, (1970).

(14) W.H. Breckenridge and A.B. Callear, Trans. Faraday Soc., 67, 2009, (1971).

(15) W.H. Breckenridge and J. FitzPatrick, J. phys. Chem., 80, 1955, (1976).

(16) W.H. Breckenridge and A.M. Renlund, J. phys. Chem., 82, 1474, (1978).

(17) A. Mandl and H.A. Hyman, J. chem. Phys., 74, 3167, (1981).

(18) W.H. Breckenridge, T.W. Broadbent and D.S. Moore, J. phys. Chem., 79, 1233, (1975).

(19) W.H. Breckenridge, R.J. Donovan and O. Kim Malmin, Chem. Phys. Letters, 62, 608, (1979).

(20) D.L. King and D.W. Setser, A. Rev. phys. Chem. 27, 407, (1976).

(21) W. Siebrand, *Dynamics of Molecular Collisions*, Vol. A, p.258, Ed. W.H. Miller, Plenum Press, New York, 1976.

(22) W.H. Breckenridge, O. Kim Malmin, W.L. Nikolai and D. Oba, Chem. Phys. Letters, 59, 38, (1978).

(23) P.D. Morten, C.G. Freeman, R.F.C. Claridge and L.F. Phillips, J. Photochem., 3, 285, (1974-75).

(24) W.H. Breckenridge and O. Kim Malmin, Chem. Phys. Letters, 68, 341, (1979).

(25) W.H. Breckenridge and O. Kim Malmin, J. chem. Phys., 74, 3307, (1981).

(26) J.R. Bates and H.S. Taylor, J. Am. chem. Soc., 50, 771, (1928).

(27) E.W.R. Steacie and D.J. LeRoy, J. chem. Phys., 11, 164, (1943).

(28) P. Young, E. Hardwidge, S. Tsunashima, G. Greig, O.P. Strausz, J. Am. chem. Soc., 96, 1946, (1974).

(29) W.H. Breckenridge and A.M. Renlund, J. phys. Chem., 83, 303, (1979).

(30) W.H. Breckenridge and A.M. Renlund, J. phys. Chem., 82, 1484, (1978).

(31) A.B. Callear and J.C. McGurk, J. chem. Soc., Faraday II, 68, 289, (1972).

(32) W.H. Breckenridge and D. Oba, Chem. Phys. Letters, 72, 455, (1980).

(33) R.P. Wayne, *Photochemistry*, p.129, Butterworths, London, 1970.

(34) S. Tsunashima, S. Hirokami and S. Sato, Can. J. Chem., 46, 995, (1968).

(35) H.E. Hunziker, J. chem. Phys., 50, 1288, (1969).

(36) S. Tsunashima and S. Sato, Bull. chem. Soc. Japan, 41, 284 (1968).

(37) S. Tsunashima, S. Satoh and S. Sato, Bull. chem. Soc. Japan, 42, 1531, (1969).

(38) H.E. Hunziker, J. chem. Phys., 50, 1294, (1969).

(39) S. Tsunashima and S. Sato, Bull. chem. Soc. Japan, 40, 2987, (1967).

(40) H. Umemoto, T. Kyogoku, S. Tsunashima and S. Sato, Chem. Phys., 52, 481, (1980).

(41) D.J. LeRoy and E.W.R. Steacie, J. chem. Phys., 10, 683, (1942).

(42) S. Tsunashima and S. Sato, Bull. chem. Soc. Japan, 41, 2281, (1968).

(43) B.L. Kalra and A.R. Knight, Can. J. Chem., 50, 2010, (1972).

(44) B.L. Kalra and A.R. Kight, Can. J. Chem., 54, 77, (1976).

(45) S. Sato, C. Takahashi and S. Tsunashima, Bull. chem. Soc. Japan, 43, 1319, (1970).

(46) S. Tsunashima, O. Ohsawa, C. Takahashi and S. Sato, Bull. chem. Soc. Japan, 46, 83, (1973).

(47) K. Yamamoto, S. Tsunashima and S. Sato, Bull. chem. Soc. Japan, 46, 3677, (1973).

(48) B.L. Kalra and A.R. Knight, Can. J. Chem., 48, 1333, (1970).

(49) E.K. Kraulinya, A.P. Bryukhovetskii and L.I. Kartasheva, Optika Spektrosk., 41, 903 (1976).

(50) L.I. Kartasheva and E.K. Kraulinya, Optika Spektrosk., 45, 1059, (1978).

(51) W. Kapuscinski, Nature, Lond., 116, 170, (1925).

(52) W. Kapuscinski, Nature, Lond., 116, 863, (1925).

(53) J.G. Winans, Phil. Mag., 7, 555, (1929).

(54) S.W. Cram, Phys. Rev., 46, 205 (1934).

(55) H. Hamada, Phyl. Mag. 12, 50, (1931).

(56) S.W. Cram and J.G. Winans, Phys. Rev., 41, 388, (1932).

(57) P. Pringsheim, *Fluorescence and Phosphorescence*, Interscience, New York, 1949.

(58) R.E. Drullinger and M. Stock, J. chem.Phys., 68, 5299, (1978).

(59) H.J. Vreede, R.F.C. Claridge and L.F. Phillips, Chem. Phys. Letters, 27, 1, (1974).

(60) M.W. McGeoch, J. chem. Phys., 72, 140, (1980).

(61) P.J. Hay, T.H. Dunning, Jr. and R.C. Raffenetti, J. chem. Phys., 65, 2679, (1976).

(62) C.F. Bender, T.N. Rescigno, H.F. Schaefer III and A.E. Orel, J. chem. Phys., 71, 1122, (1979).

(63) J.G. Winans, Phil. Mag., 7, 565, (1929).

(64) G.R. Fournier and M.W. McGeoch, J. appl. Phys., 49, 2651, (1978).

(65) M.W. McGeoch, G.R. Fournier and P. Ewart, J. Phys., B., 9, L121, (1976).

(66) M.W. McGeoch and G.R. Fournier, J. appl. Phys., 49, 2659, (1978).

(67) M.W. McGeoch, J. chem. Phys., 73, 2532, (1980).

(68) E.W. Smith, R.E. Drullinger, M.M. Hessel and J. Cooper, J. chem. Phys, 66, 5667, (1977).

(69) W.J. Stevens, Appl. Phys. Letters, 35, 751, (1979).

(70) E. Gaviola and R. W. Wood, Phil. Mag., 6, 1191, (1928).

(71) P.D. Morten, C.G. Freeman, M.J. McEwan, R.F.C. Claridge and L.F. Phillips, Chem. Phys. Letters, 16, 148, (1972).

(72) A.B. Callear and J.H. Connor, Chem. Phys. Letters, 13, 245, (1972).

(73) S. Tsunashima, T. Toyono and S.Sato, Bull. chem. Soc. Japan, 46, 2654, (1973).

(74) S. Yamamoto, S. Tsunashima and S. Sato, Bull. chem. Soc. Japan, 48, 1172, (1975).

(75) S. Yamamoto and S. Sato, Bull. chem. Soc. Japan, 48, 1382, (1975).

(76) S. Yamamoto, K. Tanaka and S. Sato, Bull. chem. Soc. Japan, 48, 2172, (1975).

(77) H. Umemoto, S. Tsunashima and S. Sato, Bull. chem. Soc. Japan, 51, 1951, (1978).

(78) S. Yamamoto, M. Yasunobu, N. Nishimura, S. Hasegawa, Mol. Photochem., 9, 277, (1979).

(79) R.H. Newman, C.G. Freeman, M.J. McEwan, R.F.C. Claridge and L.F. Phillips, Trans. Faraday Soc., 66, 2827, (1970).

(80) R.H. Newman, C.G. Freeman, M.J. McEwan, R.F.C. Claridge and L.F. Phillips, Trans. Faraday Soc., 67, 1360, (1971).

(81) H. Umemoto, S. Tsunashima and S. Sato, Chem. Phys. Letters, 53, 521, (1978).

(82) C.G. Freeman, M.J. McEwan, R.F.C. Claridge and L.F. Phillips, Chem. Phys. Letters, 9, 578, (1971).

(83) A.B. Callear and J. McGurk, Chem. Phys. Letters, 7. 491, (1970).

(84) L.F. Phillips, J. chem. Soc., Faraday II, 72, 2082, (1976).

(85) *C.R.C. Handbook of Chemistry and Physics*, Vol. 59, pE107, Ed. R.C. Weast, C.R.C. Press, West Palm Beach, 1978-79.

(86) W.S. Gleason and R. Pertel, Rev. scient. Instrum., 42, 1638, (1971).

(87) L.F. Phillips, Prog. Reaction Kinet., 7, 83, (1973).

(88) T.T. Paukert and H.S. Johnston, J. Chem. Phys., 56, 2824, (1972).

(89) A.G. Gaydon and H.G. Wolfhard, *Flames* , 3rd ed., p.212, Chapman and Hall, London, 1970 .

(90) J.C. De Vos, Physica, 20, 690, (1954).

(91) A.T. Aldred, J.D. Filby and J.N. Pratt, Trans. Faraday Soc., 55, 2030, (1959).

(92) L. Brewer, C.G. James, R.G. Brewer, F.E. Stafford, R.A. Berg and G.M. Rosenblatt, Rev. scient. Instrum., 33, 1450, (1962).

(93) A. Müller, R. Lumry and H. Kokubun, Rev. scient. Instrum., 36, 1214, (1965).

(94) B.D. Venetta, Rev. scient. Instrum., 30, 450, (1959).

(95) J.B. Birks and I.H. Munro, Prog. Reaction Kinet., 4, 239, (1967).

(96) J.B. Birks, D.J. Dyson and I.H. Munro, Proc. R. Soc., A275, 575, (1963).

(97) W.S. Metcalf, J. chem. Soc., 163, 3726, (1960).

(98) E.W. Schlag, S.J. Yao and H. von Weyssenhoff, J. chem. Phys., 50, 732, (1969).

(99) E.W. Foster, Rep. Prog. Phys. 27, 469, (1964).

(100) H.E. Hunziker, IBM J1 Res. Dev., 15, 10, (1971).

(101) R.P. Blickensderfer, W.H. Breckenridge and J. Simons, J. phys. Chem. 80, 653, (1976).

(102) G.M. Lawrence and B.D. Savage, Phys. Rev., 141, 67, (1966).

(103) K.G. Ong, C.G. Freeman, M.J. McEwan and L.F. Phillips, J. chem. Soc., Faraday II, 72, 183, (1976).

(104) A.G. Ladd, C.G. Freeman, M.J. McEwan, R.F.C. Claridge and L.F. Phillips, J. chem. Soc., Faraday II, 69, 849, (1973).

(105) L.F. Phillips, J. Photochem., 2, 255, (1973-74).

(106) K. Luther, H.R. Wendt and H.E. Hunziker, Chem. Phys. Letters, 33, 146, (1975).

(107) C.G. Freeman, M.J. McEwan, R.F.C. Claridge and L.F. Phillips, Trans. Faraday Soc.,67, 2567,(1971).

(108) C.G. Freeman and L.F. Phillips, Chem. Phys. Letters, 20, 96, (1973).

(109) A.R. Schaefer, Jnl quantve Spectros. & radiat. Transf., 11, 197, (1971).

(110) S. Yamamoto, T. Takei, N. Nishimura and S. Hasegawa, Bull. chem. Soc. Japan, 53, 860, (1980).